

博士論文（要約）

Mechanism of electron transfer between ferredoxin and
 $\alpha_3\beta_3$ -type oxygenase components of Rieske non-heme
iron oxygenase

（Rieske non-heme iron oxygenase における
フェレドキシンとオキシゲナーゼ間電子伝達機構の
解明）

サイ ビー チェン
蔡 弼丞

Table of contents 目次

Table of contents	I
Abbreviations	III
Abstract	VI
Chapter 1 Introduction	1
Chapter 2 Determination of interaction between ferredoxin and oxygenase by computational study and electron transfer efficiency analyses	
2-1 General overview	15
2-2 Prediction of the potential binding sites	
2-2-1 Homology modeling of CDO-F	16
2-2-2 Docking simulations with CDO-O and modeled CDO-F	16
2-3 Determination of interaction between CDO-F and CDO-O by electron transfer efficiency analyses	
2-3-1 Candidates of residues for alanine scanning mutagenesis study	18
2-3-2 Electron transfer efficiency analyses	18
2-4 Measurement of binding affinity between CDO-F and CDO-O	22
2-5 Conservation of binding mode in $\alpha_3\beta_3$ -type Oxy	25
Figures and Tables	28
Chapter 3 Determination of interaction between ferredoxin and oxygenase by X-ray crystallography, cross linking	
3-1 General overview	53
3-2 Crystal structure analysis of the ferredoxin-oxygenase complex of cumene dioxygenase	54
3-3 Determination of interaction between ferredoxin and oxygenase of cumene dioxygenase by cross linking and mass spectrometry	56
3-3-1 Cross linked components by chemical cross linker	
3-3-1-1 Chemical cross linking with CDO-F and CDO-O	56
3-3-1-2 Determination the chemical cross linked region by LC-MS	57
3-3-2 Cross linked components by photoreactive cross linker	59

3-3-2-1 Photo-cross-linking between ρ BPA-mutated ferredoxin and oxygenase	
3-3-2-1-1 The candidate amino acids on ferredoxin mutated with ρ BPA	59
3-3-2-1-2 Performance of photo-cross-linking between ρ BPA-substituted ferredoxin and oxygenase	59
Figures and Tables	61
Chapter 4 Conclusion and Future Prospects	89
Supplement figures for protein purification	91
Materials and Methods	119
References	143
Acknowledgements	149

Abbreviations

3'	terminus of the third carbon in the sugar-ring of DNA
5'	terminus of the fifth carbon in the sugar-ring of DNA
Å	angstrom
APS	ammonium peroxodisulphate
BDO	biphenyl dioxygenase
BLAST	The Basic Local Alignment Search Tool
BPB	bromophenol blue
BSA	bovine serum albumin
BTEX	benzene, toluene, ethylbenzene and xylene isomers
CaCl ₂	calcium chloride
CARDO	carbazole 1,9a-dioxygenase
CCP4	Collaborative Computational Project No. 4
CD	circular dichroic
CDO	cumene dioxygenase
C-terminus	end of terminus with a free carboxyl group of protein or polypeptide
DMS	dimethyl sulfoxide
DNA	deoxyribonucleic acid
DTT	dithiothreitol
EDTA	ethylene diamine tetraacetate
<i>et al.</i>	and others
FAD	flavin adenine dinucleotide
Fd	ferredoxin
FMN	flavin mononucleotide
FNR-type	ferredoxin-NADP ⁺ reductase-type
<i>g</i>	times gravity
g	gram
GFC	gel filtration chromatography
GR-type	glutathione reductase-type
h	hour
HCl	hydrochloric acid
HEPES	4-(2-hydroxyethyl)-1-piperazineethanesulfonic acid
HRP	Horseshoe peroxidase
IPTG	isopropyl β-D-1-thiogalactopyranoside
ITC	isothermal titration calorimetry
k	kilo

kb	kilobase
kDa	kilo Dalton
L	liter
LB	Luria-Bertani medium
LC	liquid chromatography
m	meter, milli (10^{-3})
M	molar
mAu	milli absorbance Unit
MES	2-(N-morpholino)ethanesulfonic acid
min	minute
MS	mass spectrometry
n	nano (10^{-9})
NaCl	sodium chloride
NADH	nicotinamide adenine dinucleotide
NH ₄ HCO ₃	ammonium hydrogen carbonate
N-terminus	start of terminus with the free amine group of protein or polypeptide
OD	optical density
<i>ox</i>	oxidized-form
Oxy	terminal oxygenase
PAGE	polyacrylamide gel electrophoresis
PAHs	polycyclic aromatic hydrocarbons
PCR	polymerase chain reaction
PCT	pre-crystallization test
pH	negative logarithm of the hydrogen ion concentration
PVDF	polyvinylidene difluoride
Q-TOF-MS	quadrupole time-of-flight mass spectrometry
Red	reductase
<i>red</i>	reduced-form
RMSD	root mean square deviation
RNA	ribonucleic acid
RNase	ribonuclease
RO	Rieske non-heme iron dioxygenase
rpm	rounds per minute
SD sequence	Shine-Dalgarno sequence
SDS	sodium dodecyl sulfate
sec	second

sulfo-SMPB	sulfosuccinimidyl 4-(N-maleimidophenyl)butyrate
TAE	Tris-Acetate-EDTA
TDO	toluene dioxygenase
TEMED	tetramethylethylenediamine
TFA	trifluoroacetic acid
TG buffer	20 mM Tris-HCl, 10% glycerol, pH7.4
Tris	Tris-aminomethane
tRNA	transfer RNA
UV	ultraviolet
UV-vis	wavelength from ultraviolet to visible
V	volt
v/v	volume / volume
WT	wild-type
ρ PBA	ρ -benzoyl-L-phenylalanine, also known as BzF
μ	micro (10^{-6})

論文の内容の要旨

応用生命工学専攻
平成28年度博士課程入学
氏名 蔡 弼丞
指導教員 野尻 秀昭

論文題目

Mechanism of electron transfer between ferredoxin and $\alpha_3\beta_3$ -type oxygenase components of Rieske non-heme iron oxygenase

(Rieske non-heme iron oxygenase におけるフェレドキシンとオキシゲナーゼ間電子伝達機構の解明)

Introduction

Aromatic compounds are utilized by microorganisms as carbon and energy sources and are transformed into non- or less-hazardous substances. Microorganisms overcome the resonance stabilization energy of aromatic ring systems using enzymes called oxygenases, which are oxidoreductases that can incorporate one (monooxygenases, also called hydroxylases) or both (dioxygenases) atoms of molecular oxygen into the molecule to cleave aromatic ring. The monooxygenases can be classified as P450-dependent systems, flavin-dependent system, non-P450 hydroxylases and non-heme-dependent oxygenases. The dioxygenases include two major classes, viz., heme-dependent iron-sulfur plant dioxygenases and Rieske non-heme iron dioxygenases (ROs).

ROs often play a key role in the initial step of bacterial degradation of various aromatic compounds, such as naphthalene, biphenyl, isopropylbenzene (cumene) and carbazole. ROs are composed of one or two electron transfer component(s) and a catalytic component (terminal oxygenase, Oxy). The reaction is triggered by electrons from NAD(P)H, which are transferred from reductase (Red) to the Oxy protein subunits directly or via a ferredoxin (Fd).

Oxy of ROs usually contains a large α -subunit having a Rieske cluster domain and a mononuclear iron-containing catalytic domain. The Rieske cluster receives electrons from electron transfer component(s) and transfers them to the mononuclear iron of the neighboring α -subunit. Apart from the large α -subunit, many Oxy contain an additional small β -subunit which contains no prosthetic group, and the function of the β -subunit is suggested to provide structural support to the overall enzyme. To date, all the structures of Oxy demonstrate that Oxy are either α_3 doughnut-shaped or $\alpha_3\beta_3$ mushroom-shaped quaternary structures.

Electron transfer is essential for triggering the degradation in ROs and it is also related with catalytic activity. In three-component RO systems, Fd shuttles electrons through non-covalent bindings between Red and Oxy. The binding manner between Fd and Oxy has been determined previously with Fd-Oxy complex structure of carbazole 1,9a-dioxygenase (CARDO) which is a α_3 -type Oxy by Ashikawa *et al.*, 2006. The study showed that Fd of CARDO (CARDO-F) binds to

the hydrophobic groove surrounded with charged residues at the interface of the α -subunits of Oxy of CARDO (CARDO-O).

Cumene dioxygenase (CDO; EC: 1.14.12.-) from *Pseudomonas fluorescens* IP01, which is a three-component RO system, catalyzes the initial reaction in cumene degradation pathway. Electrons are transferred from NADH via iron-sulfur flavoprotein Red of CDO (CDO-R) and Rieske-type Fd of CDO (CDO-F) to $\alpha_3\beta_3$ -type Oxy of CDO (CDO-O). Of the three components, only the structure of CDO-O has been determined until now and the structure revealed a $\alpha_3\beta_3$ mushroom-shaped quaternary structure. CDO is classified as a class IIB RO according to the Batie's classification, which is the same class as the well-studied ROs, biphenyl dioxygenase (BDO) and toluene dioxygenase (TDO), both of which are $\alpha_3\beta_3$ -type Oxy and are associated with Rieske-type Fd. CDO-O is possessed of 64-74%, 50-59%, 50-77% and 48-73% identities with α -, β -subunits, Fds, and Reds, respectively, of BDO from *Paraburkholderia xenovorans* LB400, BDO from *Rhodococcus jostii* RHA1, and TDO from *P. putida* F1. The structures of CDO-O α and CDO-O β have RMSD values of 0.94-1.45 Å and 0.89-1.43 Å compared to α - and β -subunits of above BDO and TDO.

The current study aimed to determine the mechanism of electron transfer between Rieske-type CDO-F and $\alpha_3\beta_3$ -type CDO-O by two different approaches. In approach I, I performed docking simulations with homology-modelled CDO-F and wild type (WT) CDO-O and electron transfer efficiency analyses to determine the residues on CDO-O involved in their interaction. Moreover, the conservation of the interaction related residues in $\alpha_3\beta_3$ -type CDO-O has also been proposed. In approach II, I tried to determine the complex structure by X-ray crystallography. The predicted interactions were further confirmed using chemical and photo cross linking followed by mass spectrometry.

Approach I: Computational study and electron transfer efficiency analyses

To determine the mechanism of electron transfer between CDO-F and CDO-O by computational studies, structures of both CDO-F and CDO-O were needed. The structures of 4 modeled CDO-Fs were generated by homology modeling using SWISS-MODEL. Then, docking simulations were performed between CDO-O and the 4 homology-modelled CDO-Fs, independently. The results showed that there were two potential docking sites on CDO-O, one was at the interface of two α -subunit at top-wise site of CDO-O molecule (on the cap of the mushroom-shaped structure), the other was at the interface of α and β -subunit at the side-wise site of CDO-O molecule (at the stem of the mushroom-shaped structure). The putative binding manner at top-wise site corresponded to that in CARDO. Both potential binding sites had similar features, which were found in the binding sites between CARDO-F and CARDO-O, and that was a hydrophobic groove surrounded by several charged residues.

Alanine-scanning mutagenesis was performed on surface-exposed residues of CARDO-O, which may be involved in the binding with CDO-F. Based on results of docking simulations, 16 charged or hydrophobic residues were chosen for alanine substitution, individually. Eight residues,

viz. Lys33, Leu35, Arg39 and Arg407 on α 1-subunit and Asp158, Trp159, Leu162, Glu180 on α 2-subunit corresponding to the top-wise site. Eight residues, viz. Lys117 and Lys141 on α 1-subunit, Leu241, Asp253 and Lys258 on α 2-subunit, Arg65 on β 1-subunit, and Leu98, Trp100 on β 2-subunit corresponding to the side-wise site.

Electron transfer efficiency were measured by the reduction of the Rieske cluster on CDO-O. The efficiencies were measured between the wild type electron transfer components and each of 16 single alanine-substituted, respectively (Fig. 1A). The mutants with alanine substitution at top-wise site showed no or negligible decrement in reduction efficiency compared with that of WT CDO-O. On the other hand, the reduction efficiency of alanine-substituents at the side-wise site significantly decreased, especially with α K117 and β R65A mutations. The efficiencies of α K117A and β R65A decreased to 21% and 46%, respectively, compared to that of the WT CDO-O. In addition, the efficiencies of α K141A and β W100A seemed to decrease slightly to 71-75%, although statistical significance was not significant. Electron transfer efficiency were also measured with 9 double-alanine-substituted Oxys (Fig. 1B). The efficiencies of mutants which included either α K117A or β R65A, decreased to less than 20%, while that of α K141A; β W100A decreased to 69%.

These results indicated that CDO-F binds at the side-wise site of CDO-O and transfers an electron to the Rieske cluster of CDO-O.

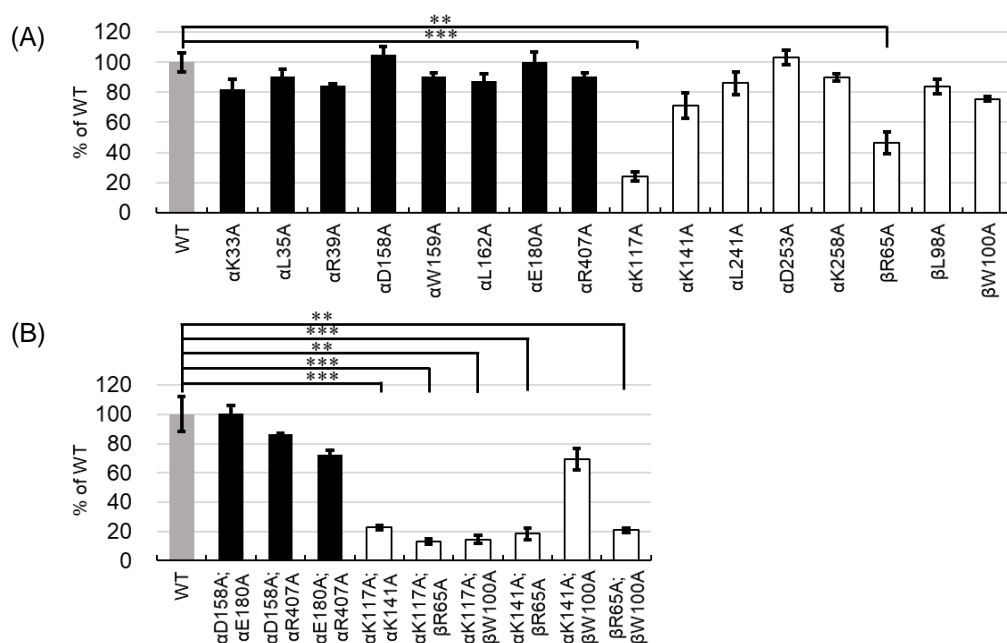


Fig. 1. Reduction efficiencies of alanine substituted CDO-O

Panels (A) and (B) show the reduction efficiencies of single alanine-substituted CDO-Os and double alanine-substituted CDO-Os, respectively. That of WT CDO-O was also shown in both panels as gray bars, which were set to be 100%. The black and white bars were the reduction efficiencies of CDO-O derivatives which had amino acid-substitution at the top-wise and side-wise potential docking site, respectively. Error bars indicate the standard deviation from three independent experiments. $n = 3$, ** $p < 0.005$, *** $p < 0.001$

Above results showed that the electron transfer was disrupted by of alanine-substitutions. To determine whether the effect by alanine substitution was disruption of the electron transfer pathway or components-binding, isothermal titration calorimetry was performed. Unfortunately, I cannot

optimize the buffer condition to measure experimental heat of CDO-F and CDO-O interaction.

Ten structures of $\alpha_3\beta_3$ -type Oxy were superimposed and the position of positive charged residues at the side-wise site were compared. The positions of α K117 and β R65 were conserved in all the Oxy. Furthermore, sequence alignment also showed that α K117 and β R65 were conserved in 73 different α - and β -subunits of ROs. It suggested a possibility that the common mechanism of electron transfer is shared by most Rieske-type Fd and $\alpha_3\beta_3$ -type Oxy combinations.

Approach II: X-ray crystallography, chemical- and photo-cross linking

X-ray crystallography was performed with mixture of WT CDO-F and WT CDO-O or its derivatives (α K117A and α R39A). Crystals were obtained within few days with following conditions, 0.7% (v/v) Jeffamine[®] ED-2001, 1.4-1.6 M sodium malonate and 0.1 M MES (pH 6.4 or 6.5) or 0.7% (v/v) Jeffamine[®] ED-2001, 1.4-1.6 M sodium malonate and 0.1 M HEPES (pH 6.6, 6.7 or 6.8). X-ray diffraction data were collected with 19 crystals and structure refinement was performed. Although the immunoblotting results showed that most of crystals contained both CDO-F and CDO-O, only CDO-O structure could be built with all X-ray diffraction data. It might be because that CDO-F was coating on the surface of crystals or not obtained in all asymmetric unit.

Chemical cross linking and photo cross linking were performed with CDO-F and CDO-O. In chemical cross linking, WT CDO-F and WT CDO-O were mixed with chemical cross linker, sulfo-SMPB or DMS for 60 min, then the mixture was separated by electrophoresis. The novel band was detected at less than 98 kDa when sulfo-SMPB was used. The band was cut off and analyzed by liquid chromatography/mass spectrometry (LC/MS). However, the binding site of CDO-F could not be identified with the mapping result of LC/MS.

On the other hand, a genetically encoded photoreactive amino acid, ρ -benzoyl-L-phenylalanine (ρ BPA), was used to survey the binding site of CDO-F. Six amino acid residues of CDO-F (Q19X, S49X, L65X, A80X, P81X and P85X) was replaced by ρ BPA, individually. Among them, only Q19X and L65X could be expressed and purified successfully. Photoreactive CDO-F and WT CDO-O were mixed in 3:1 ratio and treated with 365 nm UV light for 30 to 120 minutes. The cross linked CDO-F Q19X and CDO-O was detected by electrophoresis.

Conclusion and future prospects

The current study demonstrated that CDO-F binds at the interface of α - and β -subunit of CDO-O and that the residues, α K117 and β R65, plays critical roles in the interaction. The residues are conserved in most $\alpha_3\beta_3$ -type Oxy, suggesting a similar mode of binding in most Rieske-type Fd and $\alpha_3\beta_3$ -type Oxy. The study also revealed that the function of β -subunit of $\alpha_3\beta_3$ -type Oxy is not only structural but it also stabilizes the interaction with Rieske-type Fd. The reproducibility of photo cross linking results will be confirmed and followed by LC/MS analyses. To determine the mechanism of interaction between Rieske-type Fd and $\alpha_3\beta_3$ -type Oxy in atomic level, more detailed structural studies of complex are necessary.

Chapter 1

Introduction

Aromatic compounds are structurally diverse and widely distributed in nature. Some aromatic compounds, such as BTEX (benzene, toluene, ethylbenzene and xylene isomers) and polycyclic aromatic hydrocarbons (PAHs), are toxic, mutagenic and carcinogenic and difficult to degrade under natural conditions [IARC, 1983]. Aromatic compounds are utilized by microorganisms as the carbon source and/or energy sources and are transferred into non- or less-hazardous substances [Kanaly *et al.*, 2000]. A widely used technology, bioremediation, can remove aromatic compounds from the environment using microorganisms which is safer and more economic than physical or chemical technologies [Cerniglia *et al.*, 1993]. The challenge for microorganisms using aromatic compounds as carbon source is to overcome the stabilizing resonance energy of the aromatic ring system. Most microorganisms solve the problem by the enzymes called oxygenase, which incorporate oxygen into aromatic compounds to cleave the aromatic ring [Fuchs *et al.*, 2011].

The role of oxygen in metabolic pathway had been discovered for a long time. At beginning, it was believed that the oxygen atoms were transferred from other organic molecules or water, not from atmospheric oxygen. In 1955, it was discovered that the atmospheric oxygen was directly incorporated into the substrates with catechol 1,2-dioxygenase and phenolase [Hayaishi *et al.*, 1955; Mason, 1955]. Oxygenases were oxidoreductases which incorporate one (monooxygenases, also called hydroxylases) or both (dioxygenases) atoms of atmospheric oxygen into substrates. Microorganisms most use dioxygenase to overcome the resonance stabilization energies [Gibson and

Subramanian, 1984; Gibson and Parales, 2000]. The monooxygenase can separate to P450-dependent systems, Flavin-dependent system, non-P450 hydroxylases and non-heme-dependent oxygenases and the dioxygenases include two major classes, heme-dependent iron–sulfur plant dioxygenase and non heme-dependent iron-dependent dioxygenase, which included 2-oxoglutarate-dependent dioxygenase and Rieske non-heme iron dioxygenase (RO) [Solomon *et al.*, 2000; Burton, 2003].

Rieske non-heme iron oxygenase

ROs often play a key role in the initial step of degradation of various aromatic compounds, such as naphthalene, biphenyl, isopropylbenzene (cumene) and carbazole [Wolfe *et al.*, 2000] by oxidizing the aromatic compounds by incorporating two hydroxyl group to form *cis*-dihydrodiol [Axcell *et al.*, 1975; Gibson *et al.*, 1968]. ROs are composed of one or two electron transfer component(s) and a catalytic component (terminal oxygenase, Oxy) [Wackett, 2002]. The reaction is triggered by electrons from NAD(P)H, which are transferred directly from reductase (Red) to the Oxy protein subunits or via a ferredoxin (Fd) (Fig. 1-1) [Parales *et al.*, 1998]. There are few different methods to classify ROs [Batie *et al.*, 1992; Nam *et al.*, 2001; Kweon *et al.*, 2008; Joydeep *et al.*, 2012] and Batie's classification is used in this thesis. According to Batie's classification system, ROs are divided five different classes, IA, IB, IIA, IIB and III, on the basis of the number of components, the presence of FMN or FAD and the type of Rieske cluster present in Red, and the type of Rieske cluster contained in the Fd (Table 1) [Batie *et al.*, 1992].

Iron-sulfur clusters are common electron transfer cofactors distributed in all families of organisms, from prokaryotes to eukaryotes [Noodleman *et al.*, 2008]. The

iron-sulfur clusters contain 1 to 4 iron atoms and coordinate with inorganic sulfur (sulfide S^{2-}). Rieske cluster is a [2Fe-2S] cluster and is contained in all ROs. The iron atoms in Rieske cluster are bridged with 2 inorganic sulfur S^{2-} . One iron (Fe_1) is coordinated by 2 cysteine residues and the other iron (Fe_2) is coordinated by 2 histidine residues [Rieske *et al.*, 1964; Gurbiel *et al.*, 1989]. With other [2Fe-2S] cluster, which called putidaredoxin-type [2Fe-2S] cluster, the iron atoms are both coordinated by 2 cysteine residues (Fig. 1-2) [Hanke *et al.*, 2013].

Red is the first component of the electron transfer chain of ROs. There are two types of Red in ROs, glutathione reductase (GR)-type (EC: 1.8.1.7) and ferredoxin-NADP⁺ reductase (FNR)-type (EC: 1.18.1.2) whether or not containing a putidaredoxin type [2Fe-2S] cluster either at N- or C-terminus (Fig. 1-3) [Ferraro *et al.*, 2005].

Three-components ROs have Fd as the second electron transfer component which shuttle electrons between Red and Oxy through non-covalent binding. The Rieske-type Fd can be divided into a Rieske [2Fe-2S] cluster domain and a basal domain (Fig. 1-4) [Carrell *et al.*, 1997].

Oxy of ROs contains a large α -subunit which can be divided into a Rieske [2Fe-2S] cluster domain at N-terminus which contains a Rieske cluster receiving electrons from electron transfer component(s) and a mononuclear iron-containing catalytic domain at C-terminus which contains a mononuclear iron center as the catalytic center (Fig. 1-5A). The Rieske cluster receives electrons and transfers them to the mononuclear iron of the neighboring α subunit [Gassner *et al.*, 1993; Kauppi *et al.*, 1998]. Two histidine and two cysteine coordinate with Rieske cluster with the conserved sequence motif CXHX₁₅₋₂₁CXXH [Mason *et al.*, 1992]. Apart from the large α -subunit, most Oxy

contain an additional small β -subunit which contains no prosthetic group, and the function of β -subunit is suggested that it was structural in ROs (Fig. 1-5B) [Kauppi *et al.*, 1998; Parales *et al.*, 1998; Parales *et al.*, 1998; Beil *et al.*, 1998; Tan *et al.*, 1994; Nojiri *et al.*, 2005]. To date, structure of 14 Oxy have been determined. All the structures demonstrate either α_3 doughnut-shaped or $\alpha_3\beta_3$ mushroom-shaped quaternary structures.

Electron transfer mechanism of ROs

Electron transfer is essential for triggering the degradation in ROs and it is also related with catalytic activity. In three-component RO systems, Fd shuttles electrons through non-covalent bindings with Red and Oxy. To date, the binding manner between Red and Fd have been determined with the structures of Red-Fd complex of biphenyl dioxygenase (BDO) from *Acidovorax* sp. KKS102, Red-Fd complex of toluene dioxygenase (TDO) from *Pseudomonas putida* F1 [Senda *et al.*, 2007; Friemann *et al.*, 2009]. The binding manner between Fd and Oxy has been determined only with Fd-Oxy complex structure of carbazole 1,9a-dioxygenase (CARDO) containing α_3 -type Oxy [Ashikawa *et al.*, 2006]. That is, Fd of CARDO (CARDO-F) bound on the hydrophobic groove surrounded with charged residues at the interface of the α -subunits of Oxy of CARDO (CARDO-O) component (Fig. 1-6).

The interaction between Fd and $\alpha_3\beta_3$ -type Oxy has only been predicted by docking simulations. Friemann *et al.* (2009) and Khara *et al.* (2014) performed docking simulations with Fd and $\alpha_3\beta_3$ -type Oxy components of TDO from *P. putida* F1 and aromatic hydrocarbon dioxygenase from *Sphingobium* sp. PNB [Friemann *et al.*, 2009; Khara *et al.*, 2014]. The results suggested that Fd might bind with Oxy either at the

interface of the α -subunit at the top-wise site (on the cap of the mushroom-shaped structure), or the interface of the α - and β -subunits at the side-wise site (at the stem of the mushroom-shaped structure) Kumari *et al.* (2017) also performed docking simulation with Fd and $\alpha_3\beta_3$ -type Oxy component of 3-nitrotoluene dioxygenase from *Diaphorobacter* sp. strain DS2 and demonstrated that the Fd would bind at the interface of α -subunit [Kumari *et al.*, 2017]. The putative binding manner of the top-wise site corresponds to that in CARDO.

Cumene dioxygenase

Cumene naturally exists in crude oil and its derivatives as solvent, gasoline and diesel fuels and also the raw materials of phenol and acetone [NTP, 2009]. Exposure to high levels of cumene in short-term results in headache, dizziness, lightheadedness, unconsciousness, narcosis and coma. Long-term exposures may result in lung, liver and kidney damage [Pohanish *et al.*, 2011]. The carcinogenic activity of cumene was also been determined [NTP, 2009].

Cumene dioxygenase (CDO; EC: 1.14.12.-) from *Pseudomonas fluorescens* IP01, which is a three-component RO system, catalyzes the initial reaction in cumene degradation pathway (Fig. 1-7). The *cumA1*, *cumA2*, *cumA3* and *cumA4* genes which encode the CDO three-component oxygenase system, α -subunit and β -subunit of Oxy, Fd and Red, respectively (CDO-O α , CDO-O β , CDO-F and CDO-R) have been isolated previously [Aoki *et al.*, 1996]. Electrons are transferred from NADH via iron-sulfur flavoprotein Red of CDO (CDO-R) and Rieske-type Fd of CDO (CDO-F) to $\alpha_3\beta_3$ -type Oxy of CDO (CDO-O) (Fig. 1-1 and 1-6). Until now, only the structure of CDO-O has been determined and reported [Dong *et al.*, 2005]. The CDO-O structure confirmed that CDO-O

contains $\alpha_3\beta_3$ mushroom-shaped quaternary structure (Fig. 1-5B). CDO is classified as a class IIB according to the Batie's classification [Batie *et al.*, 1992], as same as the well-studied ROs, biphenyl dioxygenase (BDO) and TDO, which also contain Rieske-type Fd and $\alpha_3\beta_3$ -type Oxy [Furukawa, 2000; Furusawa *et al.*, 2004; Suenaga *et al.*, 2001; Suenaga *et al.*, 2002; Zielinski *et al.*, 2002; 2003]. CDO possesses 64-74% identities, 50-59% identities, 50-77% identities and 48-73% identities with α -, β -subunits, Fd and Red of BDO from *Paraburkholderia xenovorans* LB400, *Rhodococcus jostii* RHA1 and TDO from *P. putida* F1. The structures of α -, β -subunits of CDO have RMSD values of 0.94-1.45 Å and 0.89-1.43 Å to α - and β -subunit of BDO and TDO [Kumar, 2011; Furusawa *et al.*, 2004; Friemann *et al.*, 2009;]. Therefore, CDO is a good model of toluene/biphenyl dioxygenase (TDO/BDO) subfamily [Werlen *et al.*, 1996].

Objective

To date, all the binding modes between Fd and $\alpha_3\beta_3$ -type Oxy were predicted by the simulations. The current study aimed to determine the mode of binding between Rieske-type CDO-F and $\alpha_3\beta_3$ -type CDO-O by two different approaches. In approach I, I performed computational studies and reduction efficiency analyses to determine the critical residues on CDO-O which are involved in interaction. In addition, evolutionary relationships between the α -subunit, β -subunit and Fd have also been proposed. In approach II, I tried to determine the interaction between Fd and Oxy by X-ray crystallography, chemical and photo cross linking followed by mass spectrometry.

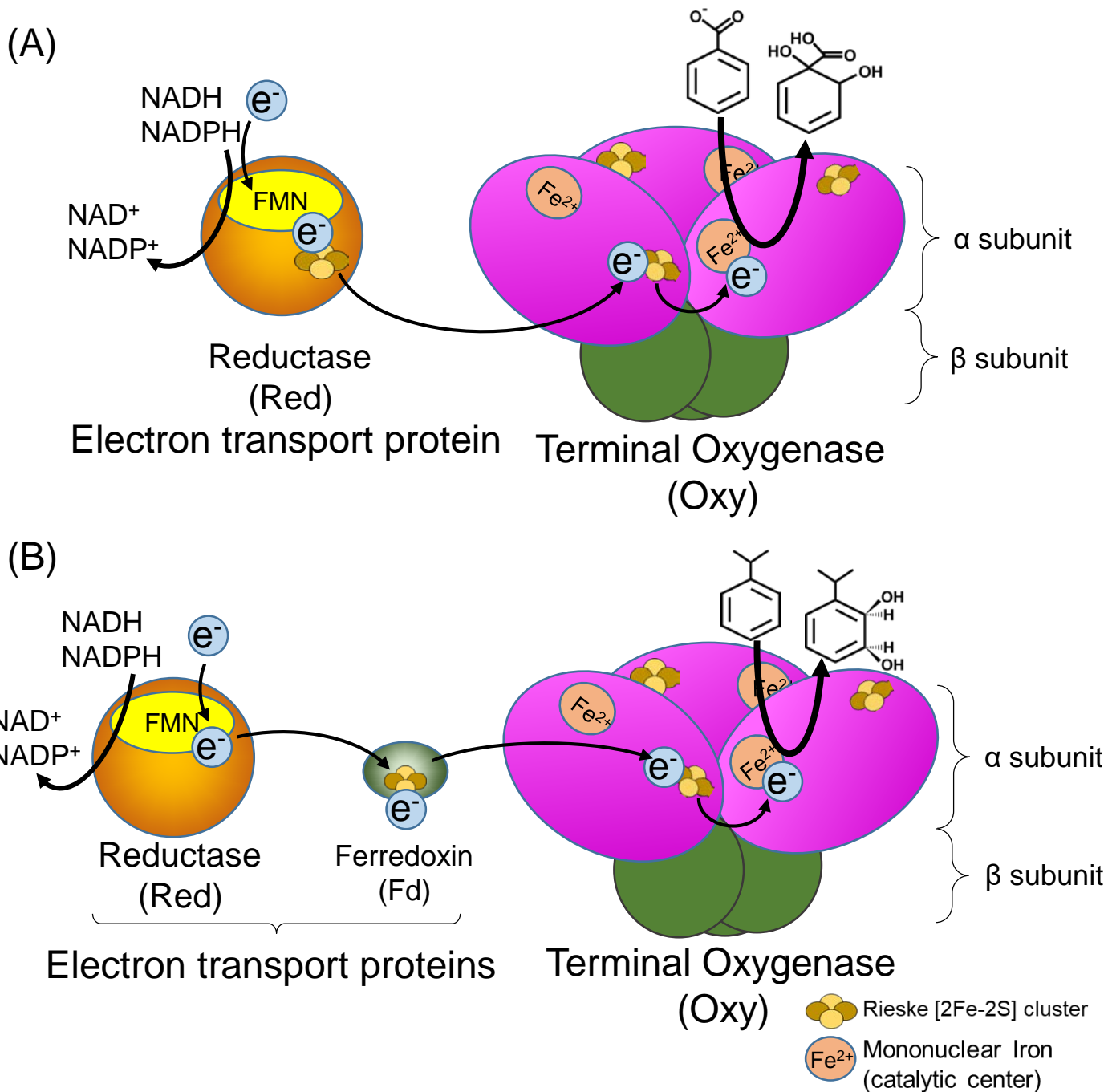


Fig. 1-1. Schematic representation of RO system

The schematic figures are the two examples of RO system. (A) The RO system contains with one electron transfer component (phthalate 4,5-dioxygenase [Gurbiel *et al.*, 1989]) and (B) two electron transfer components (CDO [Aoki *et al.*, 1996]). The reaction is triggered by the electrons from NAD(P)H which are transferred directly from Red to the terminal oxygenase or via a Fd.

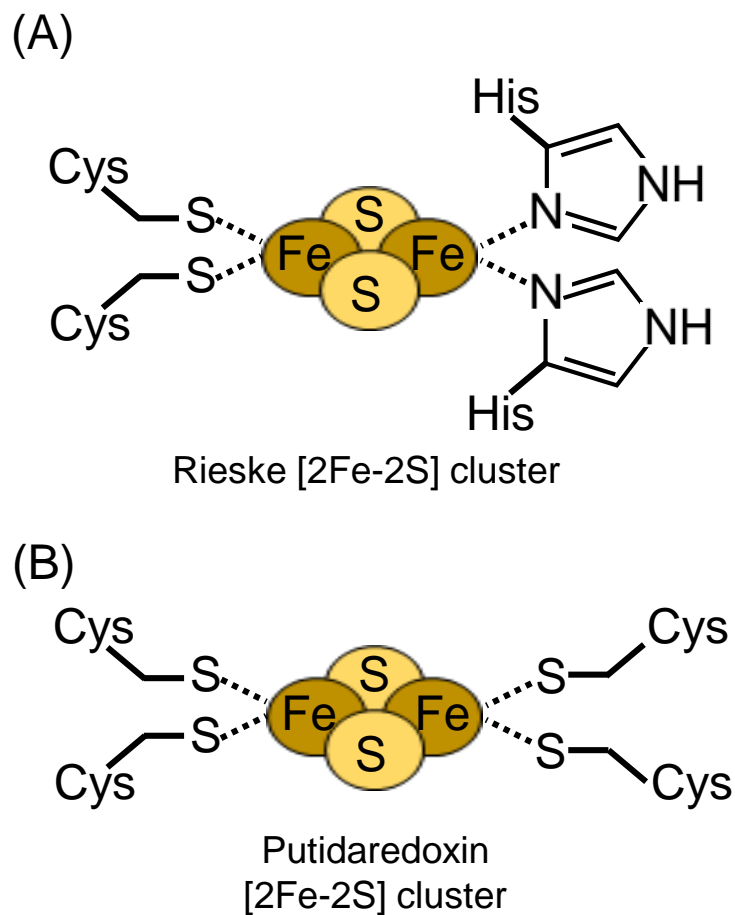


Fig. 1-2. The schematic figures of [2Fe-2S] clusters

The schematic figures of (A) Rieske [2Fe-2S] cluster and (B) putidaredoxin-type [2Fe-2S] cluster. The light brown balls show as the sulfur atoms and the heavy brown balls show as the iron atoms.

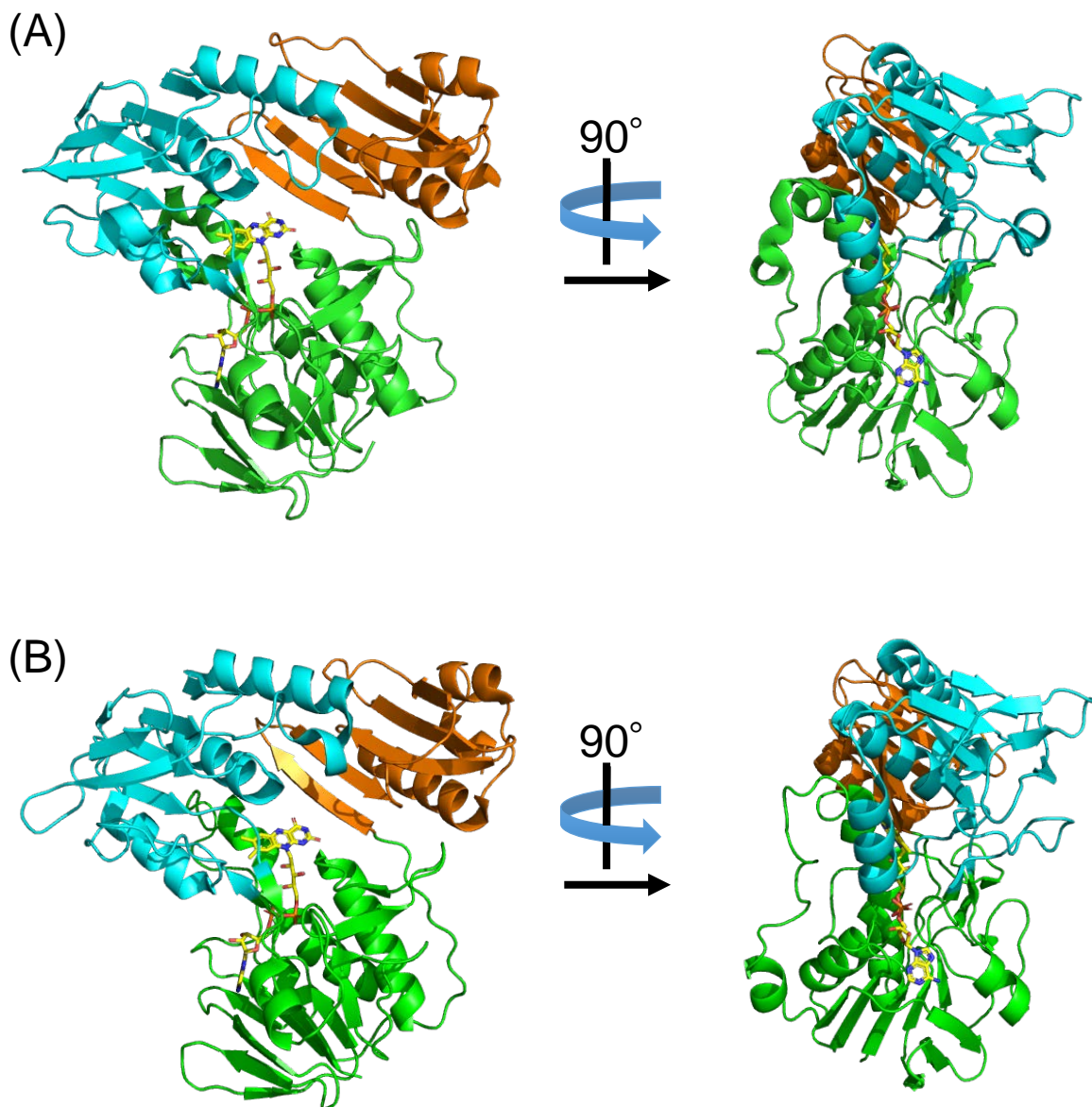


Fig. 1-3. Overall structures of Red of ROs

The crystal structure of Red with FAD of (A) biphenyl dioxygenase from *Acidovorax* sp. KKS102 [PDB ID: 2GQW; Senda *et al.*, 2007] and (B) toluene dioxygenase from *Pseudomonas putida* F1 [PDB ID: 3EF6; Friemann *et al.*, 2009] which are GR-type Reds. FAD-binding domain, NADH-binding domain and C-terminal domain are showed in green, cyans and orange. FAD is showed in sticks.

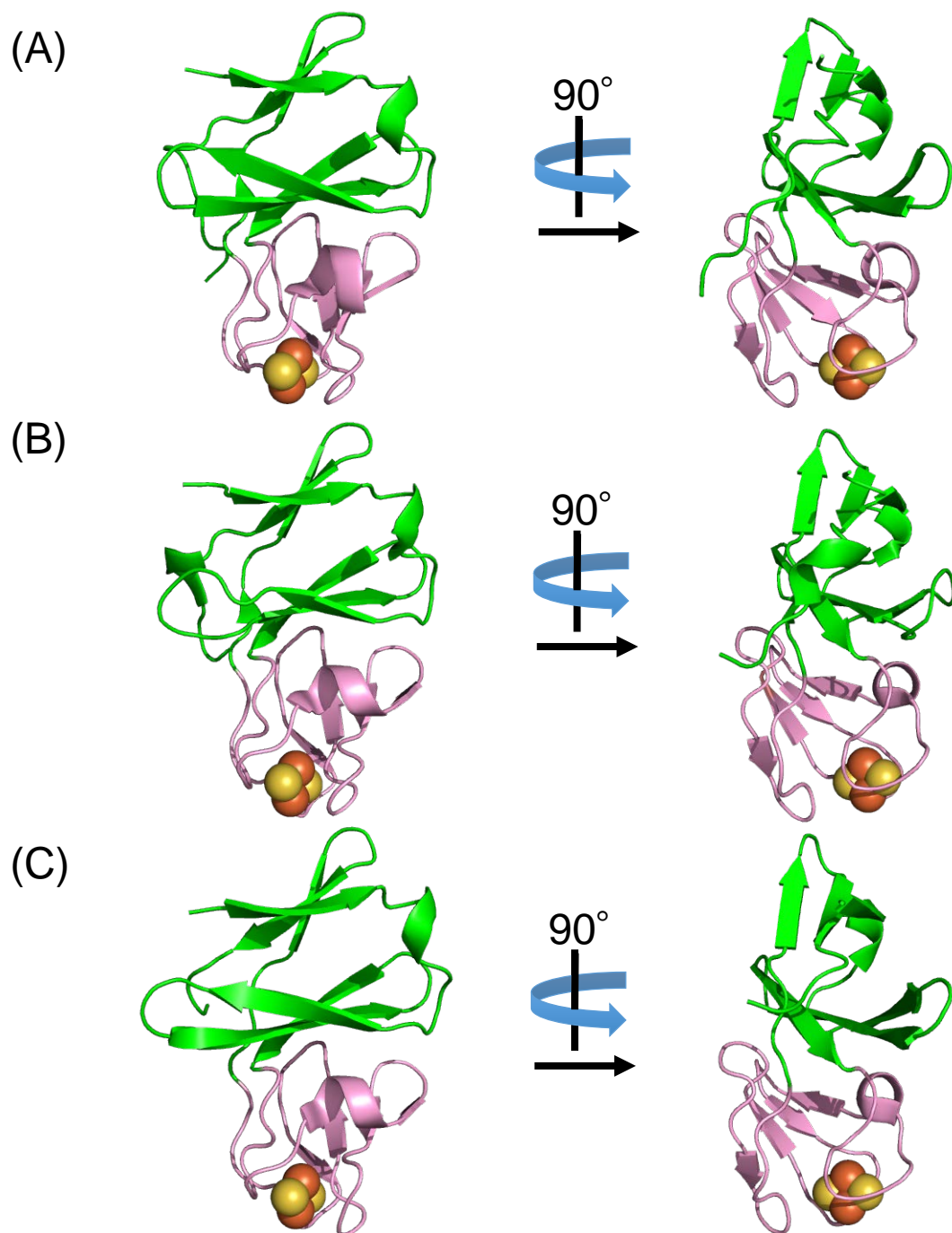


Fig. 1-4 Overall structures of Fd of ROs

The crystal structure of Fd of (A) biphenyl dioxygenase from *Acidovorax* sp. KKS102 [PDB ID: 2E4P; Senda *et al.*, 2007], (B) toluene dioxygenase from *P. putida* F1 [PDB: 3DQY; Friemann *et al.*, 2009] and (C) carbazole 1,9a-dioxygenase from *Pseudomonas resinovorans* CA10 [PDB: 1VCK; Nam *et al.*, 2005], which are Rieske-type Fd. Rieske binding domain and basal domain are showed with pink and green. The light brown balls show as the sulfur atoms and the heavy brown balls show as the iron atoms.

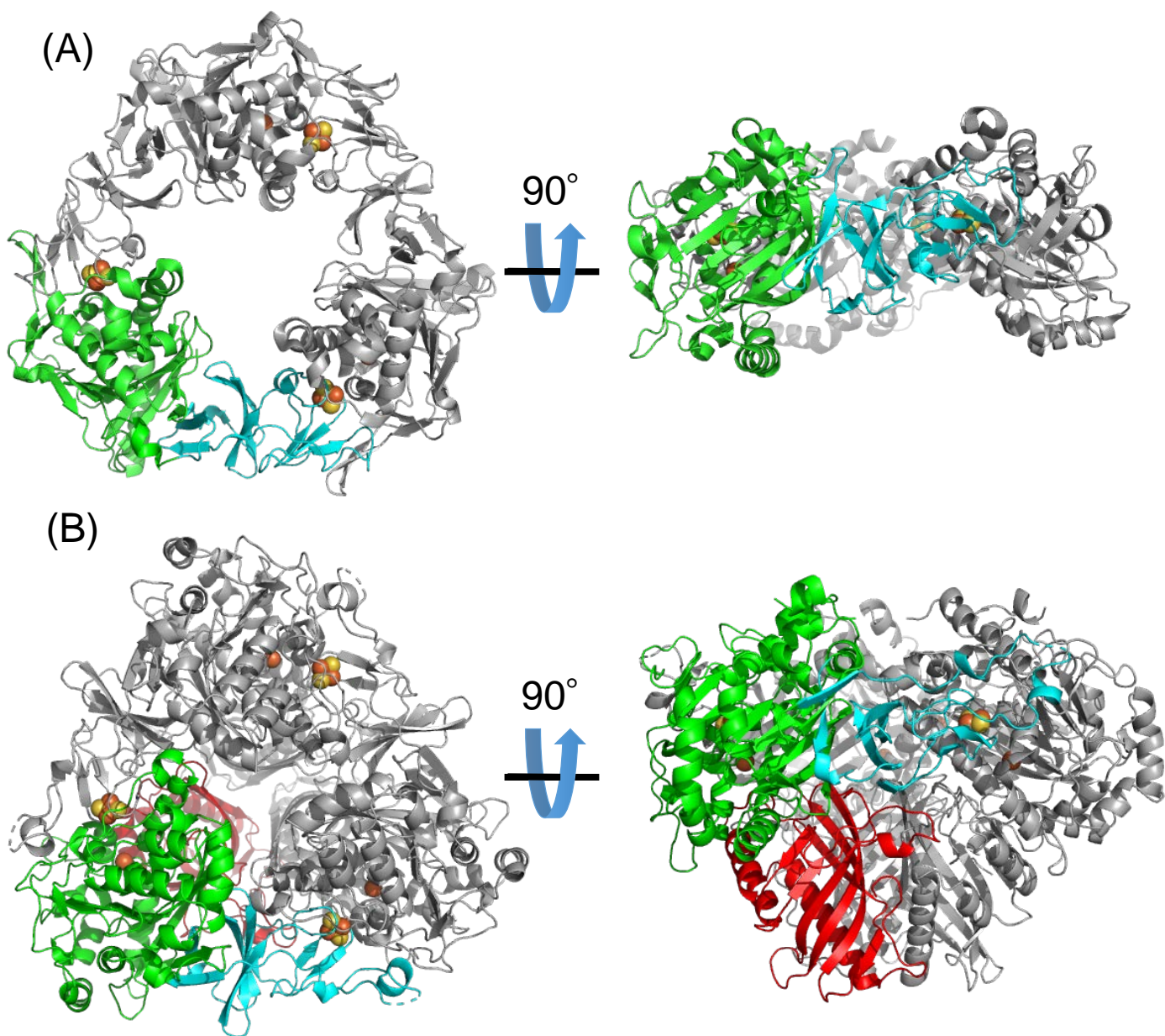


Fig. 1-5 Overall structures of terminal oxygenase of ROs

The crystal structure of α -subunit of (A) α_3 -type Oxy of CARDO from *Nocardioides aromaticivorans* IC177 [PDB: 3GCF; Inoue *et al.*, 2009] and (B) $\alpha_3\beta_3$ -type Oxy of CDO from *P. fluorescens* IP01 [PDB: 1WQL; Dong *et al.*, 2005]. Rieske cluster binding domain and catalytic domain are showed with cyan and green. The light brown balls show as the sulfur atoms and the heavy brown balls show as the iron atoms.

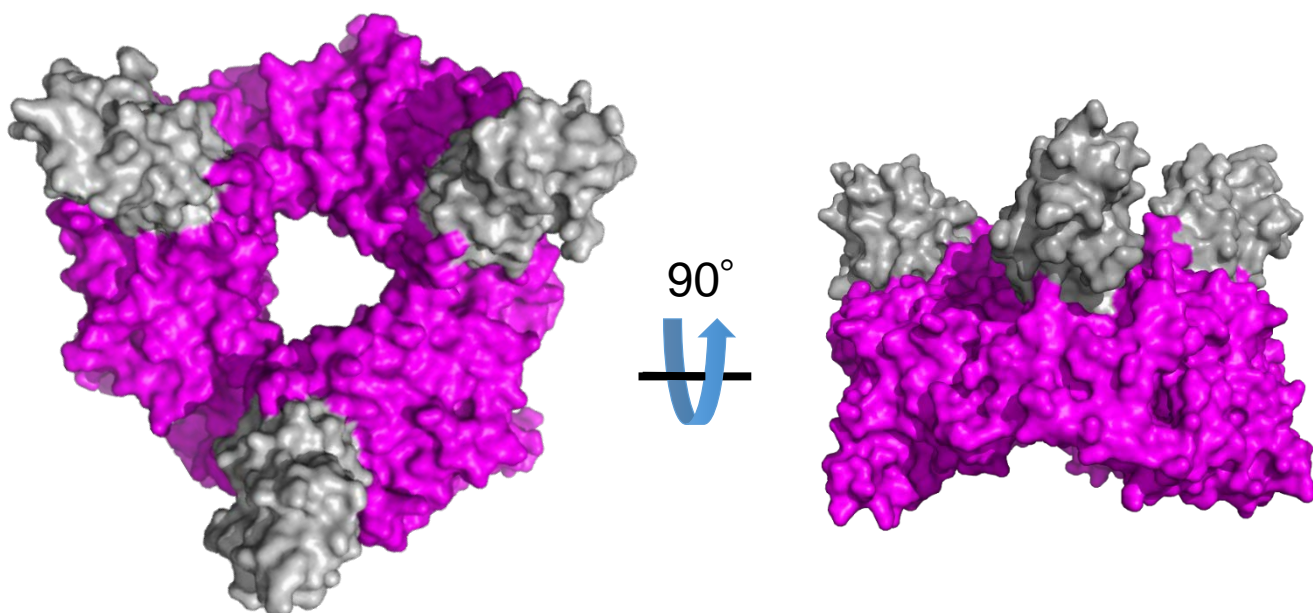


Fig. 1-6 Structure of CARDO F-O complex

The structure of CARDO F-O complex (PDB: 2DE5) [Ashikawa *et al.*, 2006]. CARDO-F and CARDO-O were showed in gray and magentas. CARDO-F bound at the interface of α -subunit.

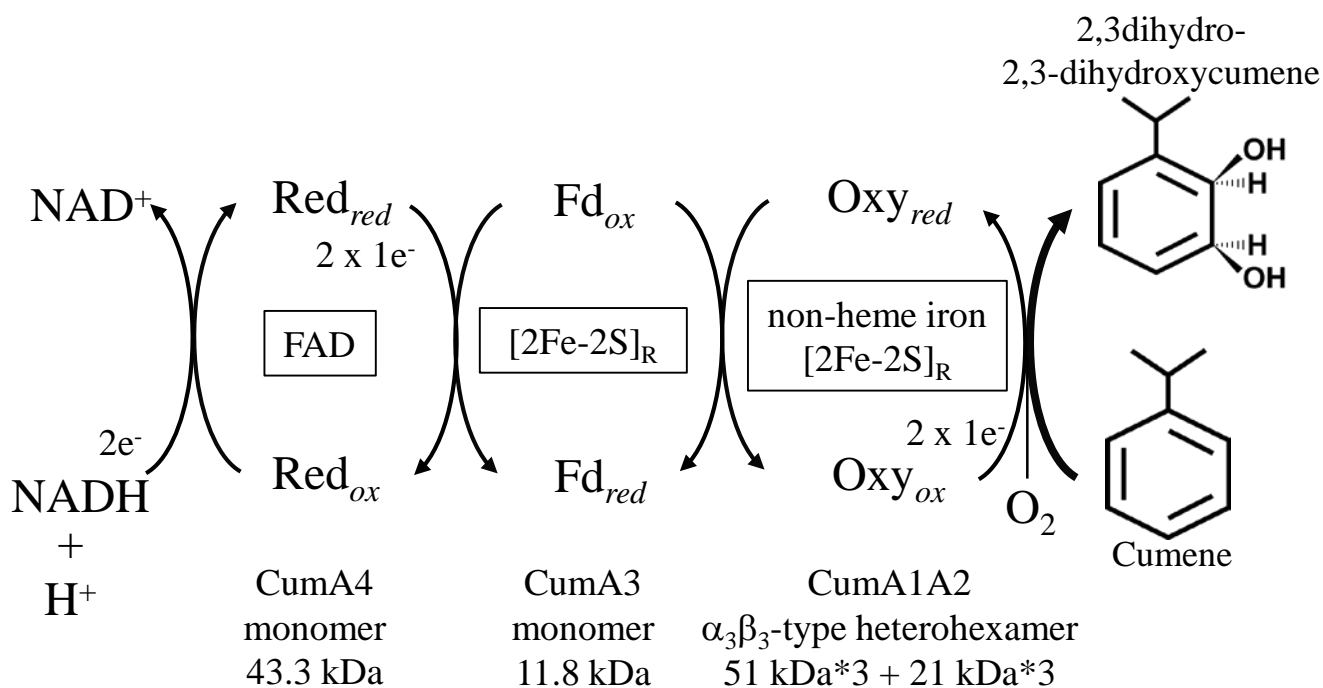
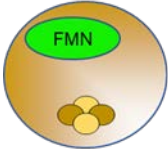

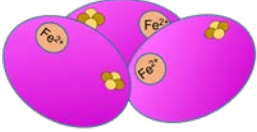
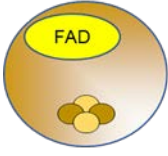
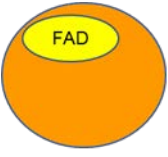

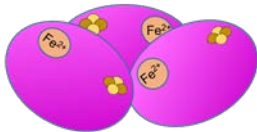
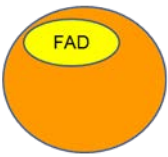

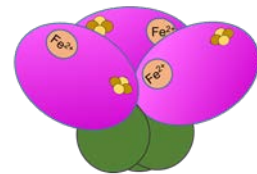
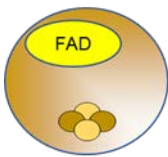

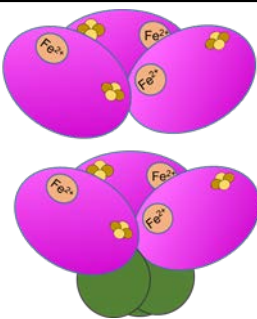
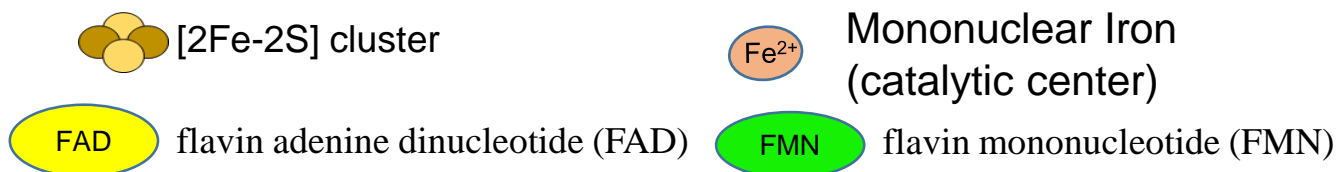


Fig. 1-7 Components of cumene dioxygenase

CDO incorporates oxygen atoms into cumene to form 2,3dihydro-2,3-dihydroxycumene by electron transfer [Aoki *et al.*, 1996]. Electrons are transferred following the arrows. The prosthetic group of CDO-R, CDO-F and CDO-O α are FAD, Rieske-type [2Fe-2S] cluster, and mononuclear iron and Rieske-type [2Fe-2S] cluster, respectively. Oxidized and reduced state are showed with subscripts ox and red. [2Fe-2S]_R means Rieske-type iron-sulfur cluster.

Table 1-1 Batie's classification system and examples.

Class		Red	Fd	Oxy	Examples
I	IA				Phthalate dioxygenase (<i>Burkholderia cepacia</i> DBO1) [Tarasev and Ballou, 2005]
	IB				2-oxoquinoline 8-monooxygenase (<i>Pseudomonas putida</i> 86) [Martins <i>et al.</i> , 2005]
II	IIA		 Putidaredoxin type		Carbazole 1,9a-dioxygenase (<i>Novosphingobium</i> sp. KA1) [Urata <i>et al.</i> , 2006]
	IIB		 Rieske type		
III			 Rieske type		Naphthalene 1,2-dioxygenase (<i>Pseudomonas</i> sp. NCIB9816-4) [Ensley and Haigler, 1990]
					Carbazole 1,9a-dioxygenase (<i>Janthinobacterium</i> sp. J3; <i>Pseudomonas resinovorans</i> CA10) [Sato <i>et al.</i> , 1997; Inoue <i>et al.</i> , 2004]



Chapter 2

Determination of interaction between ferredoxin and oxygenase by computational study and electron transfer efficiency analysis

2-1 General overview

As the state of Ch. 1, the interaction between Fd and $\alpha_3\beta_3$ Oxy was not determined by any experimental method so far.

To determine of CDO-F on the CDO-O, potential binding site was predicted. In the structure of Fd-Oxy complex of carbazole dioxygenase, the Fd bind at the interface of α -subunit. The binding site of Fd on the Oxy have two features, the hydrophobic groove and the charged amino acid around the groove. There are two similar docking sites for Fd on the CDO-O discovered by docking simulations. Alanine scanning and isothermal titration calorimetry measurement are performed to evaluate the critical residue(s) in the interaction between CDO-F and CDO-O.

「本章の内容は、学術雑誌論文として出版する計画があるため、公表できない。」

Chapter 3

Determination of interaction between ferredoxin and oxygenase by X-ray crystallography and cross linking

3-1 General overview

In this chapter, different approaches, X-ray crystallography and chemical and photo cross linking, were performed to determine the mechanism of electron transfer between CDO-F and CDO-O. WT CDO-F and 3 different CDO-Os were mixed for crystallization, respectively. Multiple crystals were obtained after optimization of crystallization conditions and X-ray diffraction data were collected. However, there was not CDO-F in all electron density maps after structure refinement. Chemical cross-linking was performed with the mixture of WT CDO-F, WT CDO-O and chemical cross linker, sulfo-SMPB. After liquid chromatography coupled with quadrupole time-of-flight mass spectrometry (LC/Q-TOF-MS) analyses, no conclusion can be made with the final mapping results. Photo cross linking was performed with genetically encoded photoreactive amino acid on 6 different residues of CDO-F, Q19X, S49X, L65X, A80X, P81X and P85X, and WT CDO-O. CDO-F Q19X was cross linked with CDO-O successfully. The reproducibility will be confirmed and will be analyzed by LC/Q-TOF-MS.

「本章の内容は、学術雑誌論文として出版する計画があるため、公表できない。」

Chapter 4

Conclusion and Future Prospects

The current study determined that CDO-F bound at the interface of α - and β -subunit of CDO-O. The residues, α_1 K117 and β_1 R65, played critical roles in the interaction. Comparison at the sequences of the binding regions of CDO-F and CDO-O with those of other Rieske-type Fds and $\alpha_3\beta_3$ -type Oxy in class IIB and III ROs indicates that the positions of negative charged residues of Rieske-type Fds and the positions of positive charged residues of $\alpha_3\beta_3$ -type Oxy are virtually conserved in all Rieske-type Fds and $\alpha_3\beta_3$ -type Oxy. The results indicate that the same binding mode may not only occur between CDO-F and CDO-O, but also occurs in all Rieske-type Fd and $\alpha_3\beta_3$ -type Oxy. Furthermore, Rieske-type Fd and $\alpha_3\beta_3$ -type Oxy may share common manner with those in CARDO containing α_3 -type oxygenase, although binding site is different. This may be an example of convergent evolution of electron transport mechanisms.

The current study also reveals that the function of β -subunit of $\alpha_3\beta_3$ -type Oxy is not only structural but also stabilize the interaction with Rieske-type Fd. Without β -subunit, the electrons cannot transfer between Fd and Oxy efficiently. It can be explained that the previous reports demonstrating that the substrate specificity or activity was disrupted after replacing or removing β -subunit of $\alpha_3\beta_3$ -type Oxy were not because the β -subunit had function in substrate specificity or activity but because the β -subunit has function in structural and stabilization of the interaction with Rieske-type Fd.

The binding site will be determined by photo cross linking. Until now, the novel bands were detected in after the reaction with mixture of CDO-O and photoreactive CDO-F. The reproducibility of photo cross linking results will be confirmed and followed by LC/MS analyses.

To determine the mechanism of interaction in atomic level, structural studies of complex are necessary to provide more detail with interaction between Rieske-type Fd and $\alpha_3\beta_3$ -type Oxy. Besides X-ray diffraction, other methods, cryo-electron microscopy or X-ray free-electron laser, may be better method to determine the structure of Fd-Oxy complex.

Supplement figures for protein purification

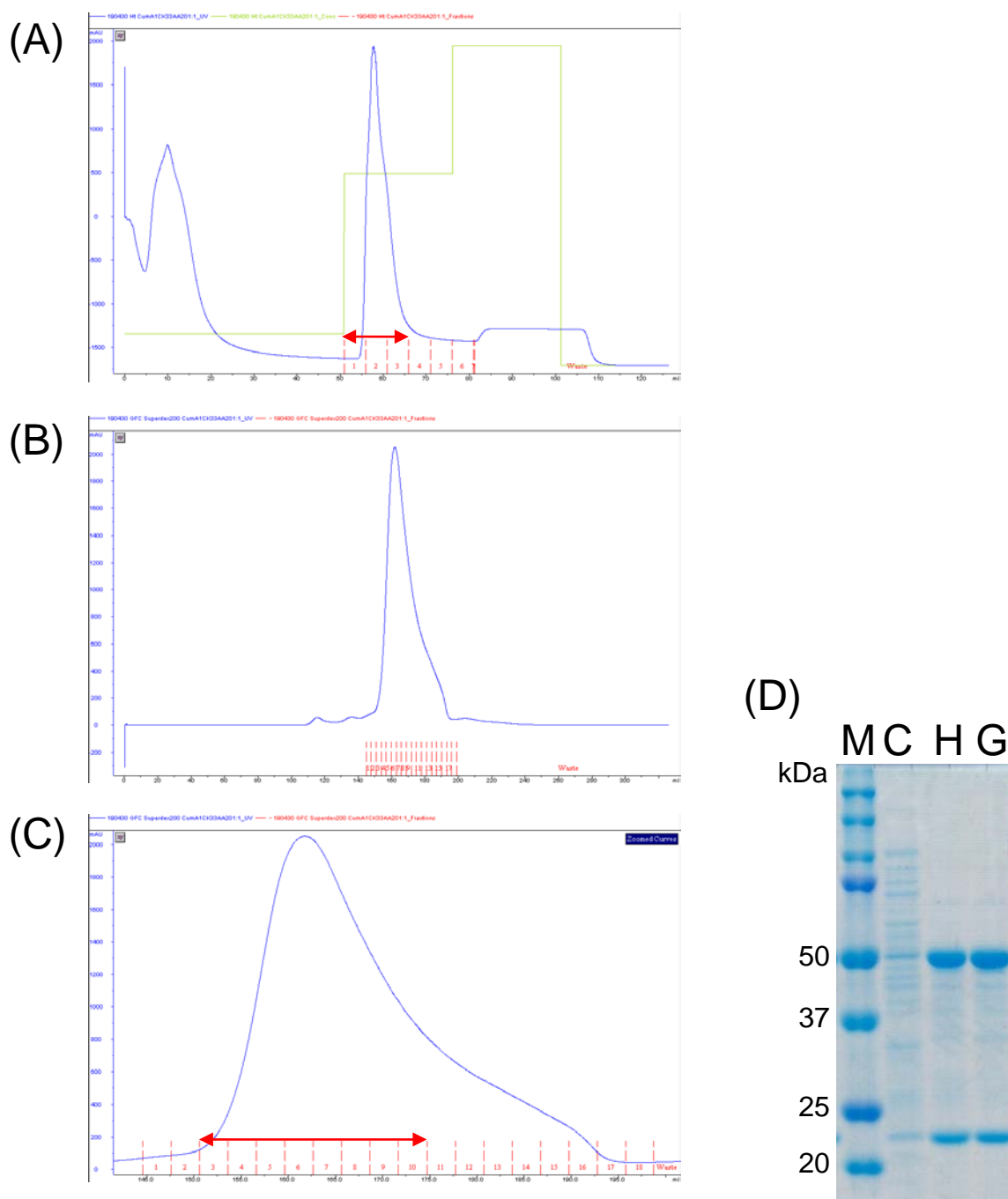


Fig. S1 Affinity purification and gel chromatography of CDO-O α K33A

(A) Elution profile of metal-chelation chromatography. Blue line indicates absorbance at 280 nm (mAU) and green line indicates imidazole concentration. (B)(C) Gel chromatography of the affinity purified CDO-O α K33A. (D) 10% Glycine SDS-PAGE of CDO-O α K33A. C: crude extract, H: purified by metal-chelation chromatography, G: purified by gel chromatography d, M: Precision Plus Protein™ Dual Color Standards. The red arrow indicated the CDO-O α K33A containing fractions.

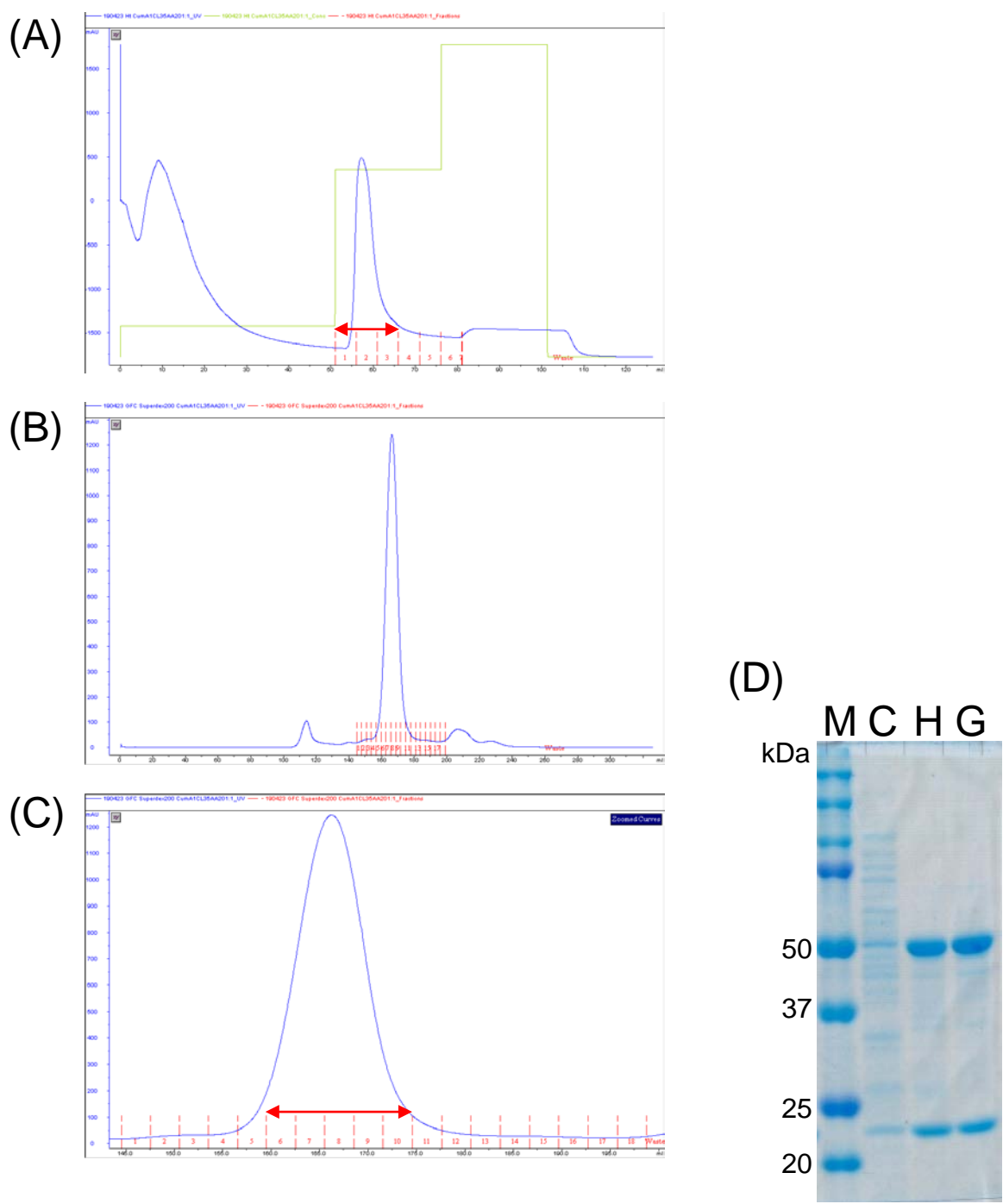


Fig. S2 Affinity purification and gel chromatography of CDO-O α L35A

(A) Elution profile of metal-chelation chromatography. Blue line indicates absorbance at 280 nm (mAU) and green line indicates imidazole concentration. (B)(C) Gel chromatography of the affinity purified CDO-O α L35A. (D) 10% Glycine SDS-PAGE of CDO-O α L35A. C: crude extract, H: purified by metal-chelation chromatography, G: purified by gel chromatography, M: Precision Plus Protein™ Dual Color Standards. The red arrow indicated the CDO-O α L35A containing fractions.

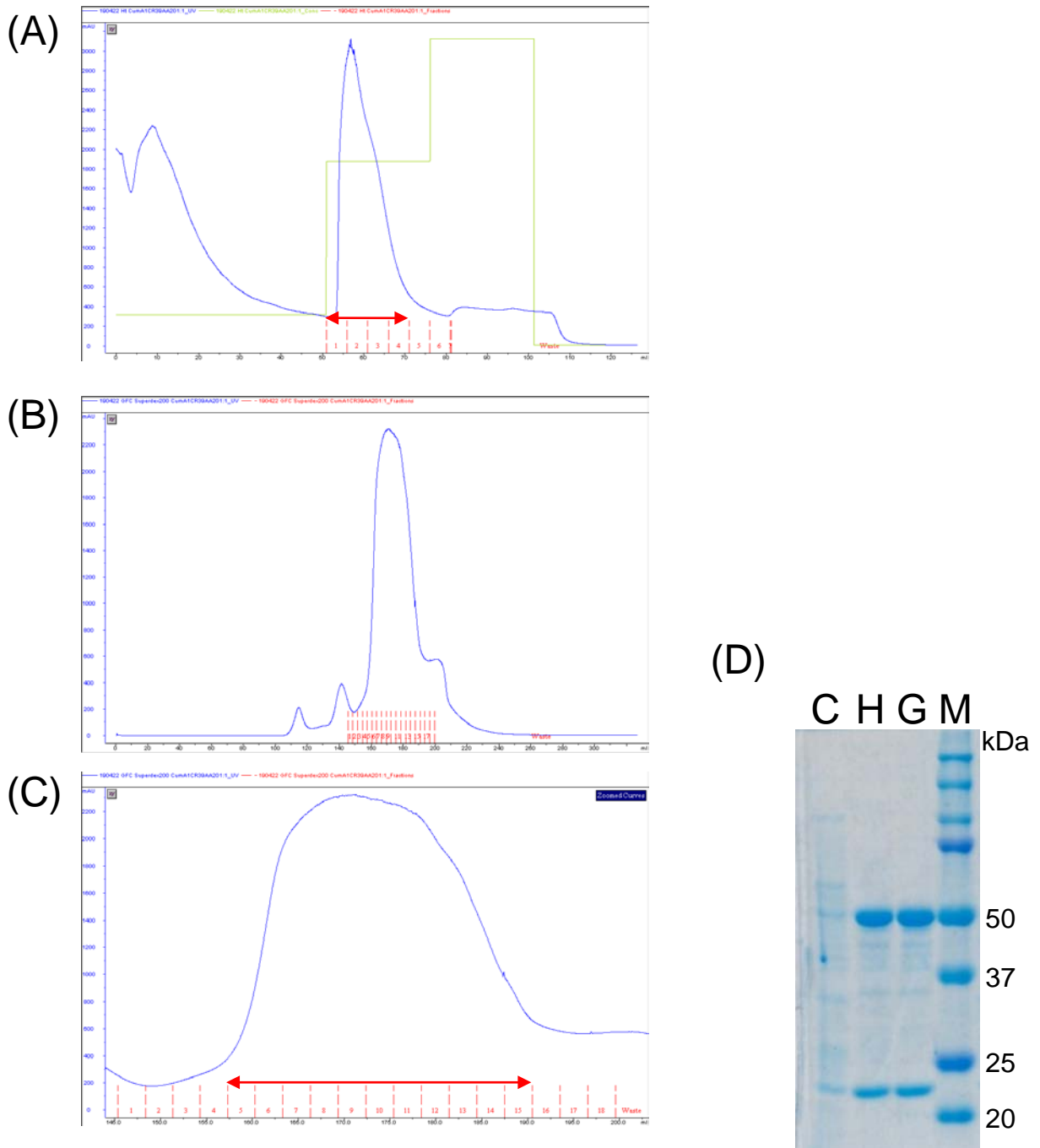


Fig. S3 Affinity purification and gel chromatography of CDO-O α R39A

(A) Elution profile of metal-chelation chromatography. Blue line indicates absorbance at 280 nm (mAU) and green line indicates imidazole concentration. (B)(C) Gel chromatography of the affinity purified CDO-O α R39A. (D) 10% Glycine SDS-PAGE of CDO-O α R39A. C: crude extract, H: purified by metal-chelation chromatography, G: purified by gel chromatography, M: Precision Plus Protein™ Dual Color Standards. The red arrow indicated the CDO-O α R39A containing fractions.

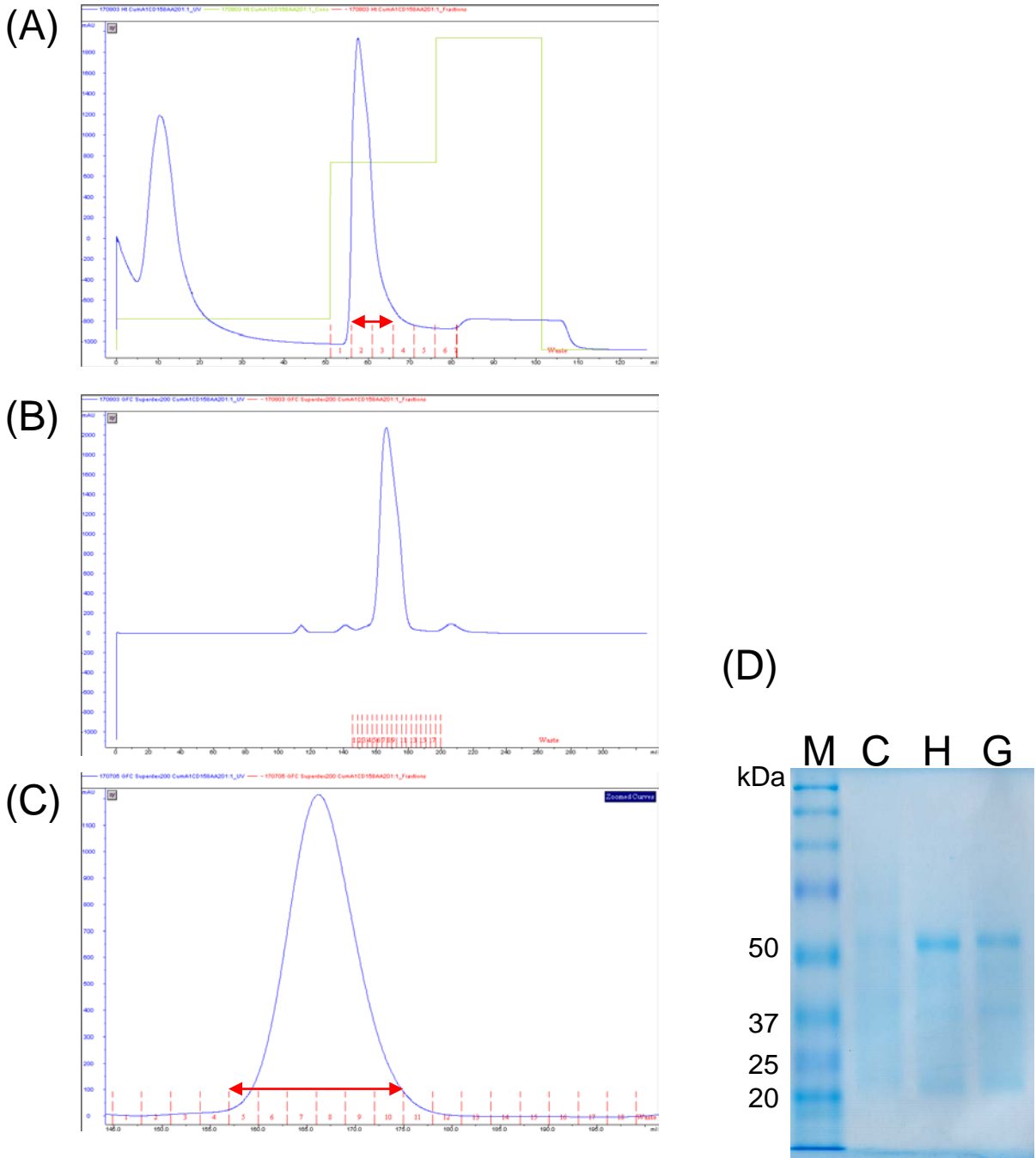


Fig. S4 Affinity purification and gel chromatography of CDO-O α D158A

(A) Elution profile of metal-chelation chromatography. Blue line indicates absorbance at 280 nm (mAU) and green line indicates imidazole concentration. (B)(C) Gel chromatography of the affinity purified CDO-O α D158A. (D) 10% Glycine SDS-PAGE of CDO-O α D158A. C: crude extract, H: purified by metal-chelation chromatography, G: purified by gel chromatography, M: Precision Plus Protein™ Dual Color Standards. The red arrow indicated the CDO-O α D158A containing fractions.

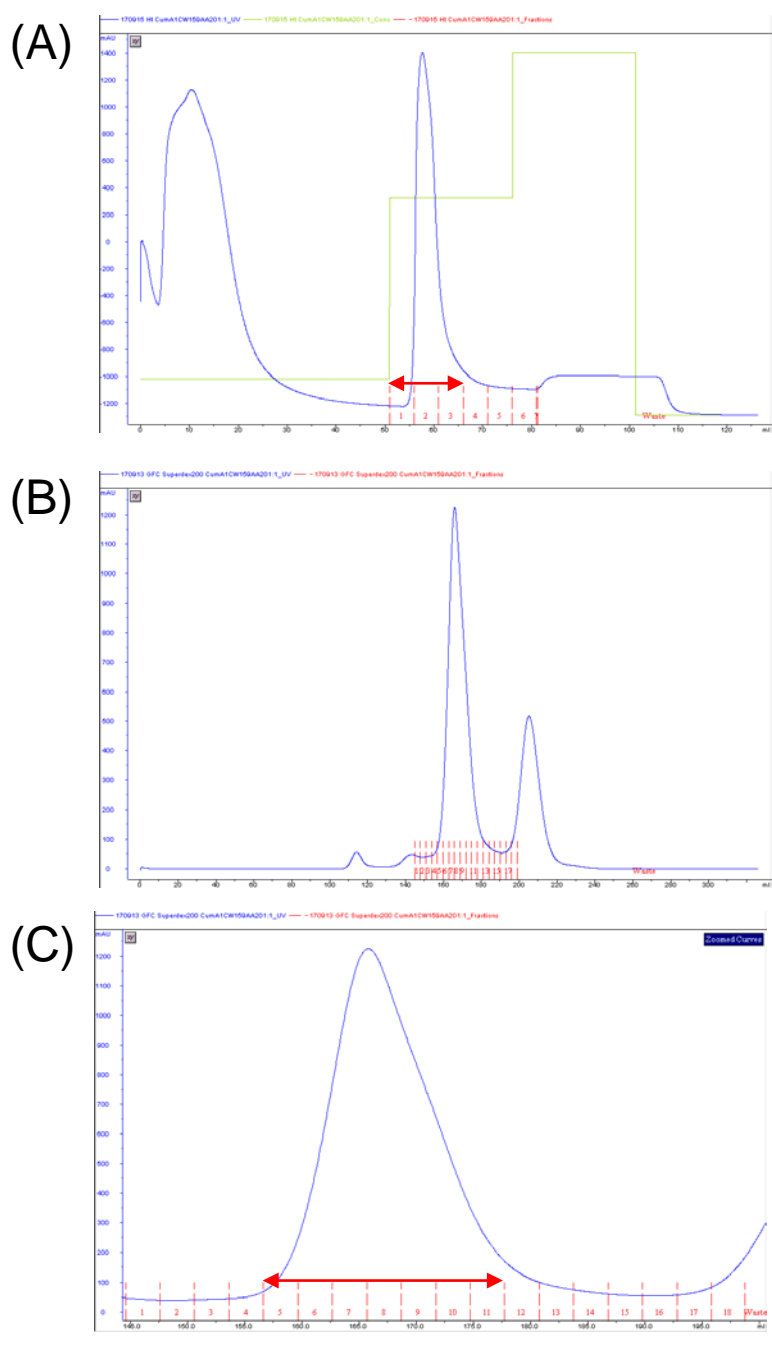


Fig. S5 Affinity purification and gel chromatography of CDO-O α W159A

(A) Elution profile of metal-chelation chromatography. Blue line indicates absorbance at 280 nm (mAU) and green line indicates imidazole concentration. (B)(C) Gel chromatography of the affinity purified CDO-O α W159A. (D) 10% Glycine SDS-PAGE of CDO-O α W159A. C: crude extract, H: purified by metal-chelation chromatography, G: purified by gel chromatography, M: SeeBlue™ Plus2 Pre-stained Protein Standard. The red arrow indicated the CDO-O α W159A containing fractions.

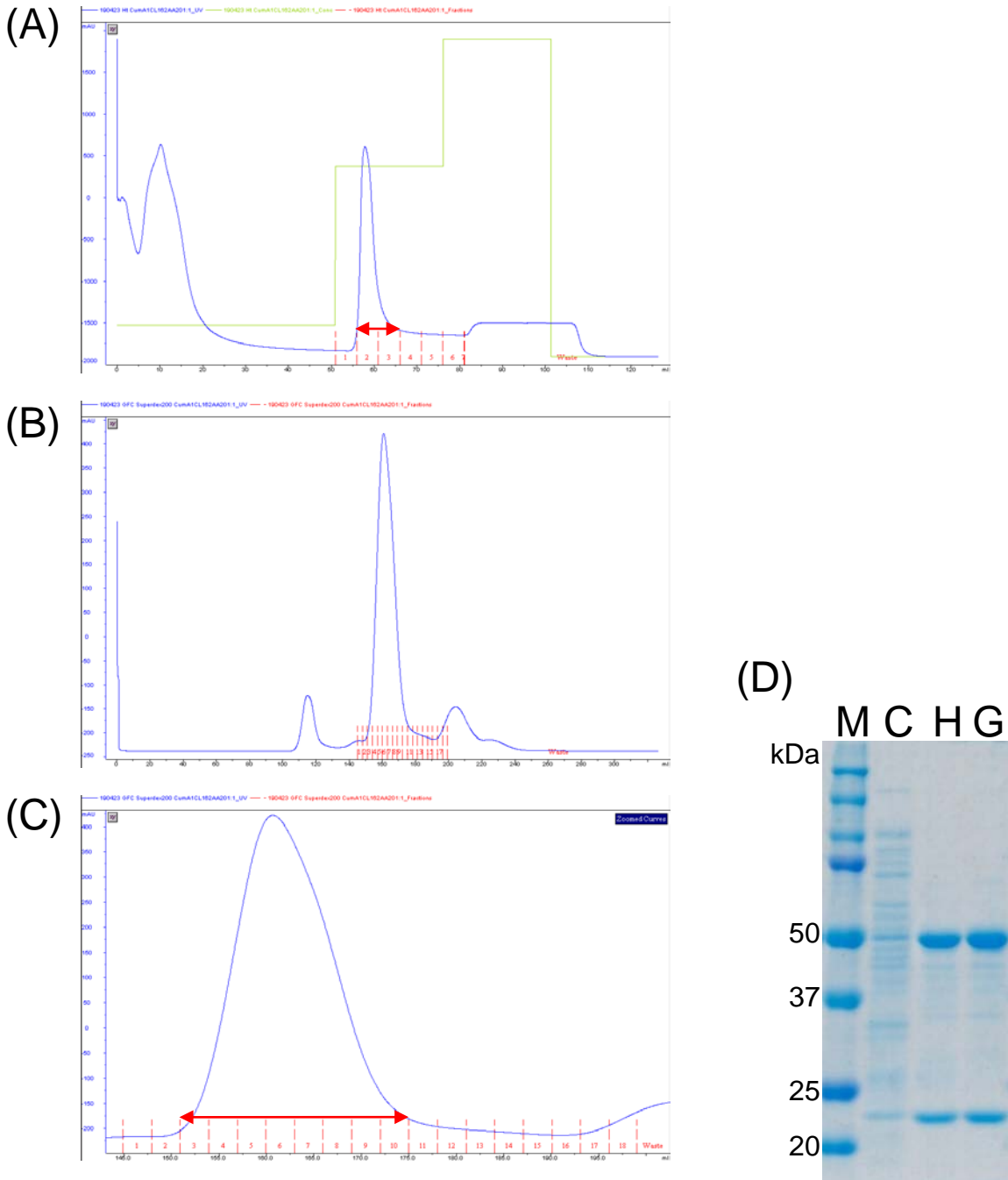


Fig. S6 Affinity purification and gel chromatography of CDO-O α L162A

(A) Elution profile of metal-chelation chromatography. Blue line indicates absorbance at 280 nm (mAU) and green line indicates imidazole concentration. (B)(C) Gel chromatography of the affinity purified CDO-O α L162A. (D) 10% Glycine SDS-PAGE of CDO-O α L162A. C: crude extract, H: purified by metal-chelation chromatography, G: purified by gel chromatography, M: Precision Plus Protein™ Dual Color Standards. The red arrow indicated the CDO-O α L162A containing fractions.

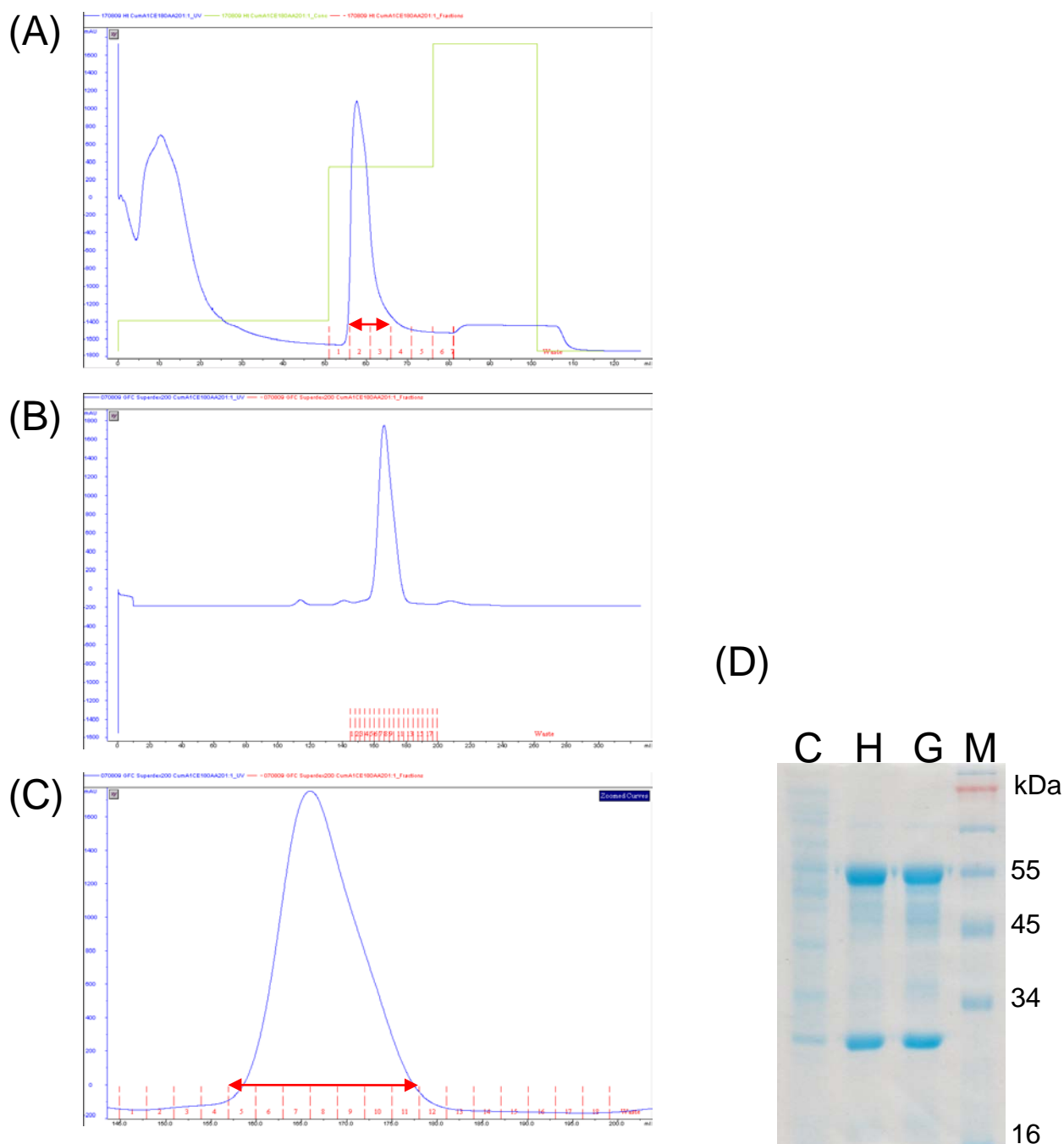


Fig. S7 Affinity purification and gel chromatography of CDO-O α E180A

(A) Elution profile of metal-chelation chromatography. Blue line indicates absorbance at 280 nm (mAU) and green line indicates imidazole concentration. (B)(C) Gel chromatography of the affinity purified CDO-O α E180A. (D) 10% Glycine SDS-PAGE of CDO-O α E180A. C: crude extract, H: purified by metal-chelation chromatography, G: purified by gel chromatography, M: SeeBlue™ Plus2 Pre-stained Protein Standard. The red arrow indicated the CDO-O α E180A containing fractions.

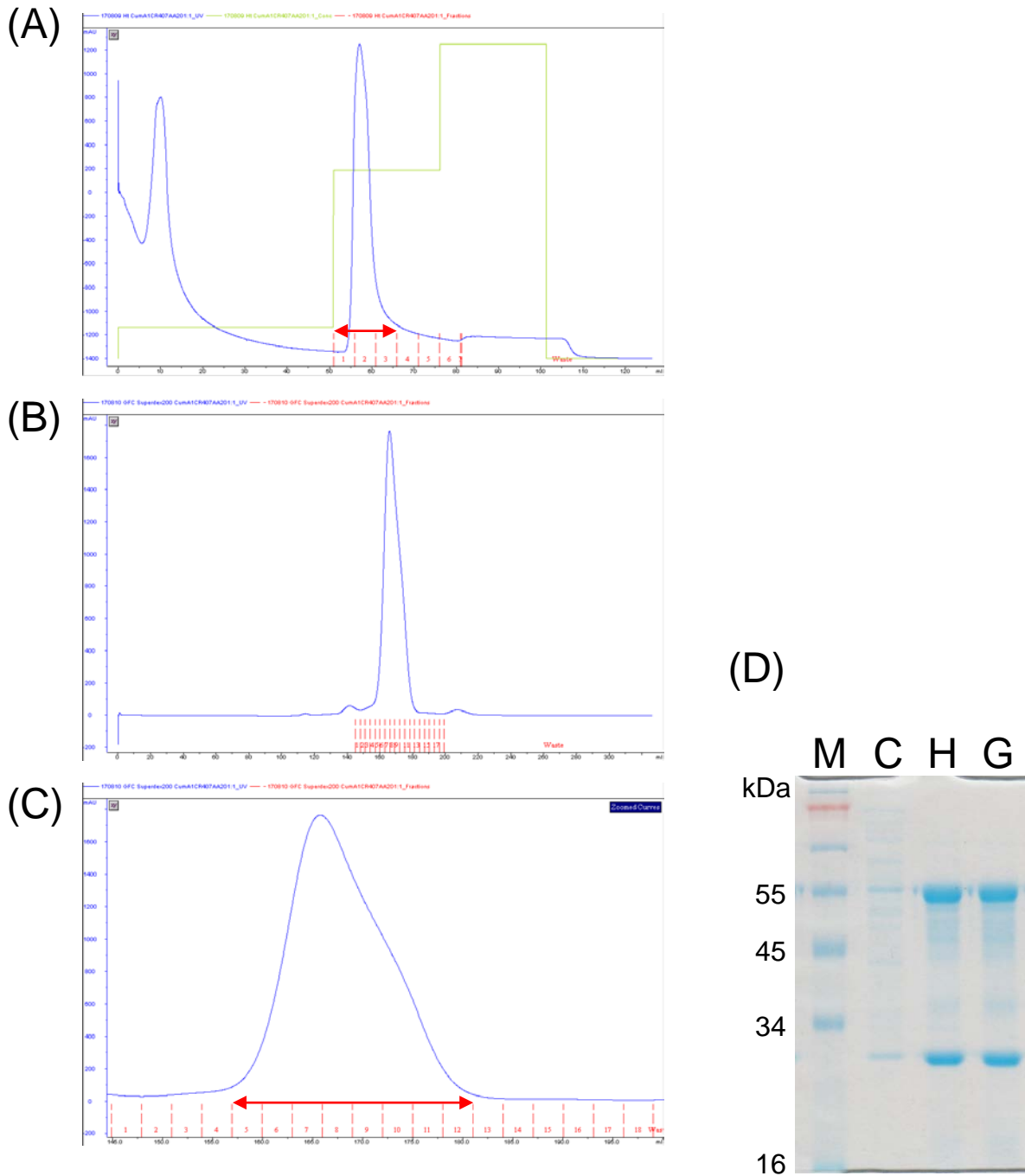


Fig. S8 Affinity purification and gel chromatography of CDO-O α R407A

(A) Elution profile of metal-chelation chromatography. Blue line indicates absorbance at 280 nm (mAU) and green line indicates imidazole concentration. (B)(C) Gel chromatography of the affinity purified CDO-O α R407A. (D) 10% Glycine SDS-PAGE of CDO-O α R407A. C: crude extract, H: purified by metal-chelation chromatography, G: purified by gel chromatography, M: SeeBlue™ Plus2 Pre-stained Protein Standard. The red arrow indicated the CDO-O α R407A containing fractions.

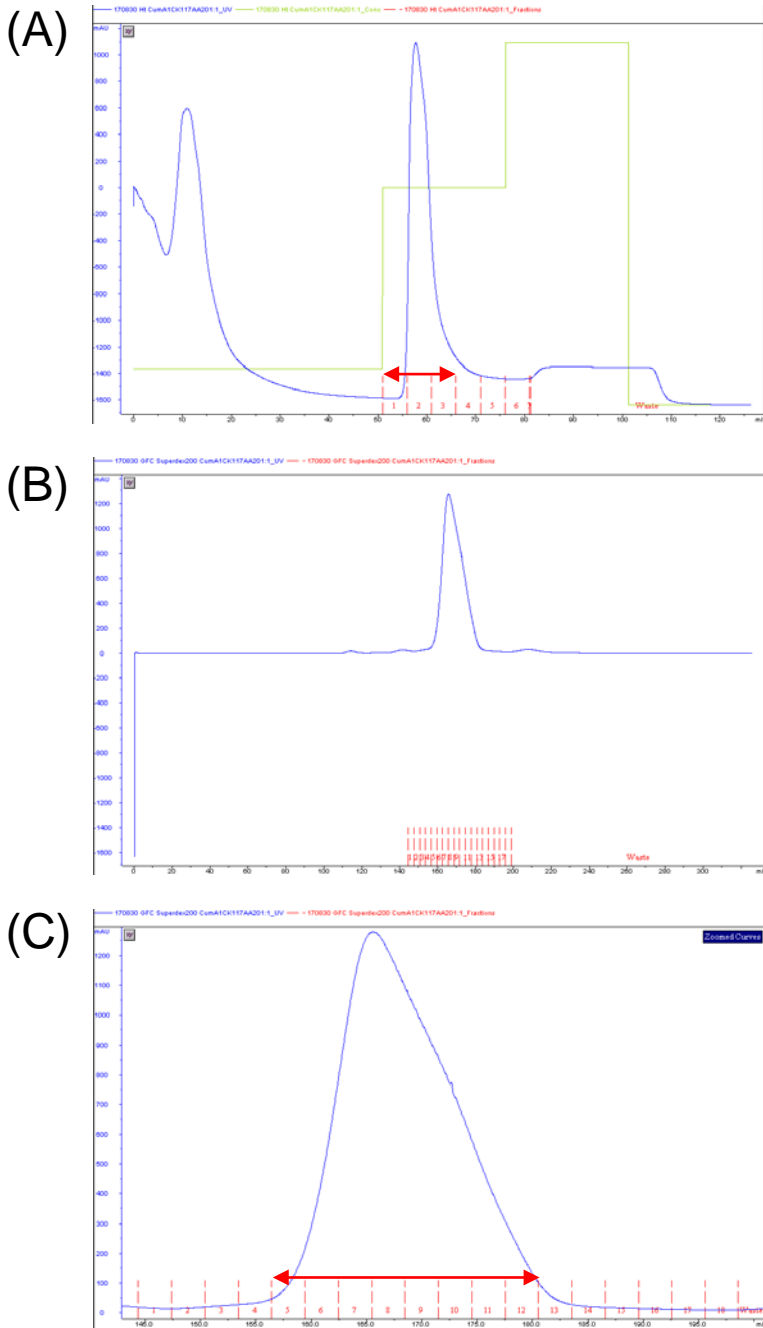


Fig. S9 Affinity purification and gel chromatography of CDO-OαK117A

(A) Elution profile of metal-chelation chromatography. Blue line indicates absorbance at 280 nm (mAU) and green line indicates imidazole concentration. (B)(C) Gel chromatography of the affinity purified CDO-OαK117A. (D) 10% Glycine SDS-PAGE of CDO-OαK117A. C: crude extract, H: purified by metal-chelation chromatography, G: purified by gel chromatography, M: Precision Plus Protein™ Dual Color Standards. The red arrow indicated the CDO-OαK117A containing fractions.

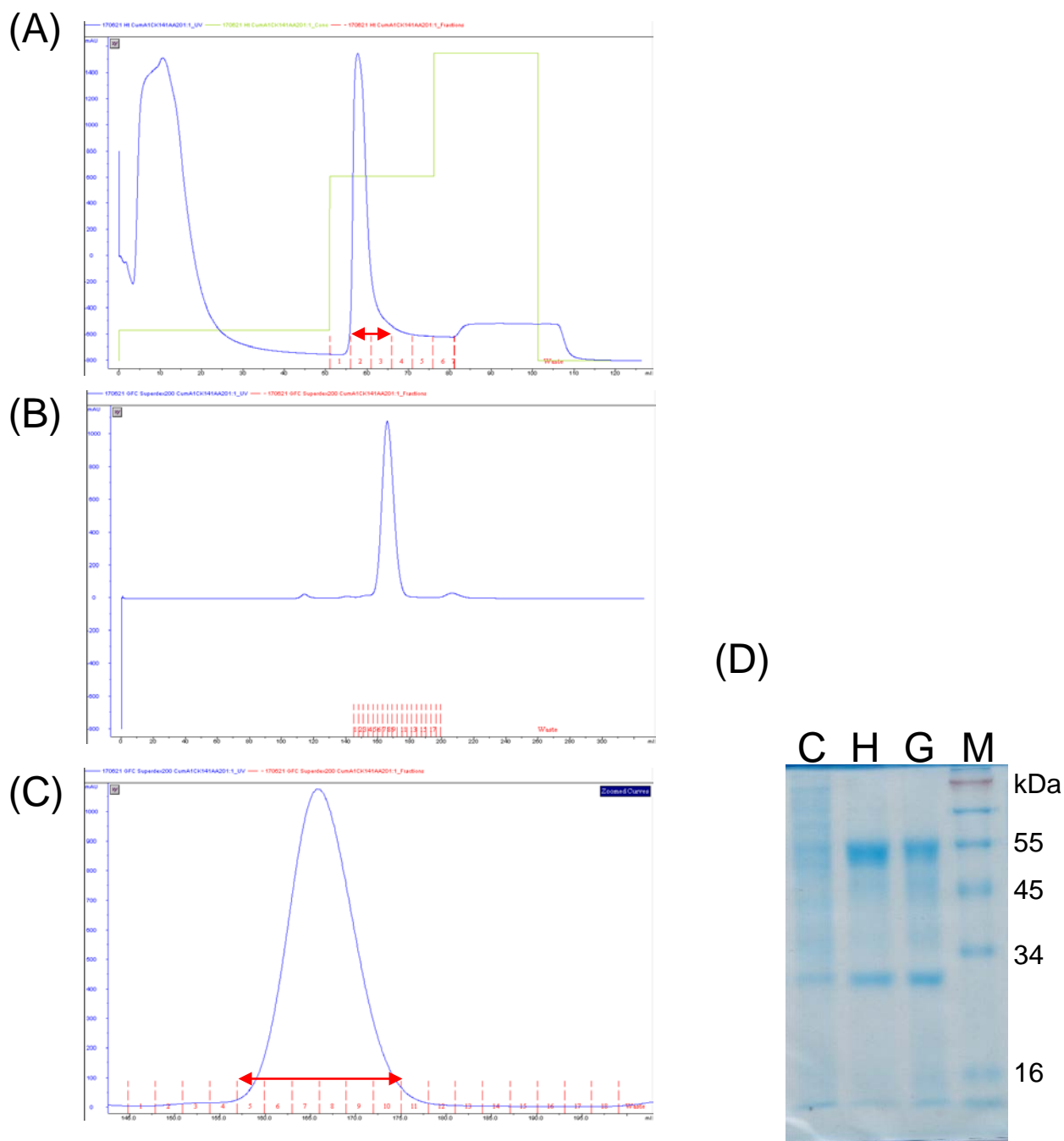


Fig. S10 Affinity purification and gel chromatography of CDO-O α K141A

(A) Elution profile of metal-chelation chromatography. Blue line indicates absorbance at 280 nm (mAU) and green line indicates imidazole concentration. (B)(C) Gel chromatography of the affinity purified CDO-O α K141A. (D) 10% Glycine SDS-PAGE of CDO-O α K141A. C: crude extract, H: purified by metal-chelation chromatography, G: purified by gel chromatography, M: SeeBlue™ Plus2 Pre-stained Protein Standard. The red arrow indicated the CDO-O α K141A containing fractions.

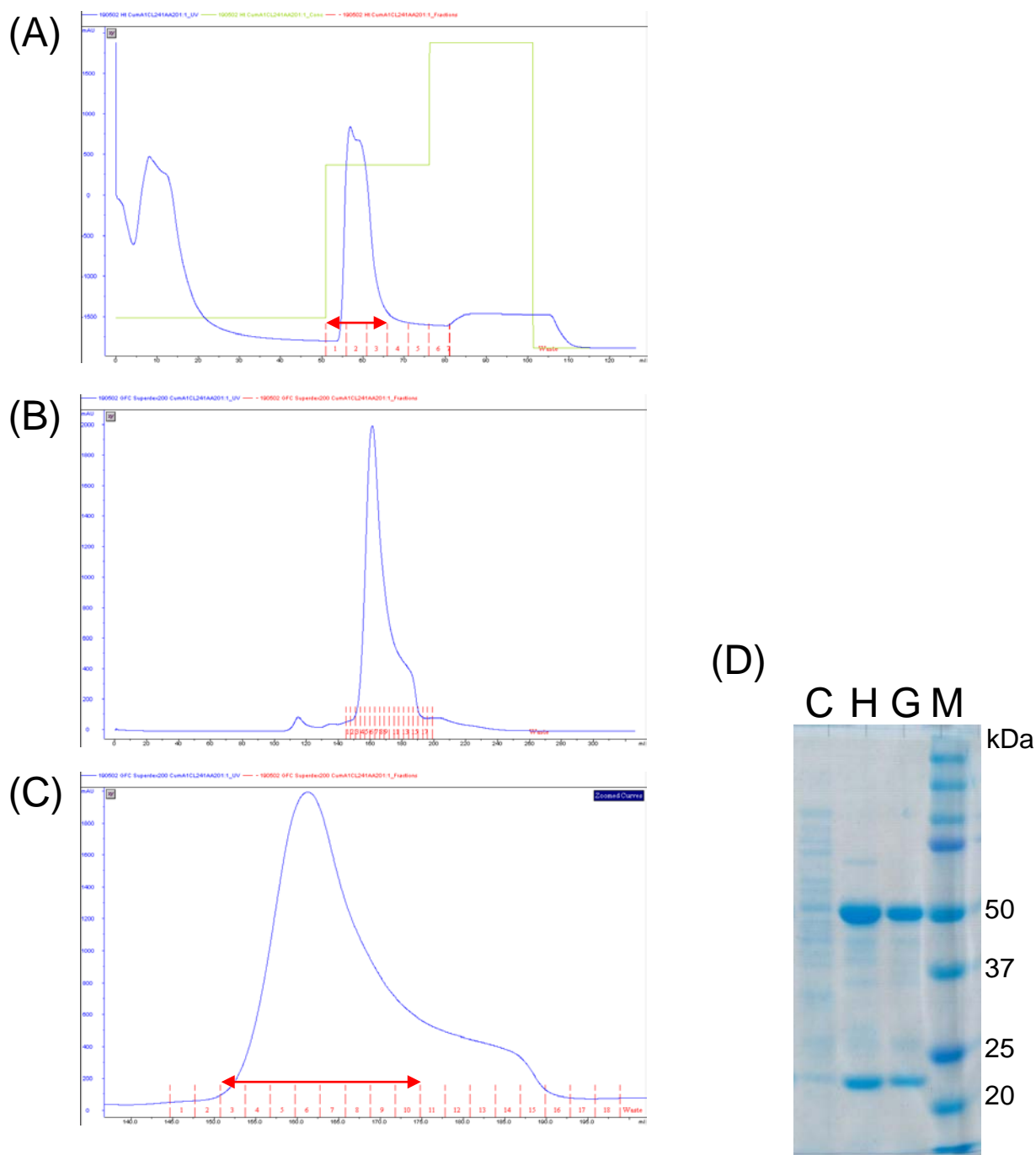


Fig. S11 Affinity purification and gel chromatography of CDO-O α L241A

(A) Elution profile of metal-chelation chromatography. Blue line indicates absorbance at 280 nm (mAU) and green line indicates imidazole concentration. (B)(C) Gel chromatography of the affinity purified CDO-O α L241A. (D) 10% Glycine SDS-PAGE of CDO-O α L241A. C: crude extract, H: purified by metal-chelation chromatography, G: purified by gel chromatography, M: Precision Plus Protein™ Dual Color Standards. The red arrow indicated the CDO-O α L241A containing fractions.

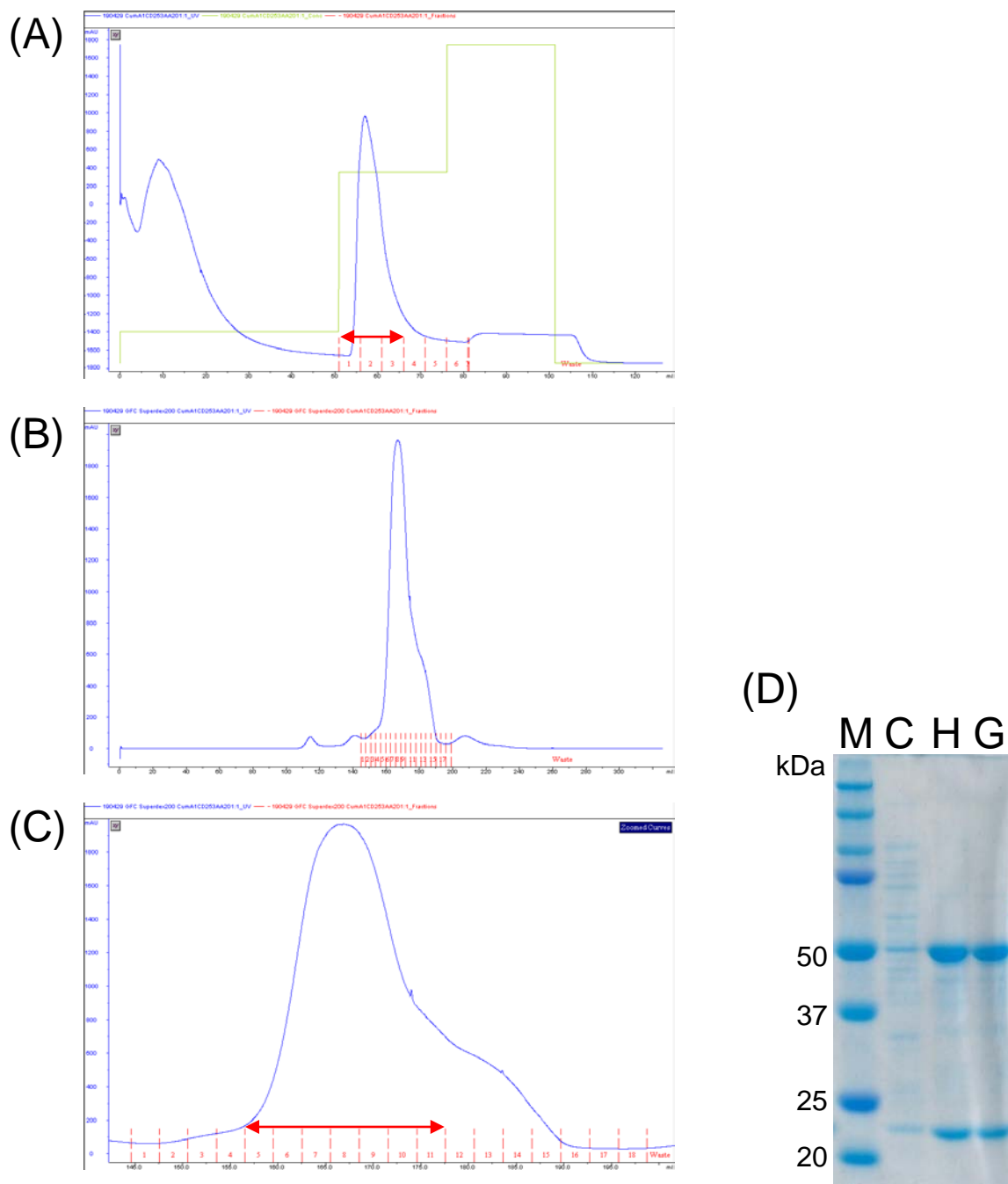


Fig. S12 Affinity purification and gel chromatography of CDO-O α D253A

(A) Elution profile of metal-chelation chromatography. Blue line indicates absorbance at 280 nm (mAU) and green line indicates imidazole concentration. (B)(C) Gel chromatography of the affinity purified CDO-O α D253A. (D) 10% Glycine SDS-PAGE of CDO-O α D253A. C: crude extract, H: purified by metal-chelation chromatography, G: purified by gel chromatography, M: Precision Plus Protein™ Dual Color Standards. The red arrow indicated the CDO-O α D253A containing fractions.

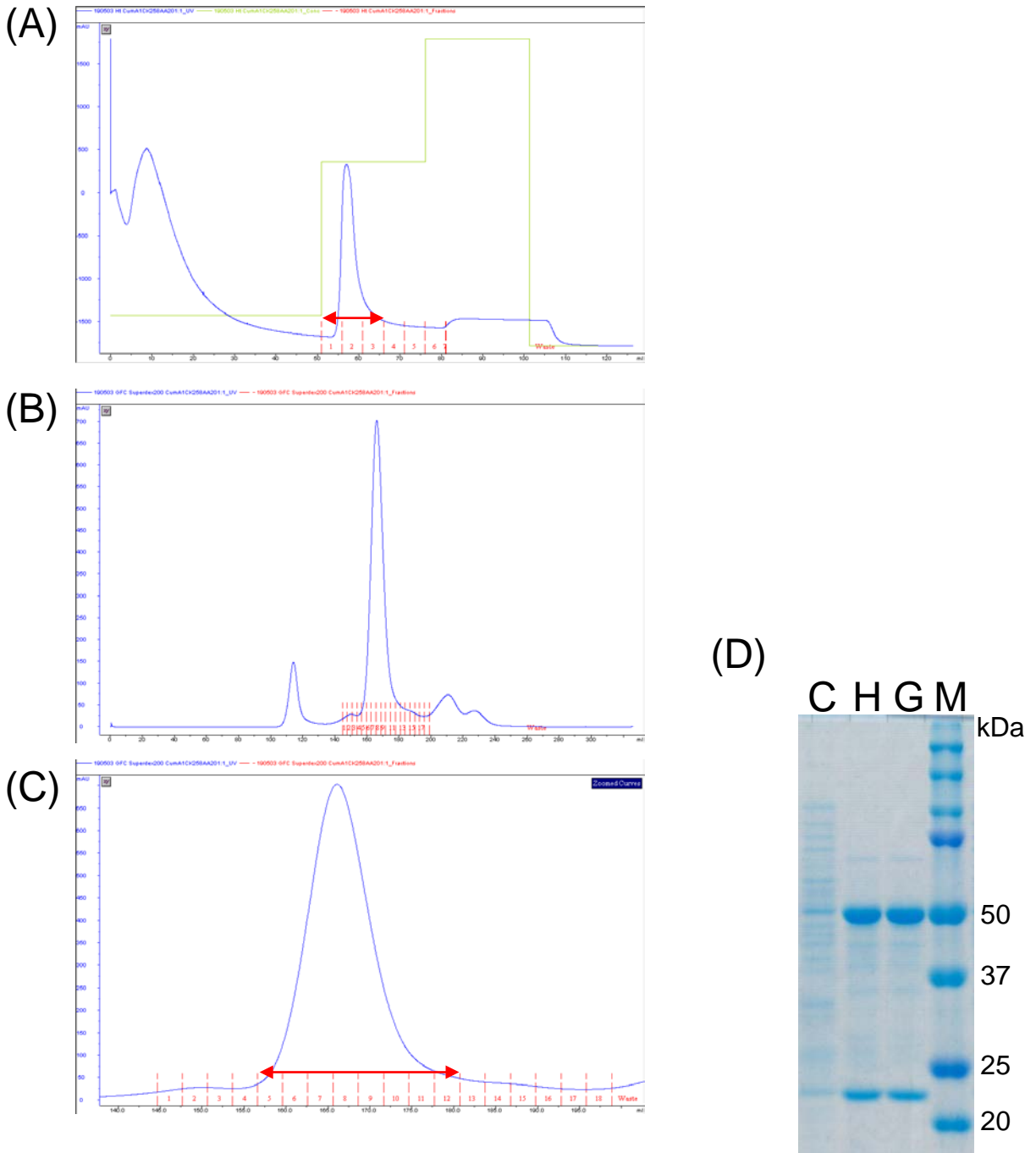


Fig. S13 Affinity purification and gel chromatography of CDO-O α K258A

(A) Elution profile of metal-chelation chromatography. Blue line indicates absorbance at 280 nm (mAU) and green line indicates imidazole concentration. (B)(C) Gel chromatography of the affinity purified CDO-O α K258A. (D) 10% Glycine SDS-PAGE of CDO-O α K258A. C: crude extract, H: purified by metal-chelation chromatography, G: purified by gel chromatography, M: Precision Plus Protein™ Dual Color Standards. The red arrow indicated the CDO-O α K258A containing fractions.

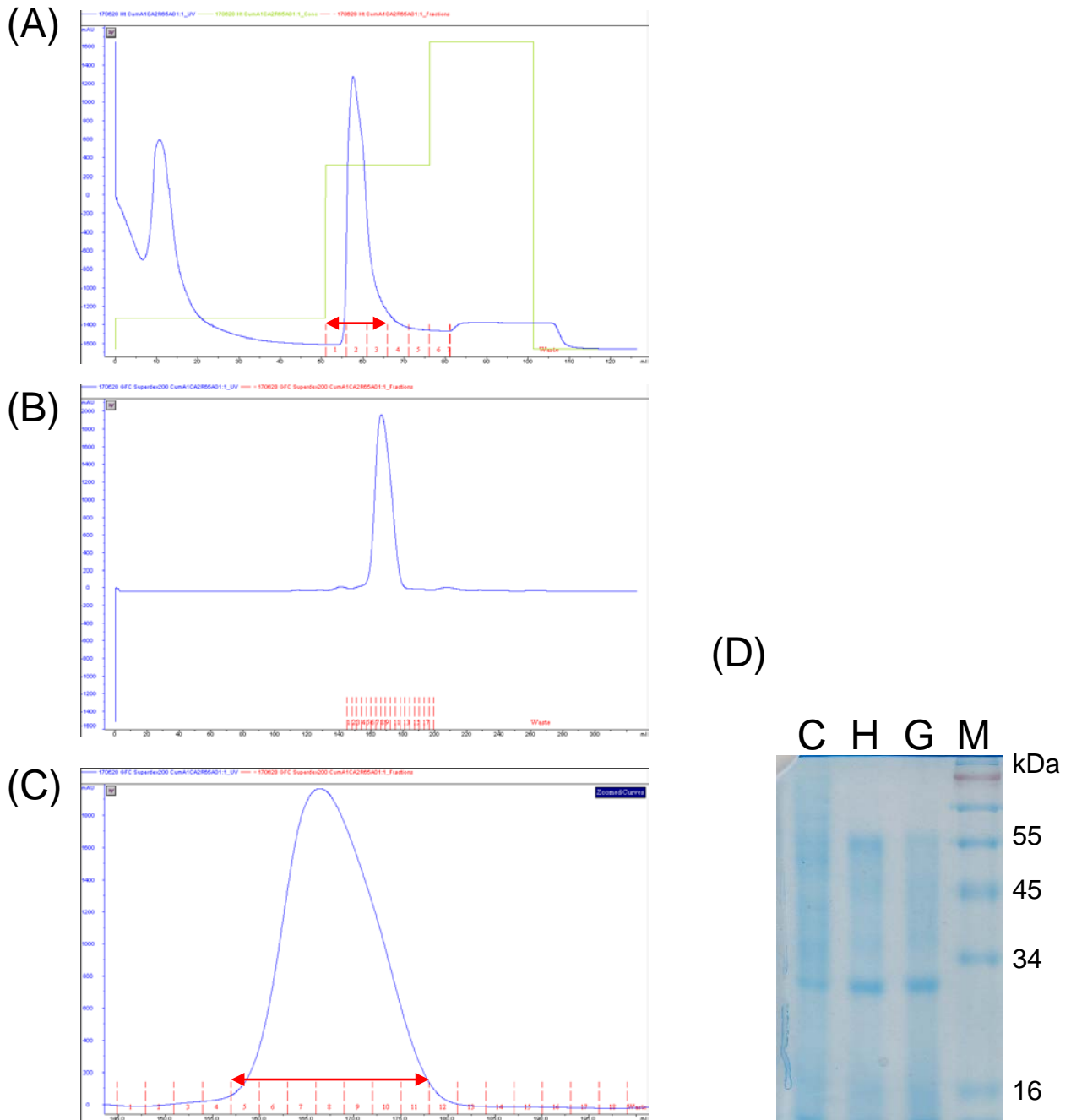


Fig. S14 Affinity purification and gel chromatography of CDO-OβR65A

(A) Elution profile of metal-chelation chromatography. Blue line indicates absorbance at 280 nm (mAU) and green line indicates imidazole concentration. (B)(C) Gel chromatography of the affinity purified CDO-OβR65A. (D) 10% Glycine SDS-PAGE of CDO-OβR65A. C: crude extract, H: purified by metal-chelation chromatography, G: purified by gel chromatography, M: SeeBlue™ Plus2 Pre-stained Protein Standard. The red arrow indicated the CDO-OβR65A containing fractions.

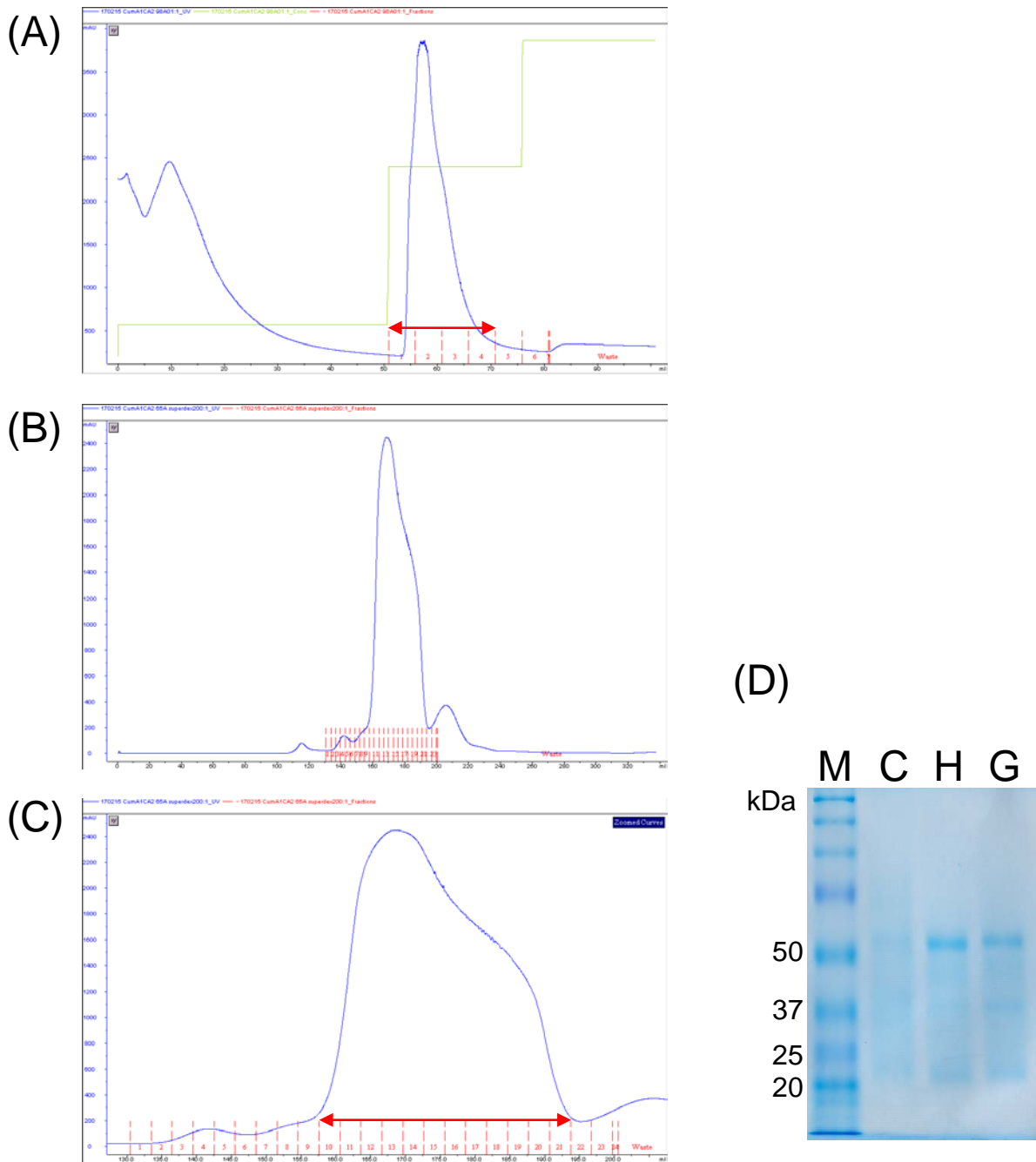


Fig. S15 Affinity purification and gel chromatography of CDO-OβL98A

(A) Elution profile of metal-chelation chromatography. Blue line indicates absorbance at 280 nm (mAU) and green line indicates imidazole concentration. (B)(C) Gel chromatography of the affinity purified CDO-OβL98A. (D) 10% Glycine SDS-PAGE of CDO-OβL98A. C: crude extract, H: purified by metal-chelation chromatography, G: purified by gel chromatography, M: Precision Plus Protein™ Dual Color Standards. The red arrow indicated the CDO-OβL98A containing fractions.

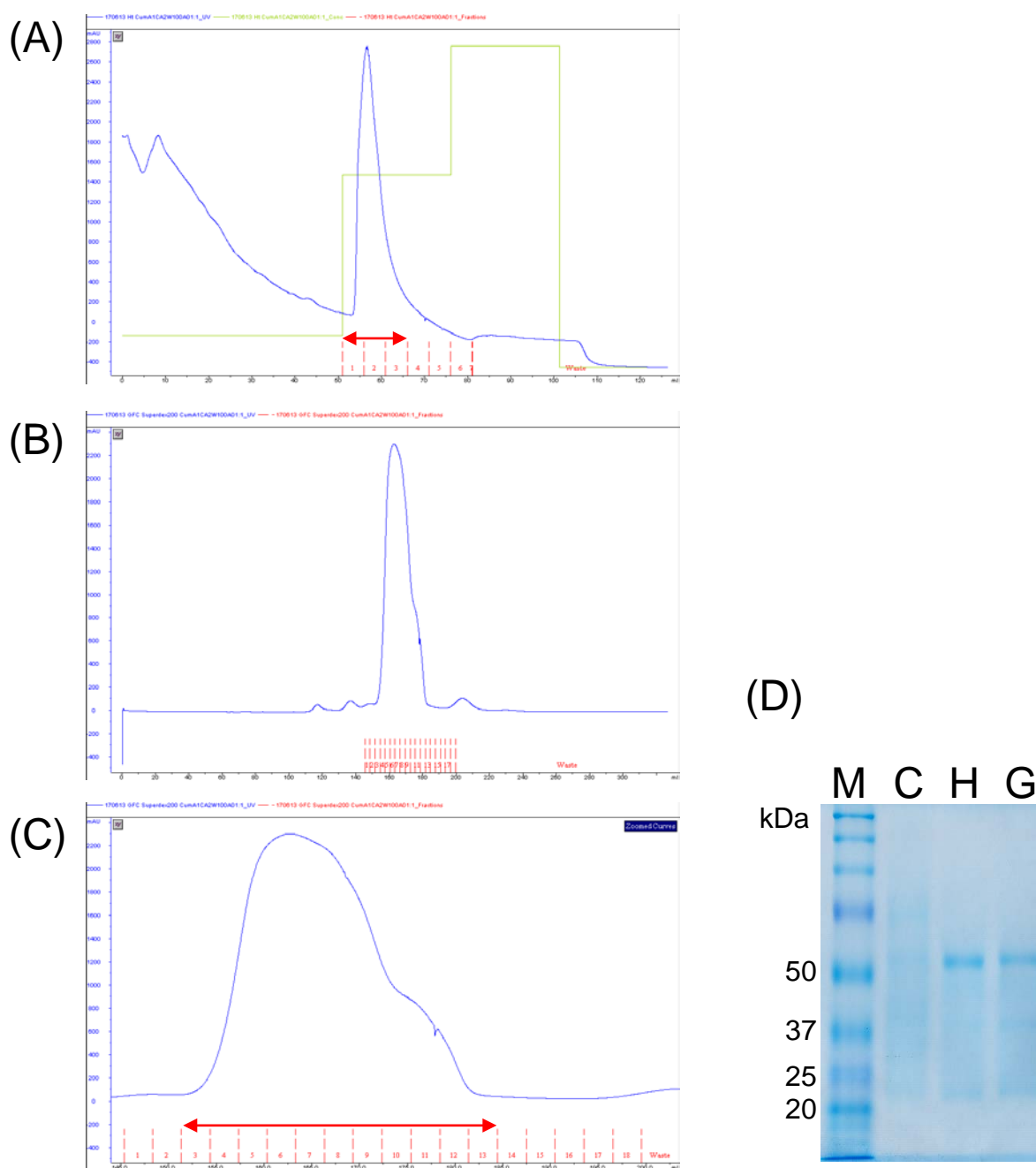


Fig. S16 Affinity purification and gel chromatography of CDO-O β W100A

(A) Elution profile of metal-chelation chromatography. Blue line indicates absorbance at 280 nm (mAU) and green line indicates imidazole concentration. (B)(C) Gel chromatography of the affinity purified CDO-O β W100A. (D) 10% Glycine SDS-PAGE of CDO-O β W100A. C: crude extract, H: purified by metal-chelation chromatography, G: purified by gel chromatography, M: Precision Plus Protein™ Dual Color Standards. The red arrow indicated the CDO-O β W100A containing fractions.

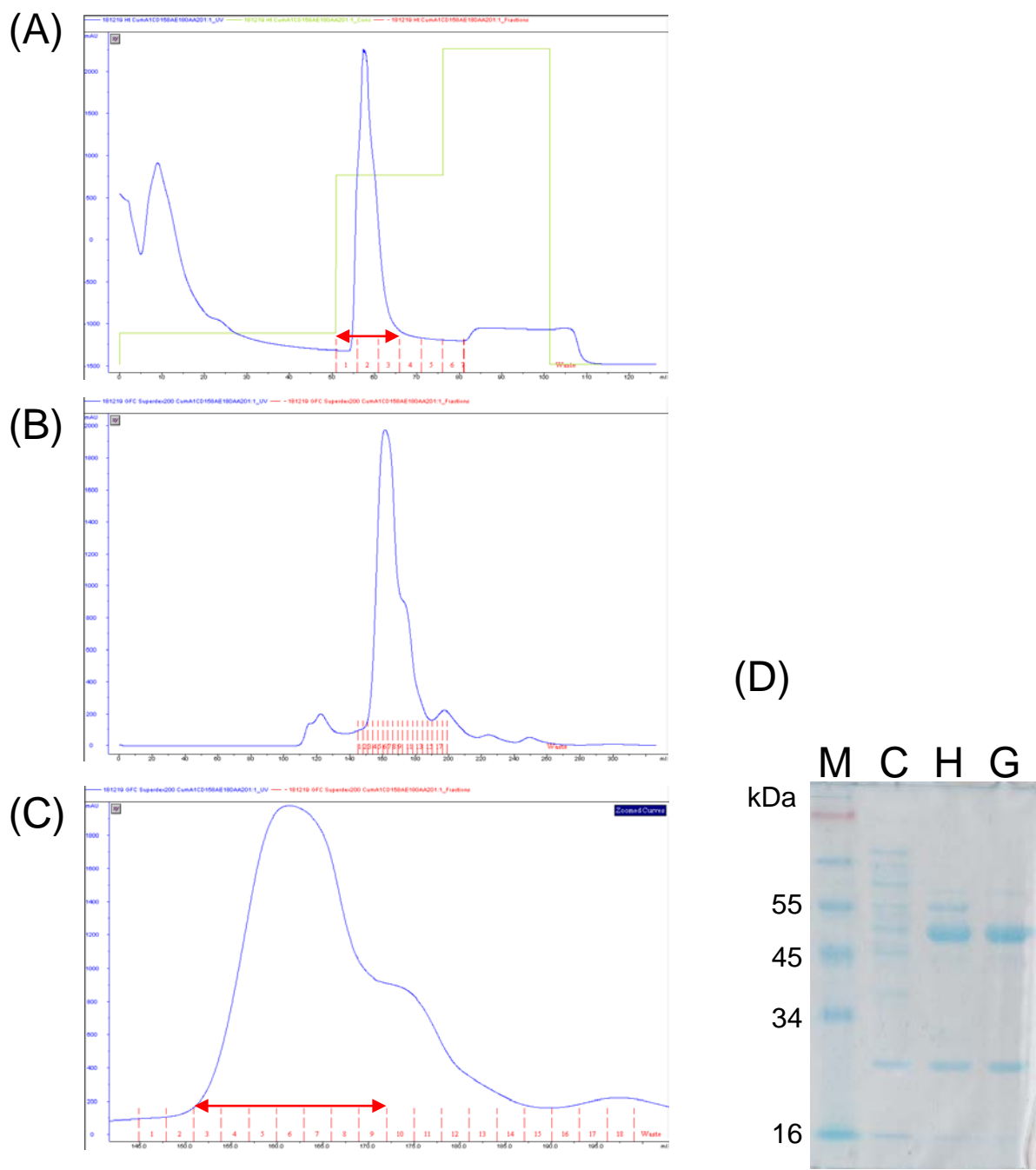


Fig. S17 Affinity purification and gel chromatography of CDO-O α D158A α E180A

(A) Elution profile of metal-chelation chromatography. Blue line indicates absorbance at 280 nm (mAU) and green line indicates imidazole concentration. (B)(C) Gel chromatography of the affinity purified CDO-O α D158A α E180A. (D) 10% Glycine SDS-PAGE of CDO-O α D158A α E180A. C: crude extract, H: purified by metal-chelation chromatography, G: purified by gel chromatography, M: SeeBlue™ Plus2 Pre-stained Protein Standard. The red arrow indicated the CDO-O α D158A α E180A containing fractions.

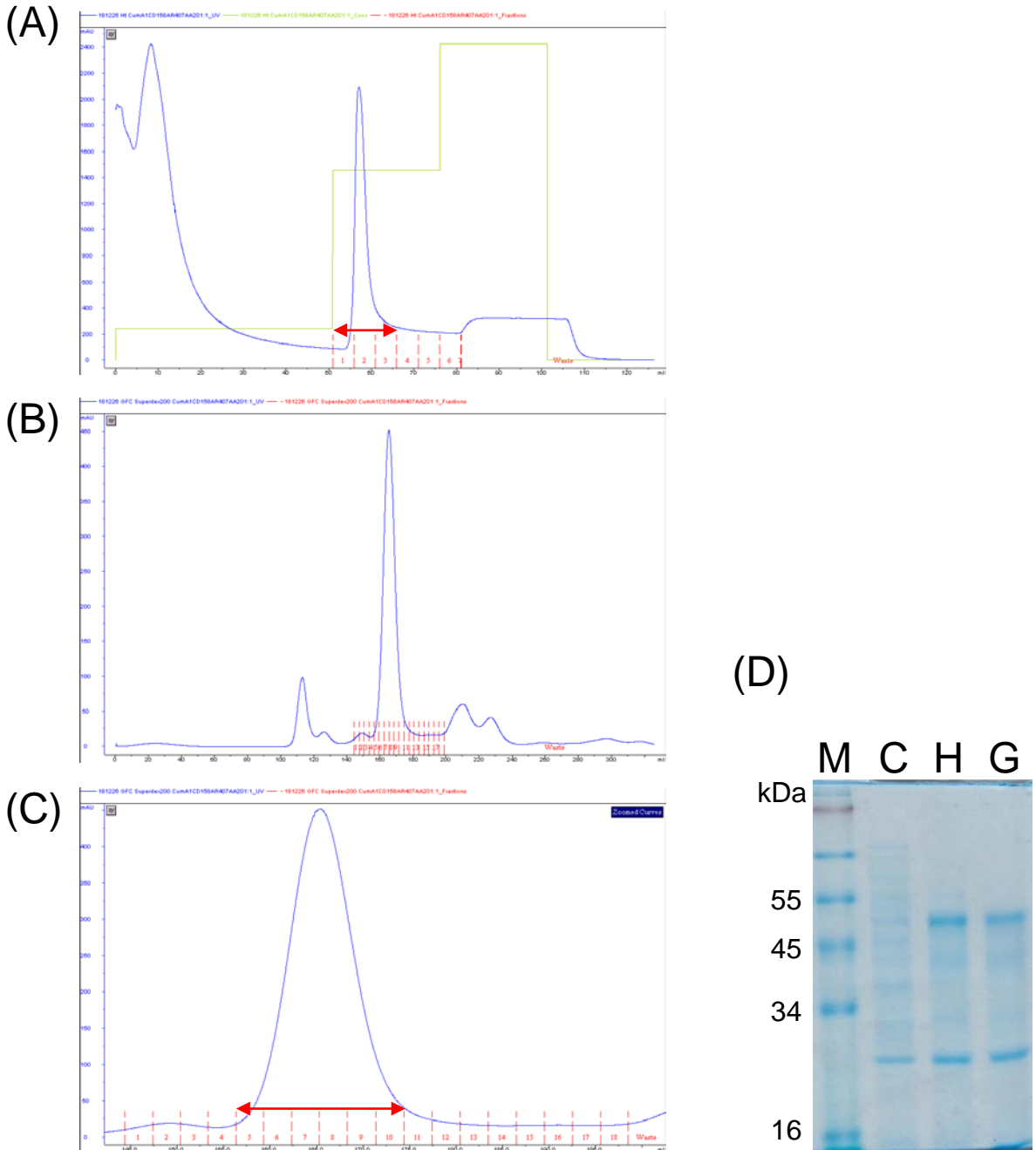


Fig. S18 Affinity purification and gel chromatography of CDO-O α D158A α R407A

(A) Elution profile of metal-chelation chromatography. Blue line indicates absorbance at 280 nm (mAU) and green line indicates imidazole concentration. (B)(C) Gel chromatography of the affinity purified CDO-O α D158A α R407A. (D) 10% Glycine SDS-PAGE of CDO-O α D158A α R407A. C: crude extract, H: purified by metal-chelation chromatography, G: purified by gel chromatography, M: SeeBlue™ Plus2 Pre-stained Protein Standard. The red arrow indicated the CDO-O α D158A α R407A containing fractions.

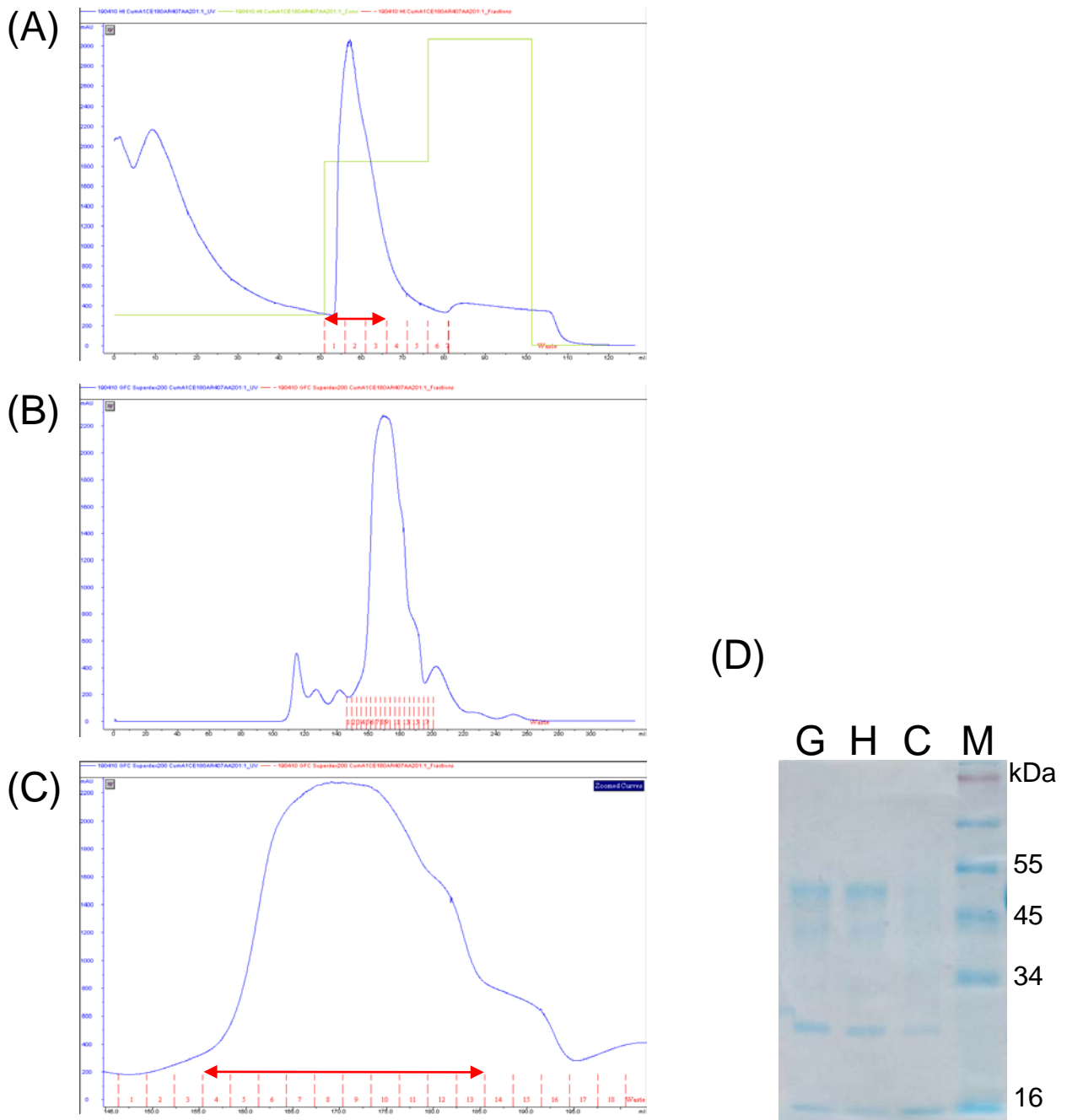


Fig. S19 Affinity purification and gel chromatography of CDO-OαE180AαR407A

(A) Elution profile of metal-chelation chromatography. Blue line indicates absorbance at 280 nm (mAU) and green line indicates imidazole concentration. (B)(C) Gel chromatography of the affinity purified CDO-OαE180AαR407A. (D) 10% Glycine SDS-PAGE of CDO-OαE180AαR407A. C: crude extract, H: purified by metal-chelation chromatography, G: purified by gel chromatography, M: SeeBlue™ Plus2 Pre-stained Protein Standard. The red arrow indicated the CDO-OαE180AαR407A containing fractions.

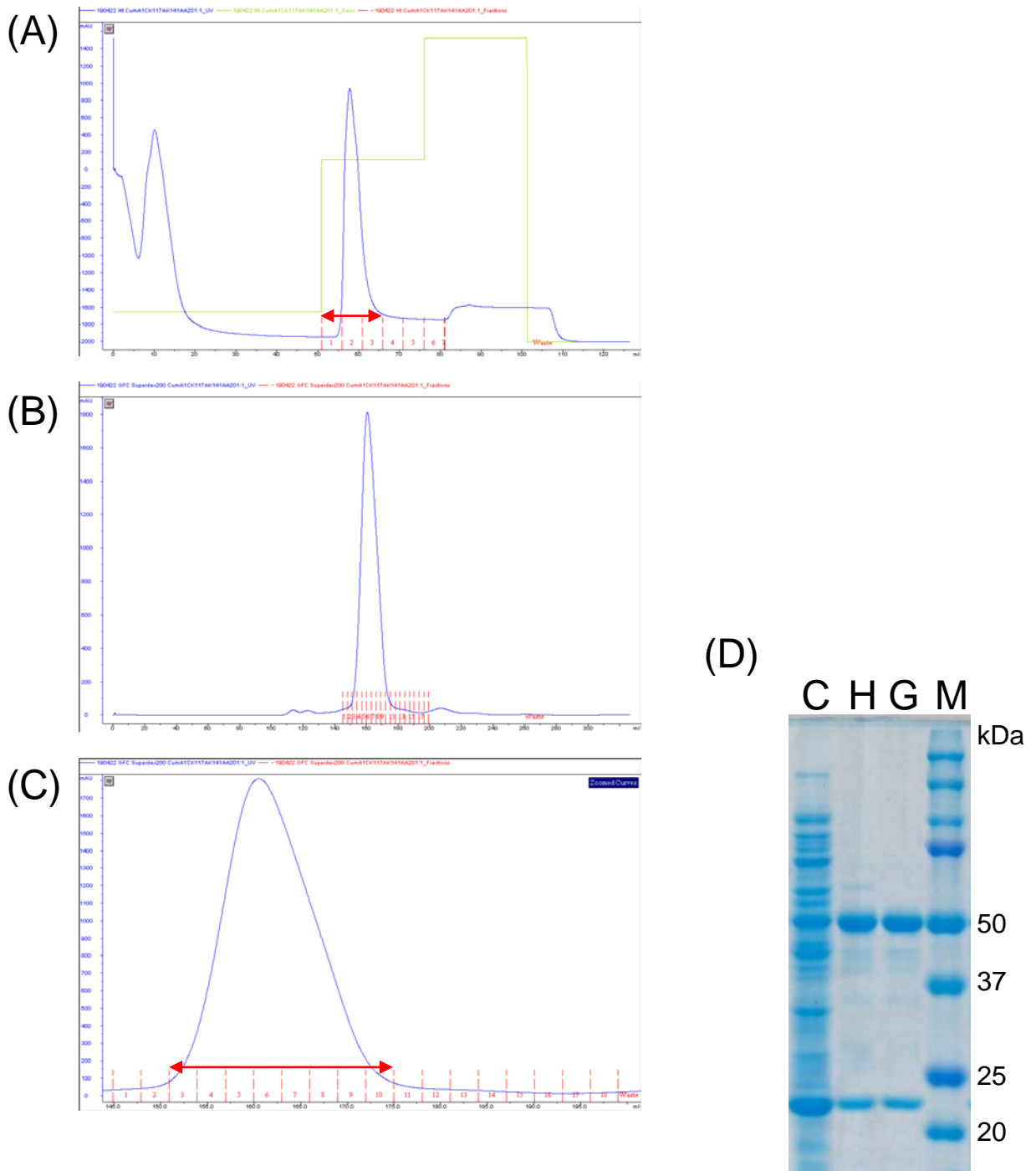


Fig. S20 Affinity purification and gel chromatography of CDO-O α K117A α K141A

(A) Elution profile of metal-chelation chromatography. Blue line indicates absorbance at 280 nm (mAU) and green line indicates imidazole concentration. (B)(C) Gel chromatography of the affinity purified CDO-O α K117A α K141A. (D) 10% Glycine SDS-PAGE of CDO-O α K117A α K141A. C: crude extract, H: purified by metal-chelation chromatography, G: purified by gel chromatography, M: Precision Plus Protein™ Dual Color Standards. The red arrow indicated the CDO-O α K117A α K141A containing fractions.

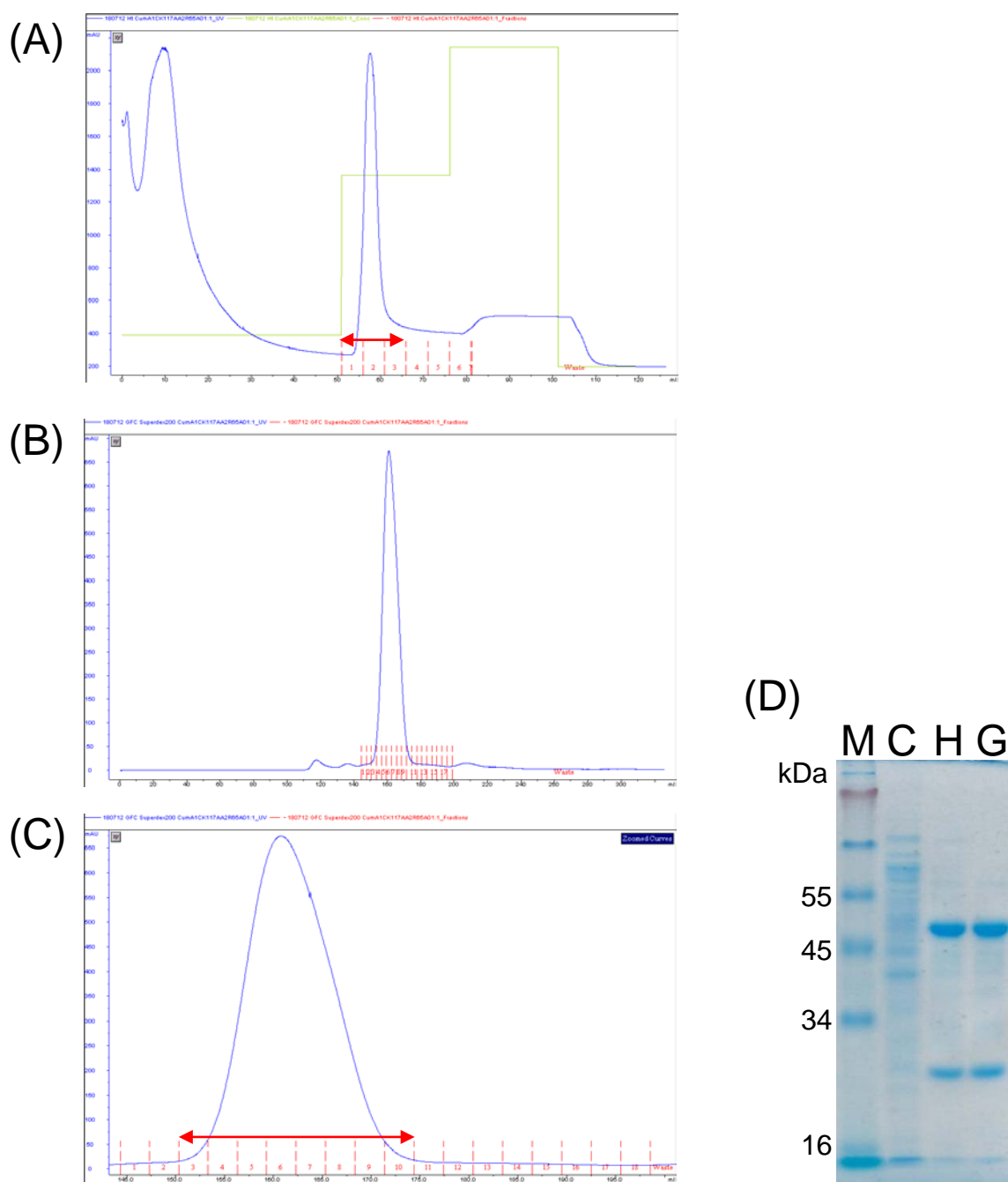


Fig. S21 Affinity purification and gel chromatography of CDO-O α K117A β R65A

(A) Elution profile of metal-chelation chromatography. Blue line indicates absorbance at 280 nm (mAU) and green line indicates imidazole concentration. (B)(C) Gel chromatography of the affinity purified CDO-O α K117A β R65A. (D) 10% Glycine SDS-PAGE of CDO-O α K117A β R65A. C: crude extract, H: purified by metal-chelation chromatography, G: purified by gel chromatography, M: SeeBlue™ Plus2 Pre-stained Protein Standard. The red arrow indicated the CDO-O α K117A β R65A containing fractions.

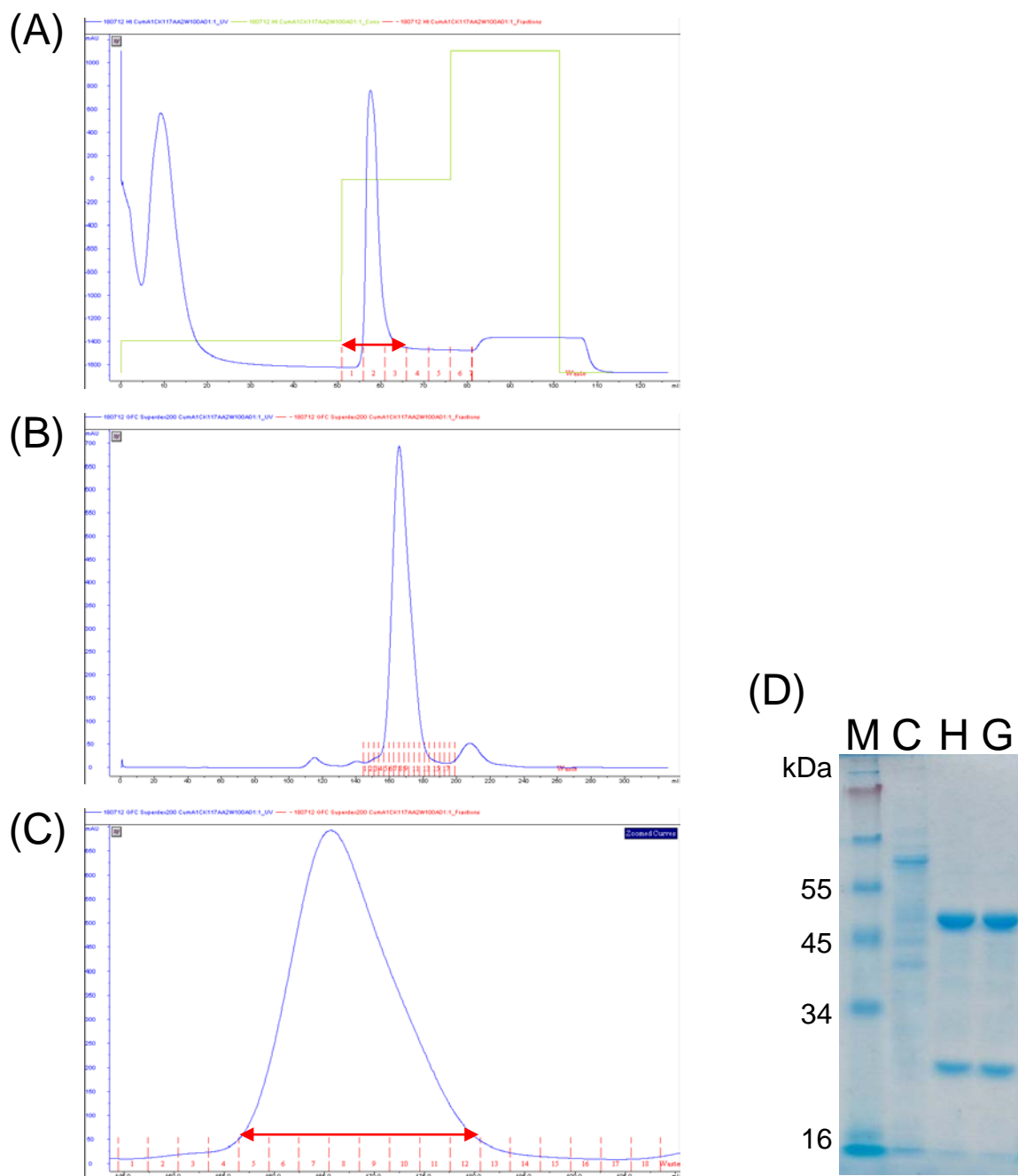


Fig. S22 Affinity purification and gel chromatography of CDO-O α K117A β W100A

(A) Elution profile of metal-chelation chromatography. Blue line indicates absorbance at 280 nm (mAU) and green line indicates imidazole concentration. (B)(C) Gel chromatography of the affinity purified CDO-O α K117A β W100A. (D) 10% Glycine SDS-PAGE of CDO-O α K117A β W100A. C: crude extract, H: purified by metal-chelation chromatography, G: purified by gel chromatography, M: SeeBlue™ Plus2 Pre-stained Protein Standard. The red arrow indicated the CDO-O α K117A β W100A containing fractions.

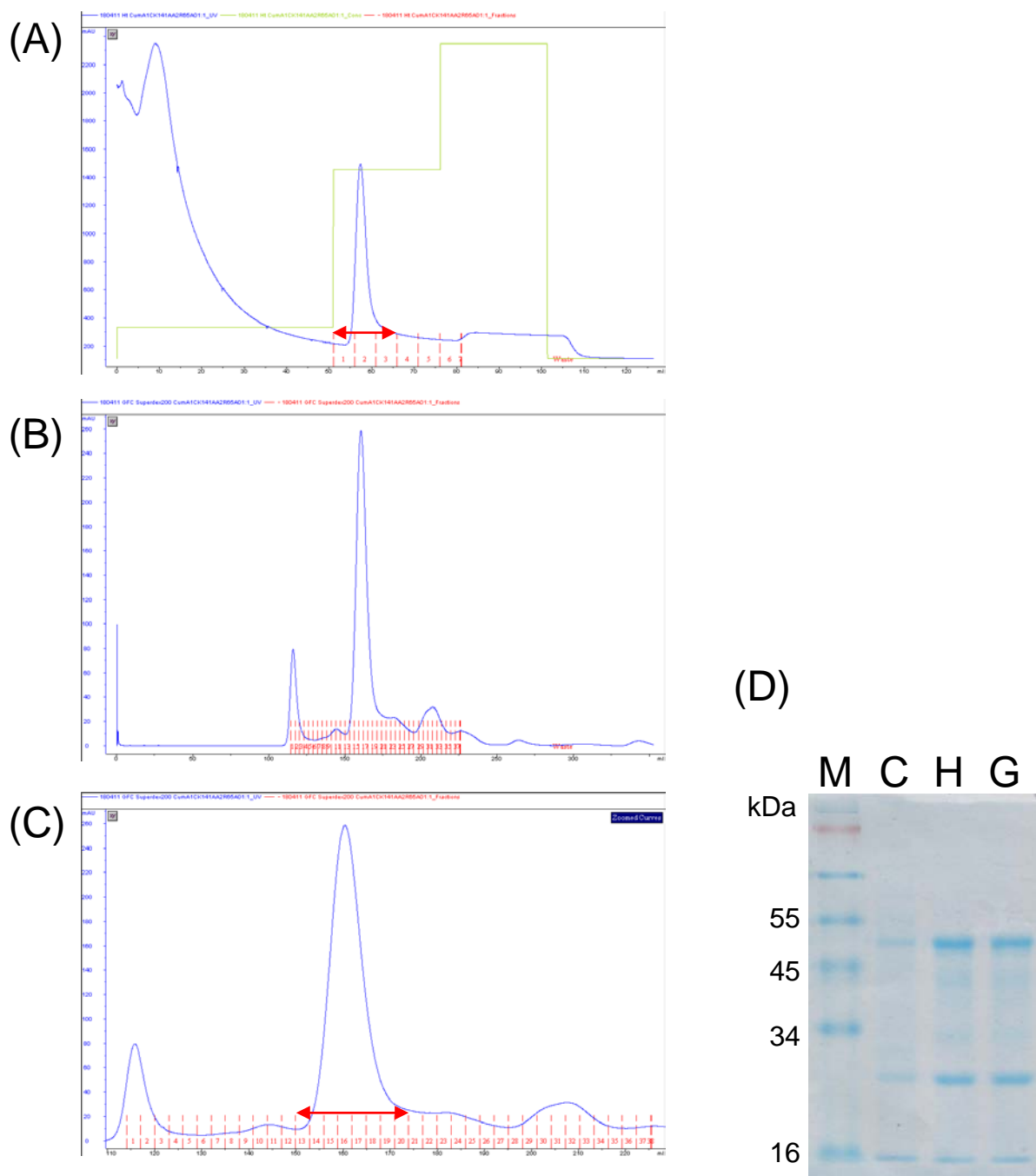


Fig. S23 Affinity purification and gel chromatography of CDO-O α K141A β R65A

(A) Elution profile of metal-chelation chromatography. Blue line indicates absorbance at 280 nm (mAU) and green line indicates imidazole concentration. (B)(C) Gel chromatography of the affinity purified CDO-O α K141A β R65A. (D) 10% Glycine SDS-PAGE of CDO-O α K141A β R65A. C: crude extract, H: purified by metal-chelation chromatography, G: purified by gel chromatography, M: SeeBlue™ Plus2 Pre-stained Protein Standard. The red arrow indicated the CDO-O α K141A β R65A containing fractions.

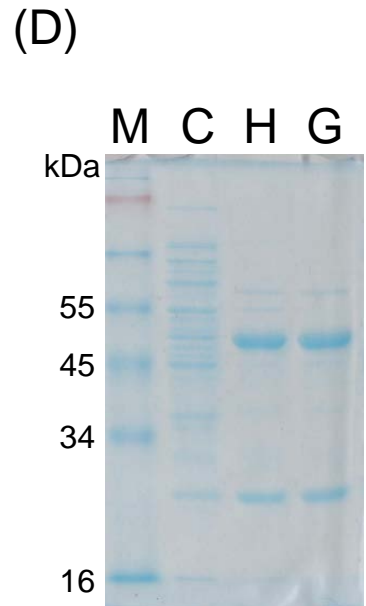
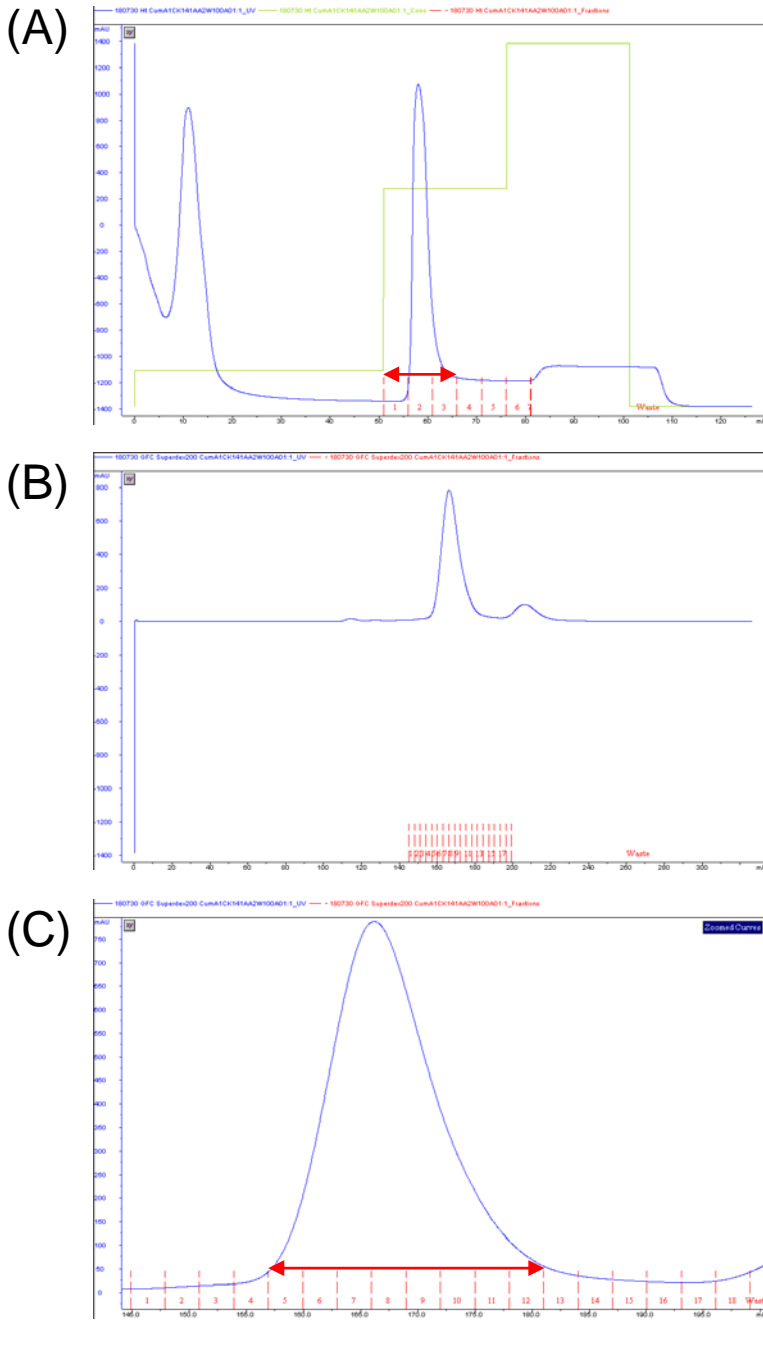


Fig. S24 Affinity purification and gel chromatography of CDO-OαK141AβW100A

(A) Elution profile of metal-chelation chromatography. Blue line indicates absorbance at 280 nm (mAU) and green line indicates imidazole concentration. (B)(C) Gel chromatography of the affinity purified CDO-OαK141AβW100A. (D) 10% Glycine SDS-PAGE of CDO-OαK141AβW100A. C: crude extract, H: purified by metal-chelation chromatography, G: purified by gel chromatography, M: SeeBlue™ Plus2 Pre-stained Protein Standard. The red arrow indicated the CDO-OαK141AβW100A containing fractions.

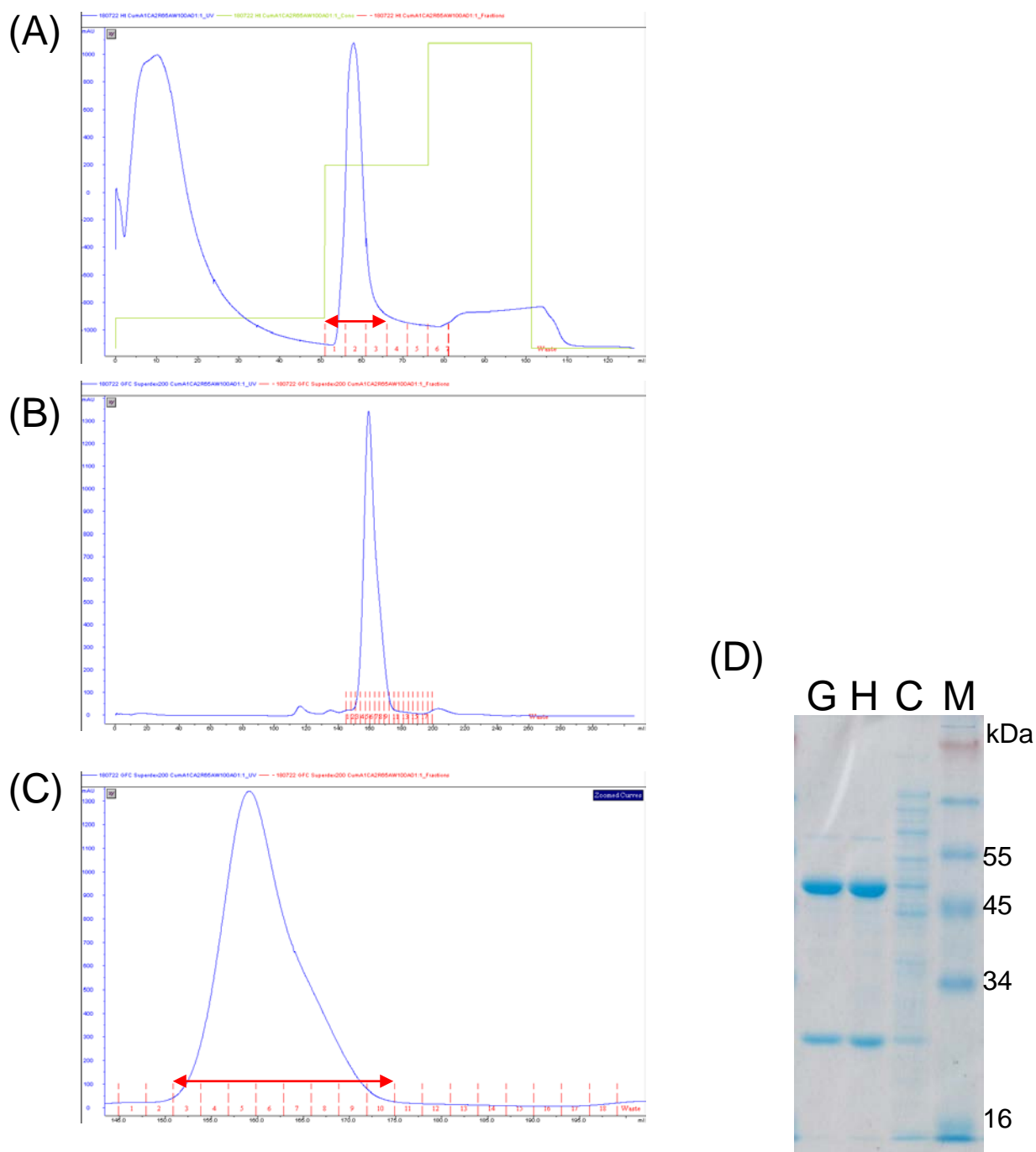


Fig. S25 Affinity purification and gel chromatography of CDO-O β R65A β W100A

(A) Elution profile of metal-chelation chromatography. Blue line indicates absorbance at 280 nm (mAU) and green line indicates imidazole concentration. (B)(C) Gel chromatography of the affinity purified CDO-O β R65A β W100A. (D) 10% Glycine SDS-PAGE of CDO-O β R65A β W100A. C: crude extract, H: purified by metal-chelation chromatography, G: purified by gel chromatography, M: SeeBlue™ Plus2 Pre-stained Protein Standard. The red arrow indicated the CDO-O β R65A β W100A containing fractions.

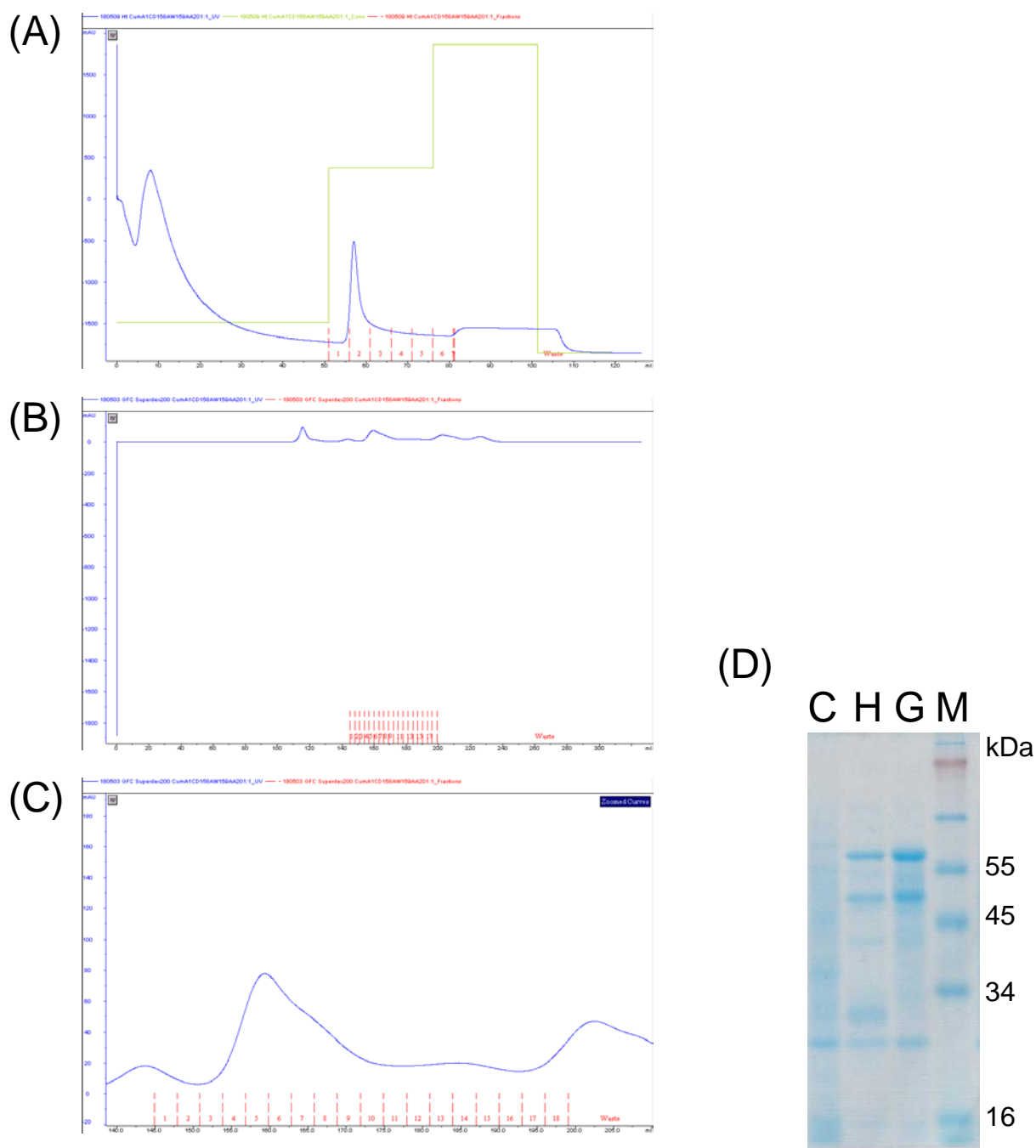


Fig. S26 Affinity purification and gel chromatography of CDO-O α D158A α W159A

(A) Elution profile of metal-chelation chromatography. Blue line indicates absorbance at 280 nm (mAU) and green line indicates imidazole concentration. (B)(C) Gel chromatography of the affinity purified CDO-O α D158A α W159A. (D) 10% Glycine SDS-PAGE of CDO-O α D158A α W159A. C: crude extract, H: purified by metal-chelation chromatography, G: purified by gel chromatography, M: SeeBlue™ Plus2 Pre-stained Protein Standard.

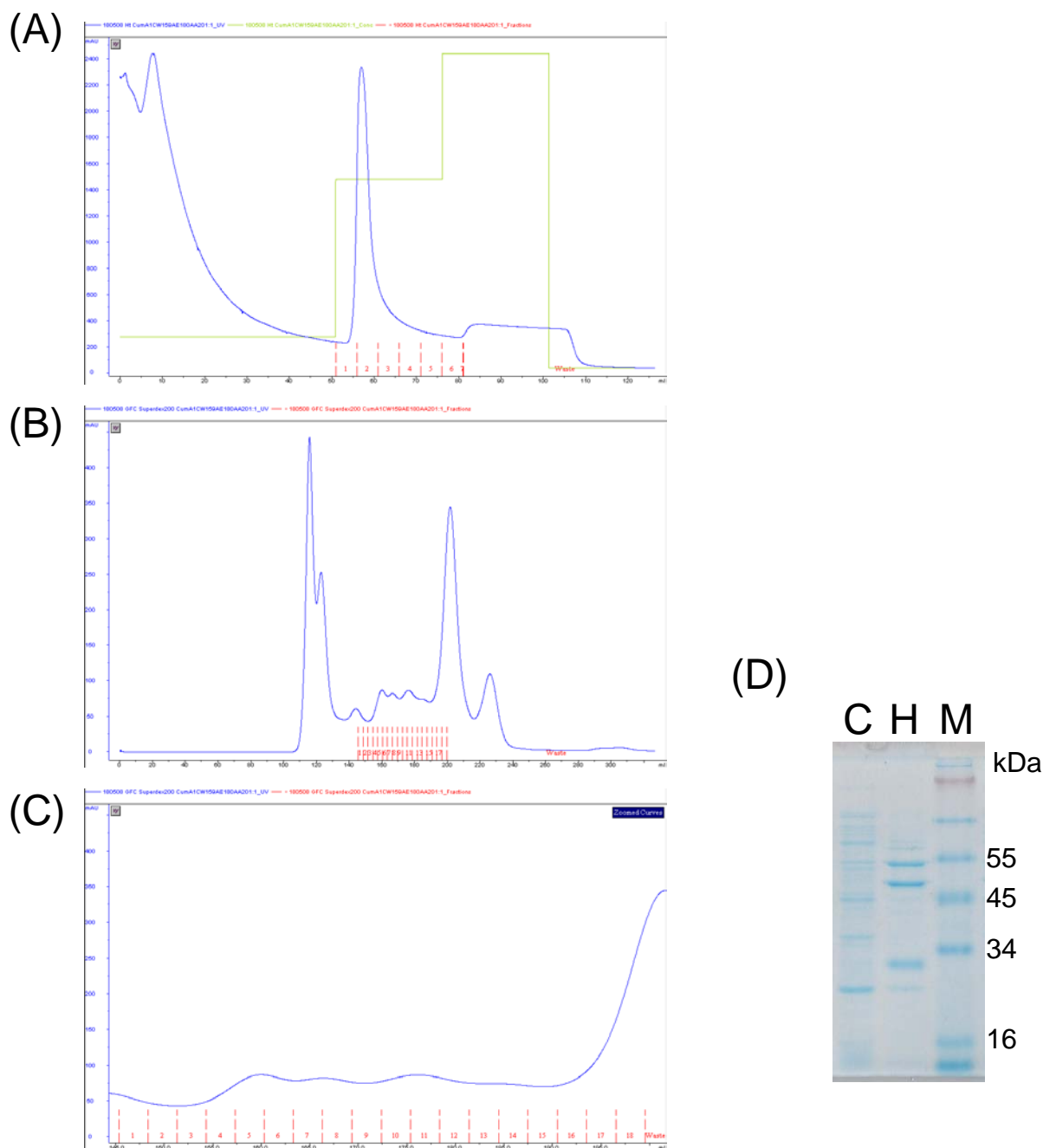


Fig. S27 Affinity purification and gel chromatography of CDO-O α W159A α E180A

(A) Elution profile of metal-chelation chromatography. Blue line indicates absorbance at 280 nm (mAU) and green line indicates imidazole concentration. (B)(C) Gel chromatography of the affinity purified CDO-O α W159A α E180A. (D) 10% Glycine SDS-PAGE of CDO-O α W159A α E180A. C: crude extract, H: purified by metal-chelation chromatography, M: SeeBlue™ Plus2 Pre-stained Protein Standard.

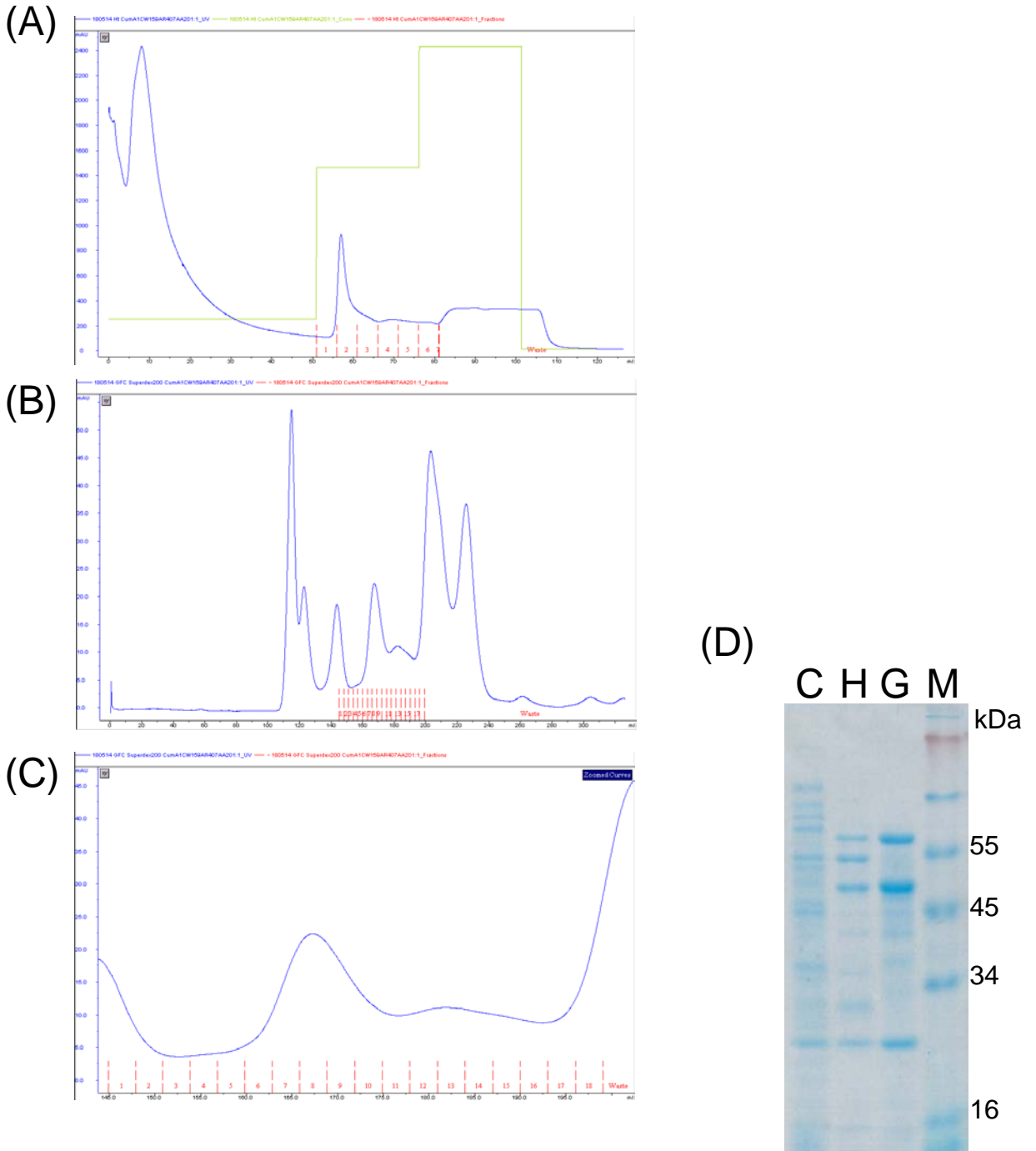


Fig. S28 Affinity purification and gel chromatography of CDO-O α W159A α R407A

(A) Elution profile of metal-chelation chromatography. Blue line indicates absorbance at 280 nm (mAU) and green line indicates imidazole concentration. (B)(C) Gel chromatography of the affinity purified CDO-O α W159A α R407A. (D) 10% Glycine SDS-PAGE of CDO-O α W159A α R407A. C: crude extract, H: purified by metal-chelation chromatography, G: purified by gel chromatography, M: SeeBlue™ Plus2 Pre-stained Protein Standard.

CCACCACCACACTTTTTCCAAAGTTTGTGAAGTATCTGATG-3' and 5'- AAAGTCGACTCATGGCGCTAGATACCCGG-3' (*NdeI* and *SalI* restriction sites were italicized). *XbaI* site, stop codon, SD sequence, *NdeI* and *SalI* sites were created on the end of *cumA4*-containing DNA fragment by using following primer set: 5'-AAATCTAGATAAGAAGGAGATATACATATGCACCACCACCACCACCACATTAATCAATCGTCATTATTGGTGCTGGC-3' and 5'-AAAGTCGACTCACTCGCATCGCTCAGCTTTAG-3' (*NdeI* and *SalI* restriction sites were italicized). The PCR amplicon of *cumA1A2* was inserted into *XbaI* and *HindIII* sites of pUC118 to produce pUCumA1CA2. The PCR amplicon of *cumA3* was inserted into *XbaI* and *SalI* sites of pET-26b(+) to produce pETumA3N. The PCR amplicon of *cumA4* was inserted into *XbaI* and *SalI* sites of pUC118 to produce pUCumA4N.

Preparation of the competent cells

For heat-shock transformation of *E. coli* DH5 α , *E. coli* JM109(DE3) and *E. coli* BL21(DE3), cells were prepared competent according Hanahan [Hanahan , 1983].

- Inoculate a single colony into 5 mL LB medium and grow overnight at 310 L.
- Preculture 1 mL medium into 100 mL fresh LB medium and propagate the cells at 310 KC until an OD600 of 0.4-0.6.
- Chill the culture on ice and pellet by centrifugation (5,000 rpm; 5 min; 277 KC).
- Rinse the tubes and the pellets with TFB I to remove traces of medium.
- Resuspend the cell pellets gently in 40 mL ice-cold TFB I. Incubate for 5 min on ice.
- Centrifugation (5,000 rpm; 5 min; 4°C). Discard the supernatants.
- Resuspend the cell pellets in 4 mL ice-cold TFB II. Incubation for 60 min on ice.
- Aliquot the 100 μ L cell suspension into each sterile 1.5-mL tubes and flash-freeze in liquid nitrogen then store at 193 K.

Table M2 composition of TFB I and TFB II

TFB I (pH 5.8)*			TFB II (pH 6.5)^		
RbCl	100	mM	MOPS	10	mM
MnCl ₂	50	mM	RbCl	10	mM
Potassium acetate	30	mM	CaCl ₂ .H ₂ O	10	mM
CaCl ₂ .H ₂ O	10	mM	Glycerol	15	% [v/v]
Glycerol	15	% [v/v]			

* The pH value was adjusted with 0.2M acetic acid. The buffer was sterile filtered and stored at 4°C.

^ The pH value was adjusted with 1N NaCl. The buffer was sterile filtered and stored at 4°C

Heat-shock transformation

Transformation of CaCl₂-competent cells of *E. coli* was performed according to the following protocol.

- Add 1 µL plasmid DNA or ligation assay to 100 µL competent cells and incubate for 20-30 min on ice.
- Perform heat shock at 42°C for 1.5 min.
- Incubate for 2 min on ice.
- Add 500 µL LB medium and incubate the cells for 1 h at 37°C with shaking (300 rpm).
- Plate 100 µL of the cell suspension on LB agar plates supplemented with the appropriate antibiotics for selection and incubate overnight at 37°C.

Plasmid extraction

Analytical and preparative plasmid isolation from cells of *E. coli* was performed using the alkaline lysis method. Cells were grown overnight in 5 ml LB medium supplemented with the appropriate antibiotics for selection.

- Pellet 5 mL cell culture in 1.5 mL microcentrifuge tube.
- Resuspend the cell pellets in 100 µL Buffer 1 by vortexing for 30 sec
- Add 200 µl Buffer 2 and invert the tube gently for 5 times. Incubate on ice for 5 min.

- Add 150 μ L Buffer 3 and invert the tube gently for 5 times. Incubate on ice for 5 min.
- Centrifugation (13,000 rpm; 5 min; 4°C). Transfer 400 μ L samples into new 1.5-mL microcentrifuge tubes.
- Add 400 μ L of Phenol:Chloroform:IAA (25:24:1) (Nacalai Tesque, Kyoto, Japan) and mix by vigorous vortexing .
- Centrifugation (13,000 rpm; 10 min; RT). Transfer 300 μ L of the upper aqueous phase into new 1.5-mL microcentrifuge tubes.
- Add 1000 μ L 99.5 % ethanol, gently mix it. Incubate on ice for 5 min.
- Centrifugation (13,000 rpm; 10 min; 4°C).
- Discard the supernatants and wash the pellets with 400 μ L 70% ethanol.
- Centrifugation (13,000 rpm; 5 min; 4°C).
- Discard the supernatants Dry the pellet with vacuum for at least 5 min.
- Resuspended the pellets in 50 μ L TE buffer and incubate with 1 μ L RNase A (Nippon Gene) for 1h at 37°C.
- Measure the concentration and 260/280 and store the samples at -20°C.

Table M3 Composition of solution for plasmid extraction

Solution I (Autoclaved)			Solution II		
	For 100 mL	Final conc.			
-D- Glucose	0.9 g	50 mM	total 1 mL		
1 M Tris-HCl	2.5 mL	25 mM		Milli Q	700 μ L
0.5 M EDTA	2.0 mL	10 mM		1 N NaOH	200 μ L
Milli Q	fill up to 100 mL				
Solution III					
	For 100 mL	Final conc.			
Potassium Acetate	29.45 g	3 M			
Acetic Acid (hood)	12 mL	2 M			
Milli Q	fill up to 100 mL				

TE buffer (Autoclaved)		
	For 100 mL	Final conc.
1 M Tris-HCl (pH 8.0)	1 mL	10 mM
0.5 M EDTA (pH 8.0)	200 mL	1mM
Milli Q	fill up to 100 mL	

Agarose gel electrophoresis

Analytical and preparative agarose gel electrophoresis of DNA fragments was carried out in horizontal electrophoresis tanks (Mupid[®]-2X, Advance, Japan) using Agarose ME (Nacalai Tesque, Japan) and 1x TAE electrophoresis buffer. Samples were mixed with 10x Loading Dye (Takara Bio, Japan) and loaded in the wells of the gel. Electrophoresis was performed at 100V for 30-40 min. The gels were then stained with ethidium bromide (Nippon Gene, Japan) for 15 min, destained in dH₂O for 15 min, and visualized using FAS (Toyobo, Japan). One STEP marker 6 (Nippon Gene, Japan) DNA ladder and 100 bp maker (GeneDireX, Japan) were routinely used in this study.

Purification of fragment of nucleotide

Wizard[®] SV Gel and PCR Clean-Up System (Promega Co., USA) was routinely used for isolation of DNA fragments from agarose gel. After sufficient separation on an agarose gel and staining with ethidium bromide, the fragments of interest were cut with a sterile scalpel under UV light and placed in clean tubes. The DNA fragments were afterwards subjected to purification as recommended by the manufacturer.

Site-directed mutagenesis

Single alanine substituted CDO-Oxy (α K33A, α L35A, α R39A, α K117A, α K141A, α D158A, α W159A, α L162A, α E180A, α L241A, α D253A, α K258A, α R407A, β R65A, β L98A, β W100A) was prepared by KOD-Plus-Mutagenesis kit (Toyobo, Japan) with the wild type Oxy (pUC118-CumA1CA2). Primer information was in Table M1. Some double alanine

substituted CDO-O (α D158A; α E180A, α D158A; α R407A, α E180A; α R407A, α K117A; α K141A, β R65A; β W100A) were artificially synthesized with exogenously added *Xba*I and *Sal*I restriction enzyme sites in α -subunit fragment and *Sal*I and *Hind*III sites in β -subunit fragment then were cloned into plasmid pUC57-Kan by GENEWIZ Japan (Saitama, Japan). The *Xba*I and *Sal*I or *Sal*I and *Hind*III fragments of double alanine mutants were inserted into corresponding sites in pUC118-CumA1CA2. The other double alanine mutants (α K117A; β R65A, α K117A; β W100A, α K141A; β R65A, α K141A; β W100A) were constructed from single alanine mutants. The *Xba*I and *Sal*I fragment of α K117A or α K141A were inserted into corresponding sites in the pUC118-CumA1CA2R65A or pUC118-CumA1CA2W100A respectively.

Table M4 The program for site directed mutagenesis

Temperature	Time	Cycle
94°C	1 min	1
98°C	10 sec	15
68°C	5 min	
4°C	∞	

Table M5 Primer list of site-directed mutagenesis		
α K33A	F	5'-GATGAGGAAG <u>CGGG</u> GTTGCTTGATCC-3'
	R	5'-GGATCAAGCAACCCCGCTTCTTCATC-3'
α L35A	F	5'-GGAAAAGGGG <u>CG</u> CTTGATCCAC-3'
	R	5'-GTGGATCAAGCGCCCCCTTTTCC-3'
α R39A	F	5'-GCTTGATCCAG <u>CG</u> ATTTTCTCTGATCAGG-3'
	R	5'-CCTGATCAGAGAAAATCGCTGGATCAAGC-3'
α K117A	F	5'-GGCAACGCAG <u>CG</u> TCATTTACCTGC-3'
	R	5'-GCAGGTAAATGACGCTGCGTTGCC-3'
α K141A	F	5'-CCCTACGAGG <u>CGG</u> AGGCTTTTTGTG-3'
	R	5'-CACAAAAGCCTCCGCTCGTAGGG-3'
α D158A	F	5'-CGACAAGGCC <u>CG</u> TGGGGGCCGC-3'
	R	5'-GCGGCCCCACGCGGCCTTGTCG-3'
α W159A	F	5'-AAGGCCGAC <u>CG</u> GGGGCCGCTGC-3'
	R	5'-GCAGCGGCCCCGCTCGGCCTT-3'
α L162A	F	5'-GGGGCCG <u>CG</u> CAAGCGGGTG-3'
	R	5'-CACCCGCGCTTGCGCCGGCCCC-3'
α E180A	F	5'-CTGGGATAC <u>CG</u> GCCCCTGATTTG-3'
	R	5'-CAAATCAGGGCCGCGGTATCCAG-3'
α L241A	F	5'-GATGGCGCAT <u>CG</u> TCAGGTGTATTGTCC-3'
	R	5'-GGACAATACACCTGACGCATGCGCCATC-3'
α D253A	F	5'-GCCTGAAATG <u>CG</u> TGTGCCAAG-3'
	R	5'-CTTGGGACAACGCCATTTTCAGGC-3'
α K258A	F	5'-GTCCAAGTAG <u>CG</u> TTACCGTCAAGTGGG-3'
	R	5'-CCCACCTTGACGGTAACGCTACTTGGGAC-3'
α R407A	F	5'-GGCTAGAAGT <u>CG</u> CCTCTTTGTGCC-3'
	R	5'-GGGCACAAAGAGGCGCACTTCTAGCC-3'
β R65A	F	5'-CTCATACATCC <u>CG</u> GAATAAGGCGATG-3'
	R	5'-CATCGCCTTATTCGCGGATGTATGAG-3'
β L98A	F	5'-GGTTTCGGGG <u>CG</u> AACTGGACTGAAG-3'
	R	5'-CTTCAGTCCAGTTCGCCCCGAAACC-3'
β W100A	F	5'-CGGGGCTTAAC <u>CG</u> ACTGAAGATCC-3'
	R	5'-GGATCTTCAGTCGCGTTAAGCCCCG-3'
Alanine mutation frames were underlined.		

Expression and purification of cumene dioxygenase

CDO-R, CDO-O, and alanine substituted CDO-O were expressed in *E. coli* JM109(DE3) transformed with pUCumA4N, pUCumA1CA2, and its derivative plasmids. For expression of CDO-F, the plasmid pETCumA3N and *E. coli* BL21(DE3) were used.

Above *E. coli* strains were grown on SB medium supplemented with either 50 µg/mL kanamycin [for BL21(DE3)(pETCumA3N)] or 100 µg/mL ampicillin [for JM109(DE3)(pUCumA4N) and JM109(DE3)(pUCumA1CA2)] in jar fermenter (BE MARUBISHI, Tokyo, Japan). The cells were initially grown at 310 K for around 2.5 hours until the OD600 reached 0.5-0.6. Then, isopropyl-β-D-thiogalactopyranoside (IPTG) was added at the final concentration of 1.0, 0.1 and 0.5 mM for expressing CDO-R, CDO-F and CDO-O, respectively. Induction by IPTG was continued for 12 hours at 298 K for CDO-R and CDO-F or 303 K for CDO-O. *E. coli* cells were then harvested by centrifugation and re-suspended in Hitrap A buffer (20 mM Tris-HCl, 0.5 M NaCl and 10% glycerol, pH 7.4).

The crude cell extract was prepared by sonication for 10 min followed by centrifugation at 25,000 g for 2 hours. All of the proteins were purified with Hitrap B buffer (20 mM Tris-HCl, 0.5 M NaCl and 10% glycerol and 300 mM imidazole, pH 7.4) by metal-chelation chromatography (HiTrap Chelating HP column, column volume: 5 mL, Amersham Biosciences, UK) with the fast protein liquid chromatography instrument (ÄKTA FPLC, GE healthcare Japan, Japan). The protein-containing fractions of CDO-O and CDO-R were pooled and concentrated by Vivaspin[®] 20 system, whose molecular cutoff is 10k (Sartorius, Germany), while CDO-F were similarly pooled by Vivaspin[®] Turbo 15 system with molecular cutoff of 5 k (Sartorius, Germany). The resultant preparation was further purified with GFC buffer (20 mM Tris-HCl, 0.2 M NaCl and 10% glycerol, pH 7.4) by gel filtration chromatography (GFC) using HiLoad_{26/60} Superdex200 per grade column (for CDO-R and CDO-O) (GE Healthcare Japan, Japan) or HiLoad_{26/60} Superdex75 per grade column (for CDO-F) (GE Healthcare Japan, Japan).

Japan). Protein-containing fractions after GFC were pooled and concentrated by the filters. Resultant CDO component solution were frozen by liquid nitrogen and stored at 193 K until use.

Tricine SDS-PAGE

- Make the gel as following table in the 50 mL baker.

Table M6 Composition of 16% Tricine SDS-PAGE

	Separating Gel (16%) (bottom)	Stacking Gel (4%) (top)
MilliQ	1 mL	1.3 mL
3X gel buffer	2 mL	0.5 mL
Glycerol	0.6 mL	-----
40 % acrylamide: bis = 19:1 (Bio-rad, USA)	2.4 mL	0.2 mL
TEMED (Nacalai Tesque, Japan)	5 μ L	3 μ L
10 % APS (Nacalai Tesque, Japan)	50 μ L	25 μ L
Total Volume	6.055 mL	2.028 mL

- Make the 10% APS from APS powder.
- After adding APS and TEMED in to separating gel, mix it well and added into module immediately.
- Add 600-800 μ L isopropanol, isopropanol or ethanol in the top of running gel, wait for gel formation.
- After the gel form, use tissue remove ethanol carefully.
- Add APS and TEMED into stacking gel, mix it well and added into module immediately.
- Insert comb into gel immediately.

Running samples

- Loading samples, blank and marker.
- Loading 10 μ L sample each well.
- Total volume should be the same in each well.
- Marker volume is 5 + 5 μ L.
- Running condition (stacking /running): 30 /100 + 150 + 200 (V)

Gel stain and destain

- Warm up the gel with MilliQ by microwave and shake it with 60 rpm for 10 min twice.
- Stain with SimplyBlue™ SafeStain (Thermo Fisher Scientific, USA). Warm up the gel with SimplyBlue™ SafeStain by microwave and shake it with 60 rpm for 15 min.
- Destain with MilliQ. Warm up the gel with MilliQ by microwave and shake it with 60 rpm overnight.
- Store the gel with little MilliQ in the zip lock bag. Scan into file and store it at 4°C.

Table M7 Composition of running buffer of Tricine SDS-PAGE

	Anode buffer (pH8.9) (10x)	Cathode buffer (10x)	Gel buffer (pH8.45) (3x)
Tris (g) (Wako, Japan)	121	121	363
Tricine (g) (Sigma-Aldrich Co., Japan)	-----	179	-----
HCl (mL) (Nacalai Tesque, Japan)	10	-----	4.5
SDS (%) (Nacalai Tesque, Japan)	-----	1.0	0.3
Final Volume (L)	1	1	0.1
pH	8.9		8.45

Table M8 Composition of protein sample buffer for all protein sample

2x SDS Sample Buffer		
	For 200 mL	Final Concentration
0.5 M Tris-HCl pH 6.8	50 mL	0.125 M
SDS	8 g	4 %
Glycerol	40 mL	20 %
Bromophenol Blue (BPB) (TCI, Japan)	20 mg	0.01 %
dithiothreitol (DTT) (Nacalai Tesque, Japan)	6.16 g	0.2 M
	Fill up to 200 mL	

Glycine SDS-PAGE

- Make the gel as following table in the 50 mL baker.

Table M9 Composition of 10% Glycine SDS-PAGE

	Separating Gel (10%) (bottom)		Stacking Gel (5%) (top)
MilliQ	2.5 mL		0.708 mL
1.5 M Tris pH 8.8	1.2 mL	0.25 M Tris pH 6.8	1 mL
40 % acrylamide: bis = 19:1	1.25 mL		0.25 mL
10% SDS	50 µL		20 µL
TEMED	10 µL		2 µL
10 % APS	20 µL		20 µL
Total Volume	5.03 mL		2 mL

- Make the 10% APS from APS powder.
- After adding APS and TEMED in to separating gel, mix it well and added into module immediately.
- Add 600-800 µL isopropanol, isopropanol or ethanol in the top of running gel, wait for gel formation.
- After the gel form, use tissue remove ethanol carefully.
- Add APS and TEMED into stacking gel, mix it well and added into module immediately.
- Insert comb into gel immediately.

Running samples

- Loading samples, blank and marker.
- Loading 10 µL sample each well.
- Total volume should be the same in each well.
- Marker volume is 5 + 5 µL.
- Running condition (stacking /running): 60 /120 (V)

Gel stain and distain

- Warm up the gel with MilliQ by microwave and shake it with 60 rpm for 10 min twice.
- Stain with SimplyBlue™ SafeStain. Warm up the gel with SimplyBlue™ SafeStain by microwave and shake it with 60 rpm for 15 min.

- Destain with MilliQ. Warm up the gel with MilliQ by microwave and shake it with 60 rpm overnight.
- Store the gel with little MilliQ in the zip lock bag. Scan into file and store it at 4°C.

Table M10 Composition of running buffer of Glycine SDS-PAGE

	Running buffer (pH8.45) (10x)	Final Concentration
Tris	30.2 g	250 mM
Glycine (Wako, Japan)	188 g	2.5 M
10% SDS	100 mL	1%
Final Volume	1 L	

Protein identification by Silver staining

After electrophoresis, the gel was fixed in 40 % ethanol, and 10 % acetic acid in water for 1 hour. It was then washed with 50 % ethanol for 10 min and then with water overnight to remove the remaining acid. The gel was sensitized by 1 min incubation in 0.02 % sodium thiosulfate, and then it was rinsed with MilliQ H₂O for 20 sec 3 times. After rinsing, the gel was incubated in 0.1 % silver nitrate and 0.02 % formaldehyde solution for 30 min at 277 K. After incubation, the gel was washed with MilliQ H₂O for 20 sec 3 times and then developed in 3 % sodium carbonate and 0.05 % formaldehyde with vigorous shaking. After the desired intensity of staining was achieved, the reaction was terminated with 5 % acetic acid.

Western blotting

After electrophoresis, the samples in the PAGE were transferred onto Sequi-Blot polyvinylidene difluoride (PVDF) membranes by 100 V for 60 min at 277 K. CDO-F and α -subunit of CDO-O was detected by anti-His-tagged antibody as the primary antibody and HRP-linked anti-mouse antibody as secondary antibody. Signals were visually by Image Quant LAS 500 (GE Healthcare Japan, Japan).

Transferring the protein from the gel to the membrane

- Prepare the sponges, filter paper, PVDF membrane.

- Cut the filter paper *4 to smaller than 6.5*9 cm, and cut PVDF *1 to just 6.5*9 cm.
- PVDF has to activate by methanol for 30 sec.
- Prepare 1x transfer buffer from 10x transfer buffer, 800 mL is enough.
- Transfer gel and PVDF to 1x transfer buffer and shake for 15 min. Also wet the sponges *2 and filter papers in transfer buffer.
- Prepare the transfer sandwich as follows, all bubbles should be removed.
- Run the transfer cell at in the ice box for 100 V for 1 hr.

Antibody staining

- Block the membrane for 1 h at room temperature using membrane blocking reagent with 20 mL 1x TBST as follows.
- Wash the membrane three times with 1×TBST, 5 min each.
- Incubate the membrane with 1000X dilution of primary antibody with 1x TBST overnight.
- Wash the membrane three times with 1x TBST, 15 min each.
- 1 h incubation the membrane with 8000 X dilution of conjugated secondary HRP Mouse antibody with 1x TBST.
- Wash the membrane three times with 1x TBST, 15 min each.
- Develop signal based on chemiluminescence (HRP substrate) (3+3 mL)

Measurement the concentration of protein samples

Protein concentrations were estimated using protein assay kit [Bio-Rad, USA; Bradford, 1994] with bovine serum albumin (BSA) as the standard. The absorbance was measured at 595 nm by spectrophotometer. Comparison to standard curve provides a relative measurement of protein concentration.

- Five times dilution of the origin dye reagent with MilliQ

- The standard curve is generated with 0, 0.1, 0.2, 0.3, 0.4 and 0.5 mg/mL BSA diluted by MilliQ.
- The 1 mL 1X dye reagent is mix with 20 μ L standards or targeted samples in 1.5 mL microcentrifuge tubes. Stand at room temperature for 10 min.
- Measure the absorbance of each sample at 595 nm wavelength by Jasco V630 spectrophotometer (Jasco Co., Japan).
- Calculate the concentrations of targeted proteins according to the standard curve.

Pre-crystallization test (PCT)

The PCT kit contains 4 reagents; A1: 0.1 M Tris-HCl (pH 8.5), 2.0 M ammonium sulfate ((NH₄)₂SO₄); B1: 0.1 M Tris-HCl (pH 8.5), 1.0 M (NH₄)₂SO₄; A2: 0.1 M Tris-HCl (pH 8.5), 0.2 M magnesium chloride hexahydrate (MgCl₂ · 6H₂O), 30% PEG 4000; B2: 0.1 M Tris-HCl (pH 8.5), 0.2 M MgCl₂ · 6H₂O, 15% PEG 4000. Different concentrations of WT CDO-F (15, 20, 25, 30, 35, 40 and 45 mg/mL) were mixed with these 4 reagents and incubated for 30 min at room temperature. After 30 min, formation of precipitate in the drops was monitored with a light microscope and compared the condition between A1/B1 and A2/B2 reagents.

Condition screening of crystallization

For crystallization experiments, WT CDO-F alone and α K117A-WT CDO-F mixture were prepared in 5 mM Tris-HCl buffer (pH 7.5). The concentration of WT CDO-F was adjusted to 5 mg/mL and 20 mg/mL. Purified Cum_OxyK117A and WT CDO-F proteins were mixed in an approximate molar ratio of 1:3 or 1:6, and the concentration was adjusted to 20 mg/mL. Crystallization was conducted by the sitting-drop vapor diffusion method at 293 K. Drops containing 0.3 μ L each of protein solution and reservoir solution was mixed using a HYDRA II-plus-One (Matrix Technologies Co., USA), and the resultant drop was equilibrated against 50 μ L reservoir solution in a 96-well crystallization plate. The screenings were performed with

Crystal Screens I and II, Salt RX, Index kits (Hampton Research, USA), Wizard Classic 1 and 2, Wizard Cryo 1 and 2, Wizard JCSG⁺ (Rigaku, USA).

Molecular replacement, model building and refinement

The structures were determined by molecular replacement with the program MOLREP integrated in the CCP4 program suite [Vagin and Teplyakov, 1997; Winn *et al.*, 2011] using CDO-O [PDB ID: 1WQL; Dong *et al.*, 2005] and BDO-F from *Acidovorax* sp. KKS102 [PDB ID: 2E4P; Senda *et al.*, 2007] as models.

Chemical Cross-linking

Chemical cross-linking reaction were conducted with purified CDO-O and WT CDO-F. The both cross-linkers, DMS (0.25 and 0.5 mg/mL) and Sulfo-SMPB (0.25 and 0.5 mM) were used. CDO-O only, WT CDO-F only, CDO-O and WT CDO-F mixture with 1:3 ratio and CDO-O WT and WT CDO-F mixture with 1:6 ratio with 10 mM phosphate buffer. The Sulfo-SMPB was dissolved in water, while DMS was dissolved in 0.4 M triethanolamine. The solution were incubated for 60 min at room temperature. After the cross-linking reaction, 10 μ L 2X protein sample buffer was added and boiled for 5 min. Samples were subjected to 10% Glycine-SDS-PAGE.

In-gel digestion for LC/ Q-TOF-MS analysis

Gel fragment preparation

- Excise the protein bands of interest from polyacrylamide gel and cut each band into 1 mm³ pieces (not cut for this time). Place gel pieces back into the 1.5 mL microcentrifuge tube. (The protein bands of interest should be visible with coomassie blue staining.)
- Wash the pieces with 500 μ L dH₂O by rotating or shaking for 10 min. Repeat the step once.

- Discard the dH₂O. Add 200 μ L acetonitrile (volume of acetonitrile should enough to cover entire gel pieces) and wait for at least 5 min until the gel pieces shrink and become white.
- Discard the acetonitrile and dry gel pieces with the vacuum centrifuge for 30 min (check the condition each 10 min).

Reduction and alkylation

Reduction and alkylation of cysteine residues improves the recovery of cystine containing peptides and minimizes the appearance of unknown masses in MS analysis from disulfide bond formation and side chain modification. Treatment with iodoacetamide will alkylate the cysteine residues. Alkylation with iodoacetamide increase the mass of a peptide by 57.02 for each cysteine residue. The size of peptides may become 1 Da larger because of the deamidation of alkylated cysteine.

- Add 50 μ L reducing buffer and incubate at 56 °C for 30 min.
- Discard reducing buffer. Add 100 μ L alkylation buffer and incubate in the dark at 37 °C for 30 min.
- Discard alkylation buffer. Wash the sample with 200 μ L 100 mM NH₄HCO₃ by tapping.
- Discard all liquid in the tube.

Digestion

- Dehydrate gel pieces with 200 μ L acetonitrile for 5 min twice until the gel pieces shrink and become white and then dry gel pieces with the vacuum centrifuge for 30 min (check the condition each 10 min).
- Add 10 μ L digestion buffer and rehydrate gel pieces for 5 min on ice. Repeat this step until the gel pieces recover to transparent.
- Discard the abundant digestion mixture. Add 20-50 μ L 50 mM NH₄HCO₃ (volume of NH₄HCO₃ should enough to cover entire gel pieces) and digest at 37 °C overnight.

Extraction

- Transfer the supernatant to a new microcentrifuge tube.
- Add 50 μL 5 % formic acid/ 50 % acetonitrile and incubate for 10 min and transfer the supernatant to the same microcentrifuge tube. Repeat the step once.
- Try the mixture with the vacuum centrifuge for around 20 min until completely dried (around 1 μL left).
- Reconstitute the peptide in 10 μL 0.1 % trifluoroacetic acid (TFA).

Equilibrate the Zip-Tip C18 (Millipore: ZTC18S096) Note: Use P10 pipette

- Pipette up 10 μL 50 % acetonitrile/ 0.1 % TFA and then discard it in the waste. Repeat the step once.
- Pipette up 10 μL 2 % acetonitrile/ 0.1 % TFA and then discard it in the waste. Repeat the step once.

Load the peptide

- Load the sample by pipetting the sample 3-7 times (discard back into the same tube).
- Wash the Zip-Tip C18 with 10 μL 2 % acetonitrile/ 0.1 % TFA and then discard it in the waste. Repeat the step once.
- Elute the sample with 10 μL 50 % acetonitrile/ 0.1 % TFA by pipetting 3-5 times in the vial. Repeat the step once.

The sample is ready for LC-based analysis. The sample can be stored at 277 K for 2-3 days.

Table M11 Composition of buffer for In-gel digestion

Reducing buffer		Alkylation buffer	
dH ₂ O	800 μL	Iodoacetamide (Nacalai Tesque, Japan)	18.5 mg
1 M NH ₄ HCO ₃	100 μL	1 M NH ₄ HCO ₃	100 μL
0.5 M DTT	100 μL	dH ₂ O	900 μL
	1000 μL		1000 μL

Photo cross linking assay

WT CDO-O is mixed with CDO-F containing pBPA in 1:3 ratio. After mixed the protein samples, aliquot 50 μ L into each PCR tube and irradiated at 5 cm distance with the 365 nm UV light using handheld UV lamp (SPECTROLINE ENF-240C/J, SPECTRONIC Co., USA). At each sampling time, 50 μ L 2X protein sample buffer is added into samples directly and boiled at 371 K for 5 min.

In silico analyses

Homology Modeling

The CDO-F was modeled using SWISS-MODEL based on 4 different models, X-ray structures of Fd of BDO (BDO-F) from *P. xenovorans* LB400 [Colbert *et al.*, 2000; PDB: 1FQT (resolution: 1.6 Å)] and BDO-F from *Acidovorax* sp. KKS102 [Senda *et al.*, 2007; PDB: 2E4P and 2YVJ (resolution: 1.8 Å and 1.9 Å)], Fd of TDO (TDO-F) from *P. putida* F1 [Lin *et al.*, 2012; PDB: 4EMJ (resolution: 2.4 Å)]. The sequence identity between CDO-F and BDO-F_{LB400}, BDO-F_{KKS102}, and TDO-F_{F1} were 78%, 73% and 57%.

Docking simulation

Docking simulation was performed with global range molecular matching (GRAMM-X) protein-protein docking web server v.1.2.0 [Tovchigrechko *et al.*, 2006]. WT CDO-O hexamer form was used as receptor protein and modeled CDO-F was as ligand protein. The 20 best docking modes were analyzed. There were two modes that Rieske clusters in Fd and Oxy were closer than 14 Å which was defined as the limit of electron tunneling in proteins [Page *et al.*, 1999].

Absorbance spectra measurement of UV-vis

UV-vis spectra were recorded at 278 K with Jasco V-630 spectrophotometer. Experimental conditions used for single scan were: bandwidth, 1.5 nm; scan speed 400 nm/min; resolution, 1 nm; temperature, 298K. The proteins were dialyzed into TG buffer (20 mM Tris-HCl, 10% glycerol, pH7.4) and diluted to either 5 μ M (for CDO-O) or 0.1 μ M (for CDO-R and CDO-F) in 2 mL TG buffer. Spectra were collected from 800 nm to 300 nm.

Electron transfer efficiency analysis

Upon received the electrons, the Rieske cluster of CDO-O would change from oxidized form to reduced form, and the absorbance at 457 nm will be decrease. Based on the initial decreasing rate of the absorbance at 457 nm, the efficiencies of electron transfer from CDO-F to CDO-O were quantified. Experimental conditions used for single scan were: bandwidth, 1.5 nm; wavelength, 457 nm; time, 80 secs; temperature, 303 K. The protein was dialyzed in TG buffer and diluted to 10 μ M for CDO-O and 0.2 μ M for CDO-R and CDO-F. The absorbance spectra were collected on a Jasco V-630 spectrophotometer as follows: At beginning, 1992 μ L TG buffer was added into the glass cuvette and sealed the cuvette with rubber cap and aluminum cap. Oxygen in the cuvette was removed by bobbling with argon gas for 5 minutes. CDO-R, CDO-F and CDO-O were injected into the sealed cuvette by Hamilton syringe. 100 mM NADH was added into cuvette after measurement started. The slope of initial rate was defined as the electron transfer efficiency. The measurements were done three times for each sample.

Circular Dichroism (CD) Spectra Measurement

CD measurements were carried out with a Jasco J-820 spectropolarimeter with 0.1 cm path length cuvette at room temperature under constant nitrogen. All the samples were prepared to 0.3 mg/mL in 10 mM phosphate buffer (pH 7.5). The CD spectra were recorded from 190 nm

to 260 nm with an interval of 0.2 nm and a scan speed of 200 nm/min. Each spectrum was the average of four successive scans.

ITC measurement

ITC measurements were conducted at constant temperature 303K on MicroCal ITC200 with a cell volume of 200 μ L and a syringe volume of 40 μ L. Each experiment consisted of an initial injection of 0.4 μ L, followed by 19 injections of 2 μ L. Stirring speed was 1000 rpm. The buffers were listed in Table M11. The concentration of samples was adjusted to 10:1 (1 CDO-F : 1 α - + 1 β -subunit of CDO-O) molar ratio and showed in each figure. All data were analyzed with the software supplied by the manufacturer.

Table M12 The list of buffer which were used in ITC measurement

buffer				
20 mM HEPES pH 6.8	20 mM HEPES 10% Glycerol pH 6.8	20 mM HEPES 10% Glycerol pH 6.6	20 mM HEPES 10% Glycerol pH 7.5	20 mM HEPES pH 7.5
20 mM Tris-HCl 10% Glycerol pH 7.5	20 mM Tris-HCl pH 7.5	20 mM Tris-HCl 10% Glycerol pH 8.47	20 mM MES 10% Glycerol pH 6.0	

Table M1 Bacterial strains and plasmids

Bacterial strains	Relevant characteristics	Source or reference
DH5 α	F ⁻ , ϕ 80d, lacZ Δ M15, Δ (lacZYA-argF)U169, <i>deoR</i> , <i>endA1</i> , <i>gyrA96</i> , <i>hsdR17</i> (rk ⁻ ,mk ⁺), <i>recA1</i> , <i>relA1</i> , <i>supE44</i> , <i>thi-1</i>	Toyobo
BL21(DE3)	F ⁻ , <i>dem</i> , <i>ompT</i> (lon), <i>hsdS_B</i> (r _B ⁻ m _B ⁻), <i>gal</i> (DE3)	Novagen
JM109(DE3)	e14-(<i>mcrA</i> -), <i>recA1</i> , <i>supE44</i> , <i>endA1</i> , <i>hsdR17</i> (rk ⁻ , mk ⁺), <i>gyrA96</i> , <i>relA1</i> , <i>thi-1</i> , Δ (lac-proAB), F ['] [<i>traD36</i> , <i>proAB</i> , <i>lacI</i> ^q , <i>lacZ</i> Δ M15], <i>gal</i> (DE3)	Toyobo
Plasmids		
pZErO-2	Kmr, T7 promoter, ColE1 and fl origin, <i>ccdB</i> lethal gene, M13 priming sites	Invitrogen
pET-26b(+)	pBR322 origin, Km ^r , <i>lacI</i> , T7 promoter	Novagen
pUC118	Ap ^r , <i>lacZ</i> , pMB9 repton, M13IG	Takara
pUCumA1CA2	Ap ^r , pUC118 with 6+3+12+3+1380+18+6+3+12+3+6+561+4=2011 bp* <i>XbaI-SalI-HindIII</i> PCR fragment containing <i>cumA1</i> gene and <i>cumA2</i> gene from <i>Pseudomonas fluorescens</i> IP01, for Oxy _{III} expression as his-tagged protein at C-terminus of <i>cumA1</i> . MW \approx 51 +21 kDa	松澤淳、未発表
pETCumA3N	Km ^r , pET-26b(+) with 6+3+12+3+18+330+6=378 bp* <i>XbaI-SalI</i> PCR fragment containing <i>cumA3</i> gene from <i>P. fluorescens</i> IP01 from pA3S502, for Fd _{III} expression as his-tagged protein at N-terminus. MW \approx 11.8 kDa	松澤淳、未発表
pUCumA4N	Ap ^r , pUC118 with 6+3+12+3+18+1236+6=1284 bp* <i>XbaI-SalI</i> PCR fragment containing <i>cumA4</i> gene from <i>P. fluorescens</i> IP01, for Red _{III} expression as his-tagged protein at N-terminus. MW \approx 43.3 kDa	松澤淳、未発表
*: <i>XbaI</i> (6)+stop codon(3)+ribosome binding site(12)+ <i>NdeI</i> (3)+6His-tag(18)+ <i>SalI</i> (6) or + <i>HindIII</i> (4)		
pUCumA1CK33AA2	pUCumA1CA2 derivative, triple codon for K33 of <i>cumA1</i> is replaced with GCG.	小竹立朗、修論、2016
pUCumA1CL35AA2	pUCumA1CA2 derivative, triple codon for L35 of <i>cumA1</i> is replaced with GCG.	小竹立朗、修論、2016
pUCumA1CR39AA2	pUCumA1CA2 derivative, triple codon for R39 of <i>cumA1</i> is replaced with GCG.	小竹立朗、修論、2016
pUCumA1CK117AA2	pUCumA1CA2 derivative, triple codon for K117 of <i>cumA1</i> is replaced with GCG.	小竹立朗、修論、2016
pUCumA1CK141AA2	pUCumA1CA2 derivative, triple codon for K141 of <i>cumA1</i> is replaced with GCG.	小竹立朗、修論、2016
pUCumA1CD158AA2	pUCumA1CA2 derivative, triple codon for D158 of <i>cumA1</i> is replaced with GCG.	小竹立朗、修論、2016
pUCumA1CW159AA2	pUCumA1CA2 derivative, triple codon for W159 of <i>cumA1</i> is replaced with GCG.	小竹立朗、修論、2016
pUCumA1CL162AA2	pUCumA1CA2 derivative, triple codon for L162 of <i>cumA1</i> is replaced with GCG.	小竹立朗、修論、2016
pUCumA1CE180AA2	pUCumA1CA2 derivative, triple codon for E180 of <i>cumA1</i> is replaced with GCG.	小竹立朗、修論、2016
pUCumA1CL241AA2	pUCumA1CA2 derivative, triple codon for L241 of <i>cumA1</i> is replaced with GCG.	小竹立朗、修論、2016
pUCumA1CD253AA2	pUCumA1CA2 derivative, triple codon for D253 of <i>cumA1</i> is replaced with GCG.	小竹立朗、修論、2016

pUCumA1CK258AA2	pUCumA1CA2 derivative, triple codon for K258 of <i>cumA1</i> is replaced with GCG.	小竹立朗、修論, 2016
pUCumA1CR407AA2	pUCumA1CA2 derivative, triple codon for R407 [^] of <i>cumA1</i> is replaced with GCG.	小竹立朗、修論, 2016
pUCumA1CA2R65A	pUCumA1CA2 derivative, triple codon for R65 [^] of <i>cumA2</i> is replaced with GCG.	小竹立朗、修論, 2016
pUCumA1CA2L98A	pUCumA1CA2 derivative, triple codon for L98 of <i>cumA2</i> is replaced with GCG.	小竹立朗、修論, 2016
pUCumA1CA2W100A	pUCumA1CA2 derivative, triple codon for W100 of <i>cumA2</i> is replaced with GCG.	小竹立朗、修論, 2016
pUC57CumA3NQ19X	Km ^r , The fragment of <i>cumA3</i> gene with amber codon at Gln19 and 6 histidine residues at N-terminus which was flanked by <i>Xba</i> I- <i>Sa</i> I sites was synthesized and inserted in pUC57.	GENEWIZ Japan
pUC57CumA3NS49X	Km ^r , The fragment of <i>cumA3</i> gene with amber codon at Ser49 and 6 histidine residues at N-terminus which was flanked by <i>Xba</i> I- <i>Sa</i> I sites was synthesized and inserted in pUC57.	GENEWIZ Japan
pUC57CumA3NL65X	Km ^r , The fragment of <i>cumA3</i> gene with amber codon at Leu65 and 6 histidine residues at N-terminus which was flanked by <i>Xba</i> I- <i>Sa</i> I sites was synthesized and inserted in pUC57.	GENEWIZ Japan
pUC57CumA3NA80X	Km ^r , The fragment of <i>cumA3</i> gene with amber codon at Ala80 and 6 histidine residues at N-terminus which was flanked by <i>Xba</i> I- <i>Sa</i> I sites was synthesized and inserted in pUC57.	GENEWIZ Japan
pUC57CumA3NP81X	Km ^r , The fragment of <i>cumA3</i> gene with amber codon at Pro81 and 6 histidine residues at N-terminus which was flanked by <i>Xba</i> I- <i>Sa</i> I sites was synthesized and inserted in pUC57.	GENEWIZ Japan
pUC57CumA3NP85X	Km ^r , The fragment of <i>cumA3</i> gene with amber codon at Pro85 and 6 histidine residues at N-terminus which was flanked by <i>Xba</i> I- <i>Sa</i> I sites was synthesized and inserted in pUC57.	GENEWIZ Japan
pUC57CumA1K117AK141A	Km ^r , The fragment of <i>cumA1</i> gene with codon replaced by GCG at Lys117 and Lys141 and 6 histidine residues at N-terminus which was flanked by <i>Xba</i> I- <i>Sa</i> I sites was synthesized and inserted in pUC57.	GENEWIZ Japan
pUC57CumA1D158AW159A	Km ^r , The fragment of <i>cumA1</i> gene with codon replaced by GCG at Asp158 and Trp159 and 6 histidine residues at N-terminus which was flanked by <i>Xba</i> I- <i>Sa</i> I sites was synthesized and inserted in pUC57.	GENEWIZ Japan
pUC57CumA1D158AE180A	Km ^r , The fragment of <i>cumA1</i> gene with codon replaced by GCG at Asp158 and Glu180 and 6 histidine residues at N-terminus which was flanked by <i>Xba</i> I- <i>Sa</i> I sites was synthesized and inserted in pUC57.	GENEWIZ Japan
pUC57CumA1D158AR407A	Km ^r , The fragment of <i>cumA1</i> gene with codon replaced by GCG at Asp158 and Arg407 and 6 histidine residues at N-terminus which was flanked by <i>Xba</i> I- <i>Sa</i> I sites was synthesized and inserted in pUC57.	GENEWIZ Japan
pUC57CumA1W159AE180A	Km ^r , The fragment of <i>cumA1</i> gene with codon replaced by GCG at Trp159 and Glu180 and 6 histidine residues at N-terminus which was flanked by <i>Xba</i> I- <i>Sa</i> I sites was synthesized and inserted in pUC57.	GENEWIZ Japan
pUC57CumA1W159AR407A	Km ^r , The fragment of <i>cumA1</i> gene with codon replaced by GCG at Trp159 and Arg407 and 6 histidine residues at N-terminus	GENEWIZ Japan

pUC57CumA1E180AR407A	which was flanked by <i>XbaI-SalI</i> sites was synthesized and inserted in pUC57. Km ^r , The fragment of <i>cumA1</i> gene with codon replaced by GCG at Glu180 and Arg407 and 6 histidine residues at N-terminus which was flanked by <i>XbaI-SalI</i> sites was synthesized and inserted in pUC57.	GENEWIZ Japan
pUC57CumA1D158AW159AE180A	Km ^r , The fragment of <i>cumA1</i> gene with codon replaced by GCG at Asp158, Trp159 and Glu180 and 6 histidine residues at N-terminus which was flanked by <i>XbaI-SalI</i> sites was synthesized and inserted in pUC57.	GENEWIZ Japan
pUC57CumA1D158AW159AR407A	Km ^r , The fragment of <i>cumA1</i> gene with codon replaced by GCG at Asp158, Trp159 and Arg407 and 6 histidine residues at N-terminus which was flanked by <i>XbaI-SalI</i> sites was synthesized and inserted in pUC57.	GENEWIZ Japan
pUC57CumA1D158AE180AR407A	Km ^r , The fragment of <i>cumA1</i> gene with codon replaced by GCG at Asp158, Glu180 and Arg407 and 6 histidine residues at N-terminus which was flanked by <i>XbaI-SalI</i> sites was synthesized and inserted in pUC57.	GENEWIZ Japan
pUC57CumA1W159AE180AR407A	Km ^r , The fragment of <i>cumA1</i> gene with codon replaced by GCG at Trp159, Glu180 and Arg407 and 6 histidine residues at N-terminus which was flanked by <i>XbaI-SalI</i> sites was synthesized and inserted in pUC57.	GENEWIZ Japan
pUC57CumA1	Km ^r , The fragment of <i>cumA1</i> gene with codon replaced by GCG at Asp158, Trp159, Glu180 and Arg407 and 6 histidine residues at N-terminus which was flanked by <i>XbaI-SalI</i> sites was synthesized and inserted in pUC57.	GENEWIZ Japan
D158AW159AE180AR407A	Km ^r , The fragment of <i>cumA2</i> gene with codon replaced by GCG at Arg65 and Trp100 and 6 histidine residues at N-terminus which was flanked by <i>SalI-HindIII</i> sites was synthesized and inserted in pUC57.	GENEWIZ Japan
pETCumA3NQ19X	Km ^r , The fragment of <i>cumA3</i> gene with amber codon at Glu19 and 6 histidine residues at N-terminus which was flanked by <i>XbaI-SalI</i> sites was synthesized and inserted in pET-26b(+).	This Study
pETCumA3NS49X	Km ^r , The fragment of <i>cumA3</i> gene with amber codon at Ser49 and 6 histidine residues at N-terminus which was flanked by <i>XbaI-SalI</i> sites was synthesized and inserted in pET-26b(+).	This Study
pETCumA3NL65X	Km ^r , The fragment of <i>cumA3</i> gene with amber codon at Leu65 and 6 histidine residues at N-terminus which was flanked by <i>XbaI-SalI</i> sites was synthesized and inserted in pET-26b(+).	This Study
pETCumA3NA80X	Km ^r , The fragment of <i>cumA3</i> gene with amber codon at Ala80 and 6 histidine residues at N-terminus which was flanked by <i>XbaI-SalI</i> sites was synthesized and inserted in pET-26b(+).	This Study
pETCumA3NP81X	Km ^r , The fragment of <i>cumA3</i> gene with amber codon at Pro81 and 6 histidine residues at N-terminus which was flanked by <i>XbaI-SalI</i> sites was synthesized and inserted in pET-26b(+).	This Study
pETCumA3NP85X	Km ^r , The fragment of <i>cumA3</i> gene with amber codon at Pro85 and 6 histidine residues at N-terminus which was flanked by <i>XbaI-SalI</i> sites was synthesized and inserted in pET-26b(+).	This Study
pUC118CumA1K117AK141A	pUCumA1CA2, where the gene CumA1 was replaced by <i>XbaI-SalI</i> fragment of CumA1K117AK141A from	This Study

pUC57CumA1K117AK141A		
pUC118CumA1K117AA2R65A	pUCumA1CA2R65A, where the gene CumA1 was replaced by <i>Xba</i> I- <i>Sa</i> I fragment of CumA1K117A from pUCumA1CK117AA2	This Study
pUC118CumA1K117AA2W100A	pUCumA1CA2W100A, where the gene CumA1 was replaced by <i>Xba</i> I- <i>Sa</i> I fragment of CumA1K117A from pUCumA1CK117AA2	This Study
pUC118CumA1K141AA2R65A	pUCumA1CA2R65A, where the gene CumA1 was replaced by <i>Xba</i> I- <i>Sa</i> I fragment of CumA1K141A from pUCumA1CK141AA2	This Study
pUC118CumA1K141AA2W100A	pUCumA1CA2W100A, where the gene CumA1 was replaced by <i>Xba</i> I- <i>Sa</i> I fragment of CumA1K141A from pUCumA1CK141AA2	This Study
pUC118CumA1D158AW159A	pUCumA1CA2, where the gene CumA1 was replaced by <i>Xba</i> I- <i>Sa</i> I fragment of CumA1D158AW159A from pUC57CumA1D158AW159A	This Study
pUC118CumA1D158AE180A	pUCumA1CA2, where the gene CumA1 was replaced by <i>Xba</i> I- <i>Sa</i> I fragment of CumA1D158AE180A from pUC57CumA1D158AE180A	This Study
pUC118CumA1D158AR407A	pUCumA1CA2, where the gene CumA1 was replaced by <i>Xba</i> I- <i>Sa</i> I fragment of CumA1D158AR407A from pUC57CumA1D158AR407A	This Study
pUC118CumA1W159AE180A	pUCumA1CA2, where the gene CumA1 was replaced by <i>Xba</i> I- <i>Sa</i> I fragment of CumA1W159AE180A from pUC57CumA1W159AE180A	This Study
pUC118CumA1W159AR407A	pUCumA1CA2, where the gene CumA1 was replaced by <i>Xba</i> I- <i>Sa</i> I fragment of CumA1W159AR407A from pUC57CumA1W159AR407A	This Study
pUC118CumA1E180AR407A	pUCumA1CA2, where the gene CumA1 was replaced by <i>Xba</i> I- <i>Sa</i> I fragment of CumA1E180AR407A from pUC57CumA1E180AR407A	This Study
pUC118CumA2R65AW100A	pUCumA1CA2, where the gene CumA2 was replaced by <i>Sa</i> I- <i>Hind</i> III fragment of CumA2R65AW100A from pUC57CumA2R65AW100A	This Study

References

- Abe, R., Caaveiro, J. M., Kozuka-Hata, H., Oyama, M., & Tsumoto, K. (2012)** Mapping ultra-weak protein-protein interactions between heme transporters of *Staphylococcus aureus*. *J Biol Chem.* **287**(20):16477–16487 doi:10.1074/jbc.M112.346700
- Aliverti, A., Pandini V., Pennati A., de, Rosa, M., Zanetti G. (2008)** Structural and functional diversity of ferredoxin-NADP⁺ reductases. *Arch. Biochem. Biophys.* **474**:283-291
- Aoki, H., Kimura, T., Habe, H., Yamane, H., Kodama, T., Omori, T., (1996)** Cloning, nucleotide sequence, and characterization of the genes encoding enzymes involved in the degradation of cumene to 2-hydroxy-6-oxo-7-methylocta-2,4-dienoic acid in *Pseudomonas fluorescens* IP01. *J Ferment Bioeng.* **81**(3): 187-196
- Ashikawa, Y., Fujimoto, Z., Noguchi, H., Habe, H., Omori, T., Yamane, H., Nojiri H. (2006)** Electron transfer complex formation between oxygenase and ferredoxin components in rieske nonheme iron oxygenase system. *Structure.* **14**(12): 1779-89
- Axcell, B.C., Geary, P.J. (1975)** Purification and some properties of a soluble benzene-oxidizing system from a strain of *Pseudomonas*, *J Biochem.* **146**(1): 173–183
- Batie, C. J., Ballou, D. P., Correll, C. C. (1992)** Phthalate dioxygenase reductase and related flavin-iron-sulfur containing electron transferases. Chemistry and Biochemistry of Flavoenzymes. *Chemistry and Biochemistry of Flavoenzymes*, **3**: 543–556
- Battye, T.G., Kontogiannis, L., Johnson, O., Powell, H.R., Leslie, A.G. (2011)** iMOSFLM: a new graphical interface for diffraction-image processing with MOSFLM. *Acta Crystallogr. D Biol. Crystallogr.* **67**:271–281
- Beil, S., Mason, J. R., Timmis, K. N., Pieper, D. H. (1998)** Identification of chlorobenzene dioxygenase sequence elements involved in dechlorination of 1,2,4,5-tetrachlorobenzene. *J Bacteriol.* **180**(21): 5520–5528
- Brown, E.N., Friemann, R., Karlsson, A., Parales, J.V., Couture, M.M., Eltis, L.D., Ramaswamy, S. (2008)** Determining Rieske cluster reduction potentials. *J. Biol. Inorg. Chem.* **13**: 1301–1313
- Burton, S.G. (2003)** Oxidizing enzymes as biocatalysts. *Trends Biotechnol.* **21**(12): 543–549
- Carl, E. C. (1993)** Biodegradation of polycyclic aromatic hydrocarbons. *Curr Opin Cell Biol.* **4**: 331-338
- Carrell, C. J., Zhang, H, Cramer, W. A., Smith, J. L. (1997)** Biological identity and diversity in photosynthesis and respiration: structure of the lumen-side domain of the chloroplast Rieske protein. *Structure*, **5**(12):1613-1625
- Chakraborty, J., Ghosal, D., Dutta, A., Dutta, T.K. (2012)** An insight into the origin and functional evolution of bacterial aromatic ring-hydroxylating oxygenases. *J. Biomol. Struct. Dyn.*, **30**:419–436
- Chang, H. K., Zylstra, G. J. (1998)** Novel organization of the genes for phthalate degradation from *Burkholderia cepacia* DBO1. *J Bacteriol.* **180**(24): 6529–6537
- Colbert, C.L., Agar, N.Y.R., Kumar, P., Chakko, M.N., Sinha, S.C., Powlowski, J.B., Eltis L.D., Bolinet, J.T. (2013)** Structural Characterization of *Pandoraea pnomenus* B-356 biphenyl dioxygenase reveals features of potent polychlorinated biphenyl-degrading enzymes. *PLoS ONE* **8**(1):e52550 doi: 10.1371/journal.pone.0052550
- Colbert, C.L., Couture, M.M.J., Eltis, L.D., Bolin, J.T. (2000)** A cluster exposed: structure of the Rieske ferredoxin from biphenyl dioxygenase and the redox properties of Rieske Fe-S protein. *Structure.* **8**(12):1267–1278

- Collaborative Computational Project, Number 4. (2011)** Overview of the CCP4 suite and current developments. *Acta Crystallogr. D Biol. Crystallogr.* **67**:235-242
- Curtis, R.A., Ulrich, J., Montaser, A., Prausnitz, J.M. Blanch, H.W. (2002)** Protein-protein interactions in concentrated electrolyte solutions: Hofmeister-series effects. *Biotechnology and Bioengineering.* **79**(4):367-380 doi: 10.1002/bit.10342
- Dong, X., Fushinobu, S., Fukuda, E., Terada, T., Nakamura, S., Shimizu, K., Nojiri, H., Omori, T., Shoun, H., Wakagi, T. (2005)** Crystal structure of the terminal oxygenase component of cumene dioxygenase from *Pseudomonas fluorescens* IP01. *J Bacteriol.* **187**(7): 2483-2490
- Dorman, G., Prestwich, G.D. (1994)** Benzophenone photophoresin biochemistry. *Biochemistry*, **33**:5661–5673
- Emsley, P., Lohkamp, B., Scott, W.G., Cowtan K.D. (2010)** Features and development of *Coot*. *Acta Crystallogr. D Biol. Crystallogr.* **66**:486-501 doi:10.1107/S0907444910007493
- Evans, P.R. (2006)** Scaling and assessment of data quality. *Acta Crystallogr. D Biol. Crystallogr.* **62**:72-82
- Evans, P.R. (2011)** An introduction to data reduction: space-group determination, scaling and intensity statistics. *Acta Crystallogr. D Biol. Crystallogr.* **67**:282-292
- Farrell, I.S., Toroney, R., Hazen, J.L., Mehl, R.A. & Chin, J.W. (2005)** Photo-cross-linking interacting proteins with a genetically encoded benzophenone. *Nat. Methods*, **2**:377–384
- Ferraro, D.J., Brown, E.N., Yu, C.L., Parales, R.E., Gibson, D.T., Ramaswamy, S. (2007)** Structural investigations of the ferredoxin and terminal oxygenase components of the biphenyl 2,3-dioxygenase from *Sphingobium yanoikuyae* B1. *BMC Struct. Biol.* **7**(10) doi: 10.1186/1472-6807-7-10
- Ferraro, D.J., Gakhar, L., Ramaswamy, S. (2005)** Rieske business: structure-function of Rieske non-heme oxygenases. *Biochem. Biophys. Res. Commun.* **338**(1):175–190. doi:10.1016/j.bbrc.2005.08.222
- Friemann, R., Ivkovic-Jensen, M.M., Lessner, D.J., Yu, C.-L., Gibson, D.T., Parales, R.E., Eklund, H., Ramaswamy, S. (2005)** Structural insight into the dioxygenation of nitroarene compounds: the crystal structure of nitrobenzene dioxygenase. *J. Mol. Biol.* **348**: 1139–1151
- Friemann, R., Lee, K., Brown, E. N., Gibson, D. T., Eklund, H., Ramaswamy, S. (2009)** Structures of the multicomponent Rieske non-heme iron toluene 2,3-dioxygenase enzyme system. *Acta Crystallographica Section D: Biological Crystallography.* **65**(1): 24–33
- Fuchs, G., Boll, M., Heider, J. (2011)** Microbial degradation of aromatic compounds—from one strategy to four. *Nat Rev Microbiol.* **9**(11): 803-816
- Furukawa, K. (2000)** Engineering dioxygenases for efficient degradation of environmental pollutants. *Curr. Opin. Biotechnol.* **11**:244–249.
- Furusawa, Y., Nagarajan, V., Tanokura, M., Masai, E., Fukuda, M., Senda, T. (2004)** Crystal structure of the terminal oxygenase component of biphenyl dioxygenase derived from *Rhodococcus* sp. strain RHA1. *J. Mol. Biol.* **342**:1041–1052.
- Gassner, G.T., Ballou, D.P., Landrum, G.A., Whittaker, J.W. (1993)** Magnetic circular dichroism studies on the mononuclear ferrous active-site of phthalate dioxygenase from *Pseudomonas cepacia* show a change of ligation state on substrate binding. *Biochemistry*, **32**:4820-4825

- Gibson, D.T., Koch, J.R., Kallio, R.E. (1968)** Oxidative degradation of aromatic hydrocarbons by microorganisms. I. Enzymatic formation of catechol from benzene. *Biochemistry* **7**(7): 2653–2662
- Gurbiel, R. J., Batie, C. J., Sivaraja, M., True, A. E., Fee, J. A., Hoffman, B. M., Ballou, D. P. (1989)** Electron nuclear double-resonance spectroscopy of N-15-enriched phthalate dioxygenase from *Pseudomonas cepacia* proves that 2 histidines are coordinated to the [2Fe-2S] Rieske-type clusters. *Biochemistry* **28**: 4861–4871.
- Haigler, B. E., Gibson, D. T. (1990)** Purification and properties of NADH-ferredoxinNAP reductase, a component of naphthalene dioxygenase from *Pseudomonas* sp. strain NCIB 9816. *J. Bacteriol.* **172**:457–464
- Hanahan, D. (1983)** Studies on transformation of *Escherichia coli* with plasmids. *J. Mol. Biol.* **166**:557-80
- Hanke, G., Mulo, P. (2013)** Plant type ferredoxins and ferredoxin-dependent metabolism. *Plant Cell Environ.* **36**:1071–1084
- Hansen, J.T., Platten, F., Wagner, D.L., Egelhaaf, S.U. (2016)** Tuning protein-protein interactions using cosolvents: specific effects of ionic and non-ionic additives on protein phase behavior. *Physical chemistry chemical physics* **18**(15):10270-10280
- Harayama, S., Rekik, M., Timmis, K. N. (1986)** Genetic analysis of a relaxed substrate specificity aromatic ring dioxygenase, toluate 1,2-dioxygenase, encoded by TOL plasmid pWW0 of *Pseudomonas putida*. *Molecular & General Genetics* **202**(2): 226–234
- Hayaishi, O., Katagiri, M., Rothberg, S. (1955)** Mechanism of the pyrocatechase reaction. *J. Am. Chem. Soc.* **77**(20):5450-5451
- Hurtubise, Y., Barriault, D., Sylvestre, M. (1998)** Involvement of the terminal oxygenase beta subunit in the biphenyl dioxygenase reactivity pattern toward chlorobiphenyls. *J Bacteriol.* **180**(22): 5828–5835
- Inoue, K., Ashikawa, Y., Umeda, T., Abo, M., Katsuki, J., Usami, Y., Noguchi, H., Fujimoto, Z., Terada, T., Yamane, H., Nojiri, H. (2009)** Specific Interactions between the ferredoxin and terminal oxygenase components of a class IIB Rieske nonheme iron oxygenase, carbazole 1,9a-dioxygenase. *J.Mol.Biol.* **392**:436-451
- International Agency for Research on Cancer (IARC) (1983)** Polynuclear Aromatic Compounds. Part 1, Chemical, Environmental and Experimental Data. IARC Monographs on the Evaluation of the Carcinogenic Risk of Chemicals to Humans. **32**: 211–224
- Jakoncic, J., Jouanneau, Y., Meyer, C., Stojanoff, V. (2007)** The crystal structure of the ring-hydroxylating dioxygenase from *Sphingomonas* CHY-1. *FEBS J.* **274**: 2470–2481
- Jiang, H., Parales, R. E., Gibson, D. T. (1999)** The α subunit of toluene dioxygenase from *Pseudomonas putida* F1 can accept electrons from reduced ferredoxin(TOL) but is catalytically inactive in the absence of the β subunit. *Appl Environ Microbiol.* **65**(1): 315–318
- Jun, H., Akiko, S., Shinsaku, H., Kensuke, F. (1994)** Construction of hybrid biphenyl (bph) and toluene (tod) genes for functional analysis of aromatic ring dioxygenases. *Gene.* **138**(1–2): 27–33
- Kabsch, W. (2010)** Integration, scaling, space-group assignment and post-refinement. *Acta Crystallogr. D Biol. Crystallogr.* **66**:133–144
- Kabsch, W. (2010)** XDS. *Acta Crystallogr. D Biol. Crystallogr.* **66**:125–132

- Kanally, R.A., Harayama, S. (2000)** Biodegradation of high-molecular-weight polycyclic aromatic hydrocarbons by bacteria. *J Bacteriol.* **182**(8): 2059-2067
- Karplus, P.A., Bruns, C.M. (1994)** Structure-function relations for ferredoxin reductase. *J. Bioenerg Biomembr* **26**:89–99 doi:10.1007/BF00763221
- Karplus, P.A., Faber, H.R. (2004)** Structural Aspects of Plant Ferredoxin : NADP⁺ Oxidoreductases. *Photosynthesis Research* **81**:303-315
- Kauer, J. C., Erickson-Viitanen, S., Wolfe, H. R., DeGrado, W. F. (1986)** p-Benzoyl-L-phenylalanine, a new photoreactive amino acid. Photolabeling of calmodulin with a synthetic calmodulin-binding peptide. *J. Biol. Chem.*, **261**:10695-10700
- Kauppi, B., Lee, K., Carredano, E., Parales, R. E., Gibson, D. T., Eklund, H., Ramaswamy, S. (1998)** Structure of an aromatic-ring-hydroxylating dioxygenase – naphthalene 1,2-dioxygenase. *Structure.* **6**(5): 571–586
- Khara, P., Roy, M., Chakraborty, J., Ghosal, D., Dutta, T. K. (2014)** Functional characterization of diverse ring-hydroxylating oxygenases and induction of complex aromatic catabolic gene clusters in *Sphingobium* sp. PNB. *FEBS Open Bio.* **4**: 290–300
- Kumar, P., Mohammadi, M., Viger, J.F., Barriault, D., Gomez-Gil, L., Eltis, L.D., Bolin, J.T., Sylvestre, M. (2011)** Structural insight into the expanded Pcb-degrading abilities of a biphenyl dioxygenase obtained by directed evolution. *J..Mol..Biol.*, **405**: 531
- Kumar, S., Stecher, G., Li, M., Knyaz, C., Tamura, K. (2018)** MEGA X: Molecular Evolutionary Genetics Analysis across computing platforms. *Molecular Biology and Evolution*, **35**:1547-1549
- Kumari, A., Singh, D., Ramaswamy, S., Ramanathan, G. (2017)** Structural and functional studies of ferredoxin and oxygenase components of 3-nitrotoluene dioxygenase from *Diaphorobacter* sp. strain DS2. *PLoS ONE.* **12**(4): e0176398
- Kweon, O., Kim, S.-J., Baek, S., Chae, J.-C., Adjei, M.D., Baek, D.-H., Kim, Y.C., Cerniglia, C.E. (2008)** A new classification system for bacterial Rieske non-heme iron aromatic ring-hydroxylating oxygenases. *BMC Biochemistry*, **9**:11.
- Lin, T.-Y., Werther, T., Jeoung, J.-H., Dobbek, H. (2012)** Suppression of Electron Transfer to Dioxygen by Charge Transfer and Electron Transfer Complexes in the FAD-dependent Reductase Component of Toluene Dioxygenase. *J. Biol. Chem.*, **287**(45):38338-38346
- Malfois, M., Bonneté, F., Belloni, L. and Tardieu, A. (1996)** A model of attractive interactions to account for fluid–fluid phase separation of protein solutions. *J. chem. phys.* **105**(8):3290-3300
- Mason, H.S., Fowlks, W.K., Peterson, E. (1955)** Oxygen transfer and electron transport by the phenolase complex. *J. Am. Chem. Soc.* **77**(10):2914 – 2915
- Mason, J. R., Cammack, R. (1992)** The electron-transport proteins of hydroxylating bacterial dioxygenases. *Annu. Rev. Microbiol.* **46**:277–305
- McCoy, A.J., Grosse-Kunstleve, R.W., Adams, P.D., Winn, M.D., Storoni, L.C. Read, R.J. (2007)** Phaser crystallographic software. *J. Appl. Cryst.* **40**:658-674
- Murshudov, G. N., Vagin, A. A. Dodson, E. J. (1997)** Refinement of Macromolecular Structures by the Maximum-Likelihood Method. *Acta Crystallogr. D Biol. Crystallogr.* **53**:240-255 doi:10.1107/S0907444996012255
- Murshudov, G.N., Skubák, P., Lebedev, A.A., Pannu, N.S., Steiner, R.A., Nicholls, R.A., Winn, M.D., Long, F., Vagin, A.A. (2011)** REFMAC5 for the refinement of macromolecular

crystal structures. *Acta Crystallogr. D Biol. Crystallogr.* **67**:355–367
doi:10.1107/S0907444911001314

Nam, J.W., Noguchi, H., Fujiomoto, Z., Mizuno, H., Ashikawa, Y., Abo, M., Fushinobu, S., Kobashi, N., Wakagi, T., Iwata, K., Yoshida, T., Habe, H., Yamane, H., Omori, T., Nojiri, H. (2005) Crystal structure of the ferredoxin component of carbazole 1,9a-dioxygenase of *Pseudomonas resinovorans* strain CA10, a novel Rieske non-heme iron oxygenase system. *Proteins*. **58**:779-789

Nam, J.W., Nojiri, H., Yoshida, T., Habe, H., Yamane, H., Omori, T. (2001) New classification system for oxygenase components involved in ring-hydroxylating oxygenations. *Bioscience, Biotechnology, and Biochemistry*, **65**:254–263.

Naruya, S, Masatoshi, N. (1987) The neighbor-joining method: a new method for reconstructing phylogenetic trees. *Molecular Biology and Evolution*, **4**:406–425.

National Toxicology Program. (2009) Toxicology and carcinogenesis studies of cumene (CAS No. 98-82-8) in F344/N rats and B6C3F1 mice (inhalation studies). *Natl Toxicol Program Tech Rep Ser* **542**: 1–200.

Nojiri, H., Ashikawa, Y., Noguchi, H., Nam, J. W., Urata, M., Fujimoto, Z., Uchimura, H., Terada, T., Nakamura, S., Shimizu, K., Yoshida, T., Habe, H., Omori, T. (2005) Structure of the terminal oxygenase component of angular dioxygenase, carbazole 1,9a-dioxygenase. *Journal of Molecular Biology*. **351**(2): 355–370

Noodleman, L., Pique, M. E., Roberts, V. A. (2008) Iron–Sulfur Clusters: Properties and Functions. *Wiley Encyclopedia of Chemical Biology*. pp. 458-468

Page, C. C., Moser, C. C., Chen, X., Dutton, P. L. (1999) Natural engineering principles of electron tunneling in biological oxidation-reduction. *Nature*. **402**(6757): 47–52

Parales, J. V., Parales, R. E., Resnick, S. M., Gibson, D. T. (1998) Enzyme specificity of 2-nitrotoluene 2,3-dioxygenase from *Pseudomonas* sp. strain JS42 is determined by the C-terminal region of the beta subunit of the oxygenase component. *J Bacteriol.* **180**(5): 1194–1199

Parales, R. E., Emig, M. D., Lynch, N. A., Gibson, D. T. (1998) Substrate specificities of hybrid naphthalene and 2,4-dinitrotoluene dioxygenase enzyme systems. *J Bacteriol.* **180**(9): 2337–2344

Piazza, R. (1999) Interactions in protein solutions near crystallisation: A colloid physics approach. *Journal of Crystal Growth*. **196**:415-423

Pohanish, R. P., Sittig, M. (2011) Sittig's handbook of toxic and hazardous chemicals and carcinogens. 6th edition, Norwich, N.Y., U.S.A: Noyes Publications.

Rieske, J.S., Hansen, R.E., Zaugg, W.S. (1964) Studies on the electron transfer system. 58. Properties of a new oxidation-reduction component of the respiratory chain as studied by electron paramagnetic resonance spectroscopy. *J. Biol. Chem.*, **239**:3017-3022

Rosche, B., Tshisuaka, B., Fetzner, S., and Lingens, F. (1995) 2-Oxo-1,2-dihydroquinoline 8-monooxygenase, a two-component enzyme system from *Pseudomonas putida* 86. *J. Biol. Chem.* **270**:17836–17842

Sambrook, J., Fritsch, E F., Maniatis, T. (1989) Molecular cloning: a laboratory manual, 2nd ed. Cold Spring Harbor Laboratory Press, Cold Spring Harbor, N.Y.

Schluchter, W.M., Bryant, D.A. (1992) Molecular characterization of ferredoxin-NADP⁺ oxidoreductase in cyanobacteria: cloning and sequence of the petH gene of *Synechococcus* sp. PCC 7002 and studies on the gene product. *Biochemistry* **12**: 3092-3102

- Senda, M., Kishigami, S., Kimura, S., Fukuda, M., Ishida, T., Senda, T. (2007)** Molecular mechanism of the redox-dependent interaction between NADH-dependent ferredoxin reductase and Rieske-type [2Fe-2S] Ferredoxin. *Journal of Molecular Biology*. **373**(2): 382–400
- Solomon, E. I., Brunold, T. C., Davis, M. I., Kemsley, J. N., Lee, S.-K., Lehnert, N., Neese, F., Skulan, A. J., Yang, Y.-S., Zhou, J. (2000)** Geometric and electronic structure/function correlations in non-heme Iron Enzymes. *Chem. Rev.* **100**(1):235-350
- Suenaga, H., Mitsuoka, M., Ura, Y., Watanabe, T., Furukawa, K. (2001)** Directed evolution of biphenyl dioxygenase: emergence of enhanced degradation capacity for benzene, toluene, and alkylbenzenes. *J. Bacteriol.* **183**: 5441–5444.
- Suenaga, H., Watanabe, T., Sato, M., Ngadiman, Furukawa, K. (2002)** Alteration of regiospecificity in biphenyl dioxygenase by active-site engineering. *J. Bacteriol.* **184**:3682–3688.
- Tan, H.-M., Cheong, C.-M. (1994)** Substitution of the ISP alpha-subunit of biphenyl dioxygenase from *Pseudomonas* results in a modification of the enzyme activity. *Biochem Biophys Res Commun.* **204**(2): 912–917
- Tovchigrechko, A., Vakser, I. A. (2006)** GRAMM-X public web server for protein-protein docking. *Nucleic Acids Res.* **34**:W310-314.
- Tovchigrechko, A., Vakser, I.A. (2005)** Development and testing of an automated approach to protein docking. *Proteins* **60**(2):296-301.
- Vagin, A., Teplyakov, A. (1997)** *MOLREP*: an Automated Program for Molecular Replacement. *J. Appl. Cryst.* **30**:1022-1025 doi:10.1107/S0021889897006766
- Wackett, L.P. (2002)** *Mechanism and applications of Rieske non-heme iron dioxygenases.* *Enzyme Microb Technol.* **31**(5): 577-587
- Werlen, C., Kohler, H.-P. E., van der Meer, J. R. (1996)** The broad substrate chlorobenzene dioxygenase and cis-chlorobenzene dihydrodiol dehydrogenase of *Pseudomonas* sp. strain P51 are linked evolutionarily to the enzymes for benzene and toluene degradation. *J. Biol. Chem.*, **271**:4009-4016
- Winn, M.D., Ballard, C.C., Cowtan, K.D., Dodson, E.J., Emsley, P., Evans, P.R., Keegan, R.M., Krissinel, E.B., Leslie, A.G., McCoy, A., McNicholas, S.J., Murshudov, G.N., Pannu, N.S., Potterton, E.A., Powell, H.R., Read, R.J., Vagin, A., Wilson, K.S. (2011)** Overview of the CCP4 suite and current developments. *Acta Crystallogr. D Biol. Crystallogr.* **67**:235–242
- Wolfe, M.D., Parales, J.V., Gibson, D.T., Lipscomb, J.D. (2000)** Single turnover chemistry and regulation of O₂ activation by the oxygenase component of naphthalene 1,2-dioxygenase. *J Biol Chem.* **276**(3):1945-1953
- Zielinski, M., Backhaus, S., Hofer, B. (2002)** The principal determinants for the structure of the substrate-binding pocket are located within a central core of a biphenyl dioxygenase alpha subunit. *Microbiology* **148**:2439–2448.
- Zielinski, M., Kahl, S., Hecht, H. J., Hofer, B. (2003)** Pinpointing biphenyl dioxygenase residues that are crucial for substrate interaction. *J. Bacteriol.* **185**:6976–6980.
- den, Dunnen, J.T., Dagleish, R., Maglott, D.R., Hart, R.K., Greenblatt, M.S., McGowan-Jordan, J., Roux, A.-F., Smith, T., Antonarakis, S.E., Taschner, P.E. (2016)** HGVS Recommendations for the Description of Sequence Variants: 2016 Update. *Human Mutation*, **37**:564-569. doi:10.1002/humu.22981

小竹立朗, 2016, 東京大学修士論文

Acknowledgements

First I would like to express my gratitude to Prof. Hideaki Nojiri for giving me the opportunity to pursue a doctoral degree in his laboratory and for his guidance and support. My grateful thanks are extended to Associate Prof. Okada Kazunori and Assistant Prof. Chiho Suzuki-Minakuchi for helpful discussions and support.

Furthermore, I would like to thank PhD Shumpei Asamizu for his support with preparation of the protein samples for MS sampling, analysis of the data, useful discussions of the results of MS. I am also thankful to Assistant Prof. Takatoshi Arakawa for his support with measurement of CD spectrum. I would also thank Associate Prof. Satoru Nagatoishi for providing the plasmid and useful discussions for photo cross linking. I would like also to thank PhD Zui Fujimoto from NARO for providing the Hydra II Plus-One robot and all chemicals for pre-crystallization screening of complex of CDO-F and CDO-O. This work was performed under the approval of the Photon Factory Program Advisory Committee (Proposal No. 2015G625 and 2019G102).

I am thankful to Dr. Aya Kubo (久保 彩) for her helping at beginning of my life in Japan, like applied the cell phone number, applied bank account or submitted documents to city office. And thankful to Mr. Jun Matsuzawa (松澤 淳) for teaching me the experimental method relating with protein research. I am especially thankful Miss Ayako Sakuda (作田 郁子) for her supporting and helping, for taught me plasmid extraction at beginning, modified my Japanese articles, gave advice when I have problems with my experiment and also supported me all the time especially when I depressed. My thankful to her is beyond words.

I am also thankful to all the present and former members of the Laboratory for Environmental Biochemistry at the University of Tokyo who have immensely contributed to my personal and professional life in Japan. I am especially grateful to my family for all their love, encouragement and infinite support.

2020年2月

蔡弼丞